5-2021

Spatial and Temporal Patterns of River Incision and Terrace Deposition in Response to Climate and Tectonics in Southern Taiwan

Dominique M. Shore
Utah State University

SPATIAL AND TEMPORAL PATTERNS OF RIVER INCISION AND TERRACE DEPOSITION IN RESPONSE TO CLIMATE AND TECTONICS IN SOUTHERN TAIWAN

by

Dominique M. Shore

A thesis submitted in partial fulfillment
of the requirements for the degree

of

MASTER OF SCIENCE

in

Geology

Approved:

_____	_____
Tammy M. Rittenour, Ph.D. Major Professor	Brian J. Yanites, Ph.D. Committee Member
_____	_____
Patrick Belmont, Ph.D. Committee Member	D. Richard Culter, Ph.D. Interim Vice Provost of Graduate Studies

UTAH STATE UNIVERSITY
Logan, Utah

2021

ABSTRACT

Spatial and Temporal Patterns of River Incision and Terrace Deposition in response to Climate and Tectonics in Southern Taiwan

by

Dominique M. Shore, Master of Science

Utah State University, 2021

Major Professor: Tammy M. Rittenour, Ph.D.
Department: Geology

The incision of bedrock rivers is often thought of as a detachment limited system reflecting the underlying tectonics. Recent studies have shown sediment supply also plays a crucial role in understanding landscape response to uplift, and can obscure tectonic forcings. This thesis investigates river incision patterns across a steep gradient of topography and accumulated uplift in southern Taiwan to better understand the role of climate and tectonics in landscape development. Taiwan is a young island undergoing rapid, southward propagating uplift resulting from the oblique collision of the Philippine Sea Plate and Eurasian Plate. Rapid uplift coupled with a warm, wet climate heavily influenced by the East Asian Summer Monsoon (EASM) allows processes of erosion to occur quickly resulting in a steep, dynamic landscape.

Age control from luminescence dating and field measurements were used to determine timing of terrace deposition and rates of river incision along the southern 100 km of Taiwan. Preliminary terrace deposition ages ranging from late-Pleistocene to late-

Holocene reveal periods of regional terrace deposition around 1, 11, 18, 28, and 40 ka. Periods of terrace deposition coincident with precession-driven cyclicity of the EASM during the Holocene and Pleistocene. Periods of terrace deposition also correlate with periods of increased hillslope erosion recorded in Holocene mass-wasting records from central and southern Taiwan. Results suggest that climate-driven changes in sediment supply are able to obscure tectonic drivers of incision on short-term timescales (10^0-10^3 yrs).

Preliminary incision rates range from 6 ± 2.6 to 0.2 ± 0.1m/kyr with an average of 2.4 ± 1.2 m/kyr. Incision rates increase northward along with hillslope denudation rates until a critical hillslope threshold is met ~80 km northward at which point hillslope denudation decreases and rates of incision continue to increase. Northward increasing rates of denudation mirroring the assumed pattern of uplift suggest that that tectonics is the primary driver of river incision on longer-term scales (10^3-10^6 yrs). The influence of climate on shorter timescales suggests that caution should be taken in using short-term incision rates to understand underlying geomorphic response to tectonics in Taiwan.

(107 pages)

PUBLIC ABSTRACT

Spatial and Temporal Patterns of River Incision and Terrace Deposition in response to Climate and Tectonics in Southern Taiwan

Dominique Shore

Geologists often look at the Earth's surface to understand the underlying processes that cause mountain formation. As tectonic forces drive uplift of Earth's surface, processes of erosion transport sediment to lower elevations. Climate can play a large role in landscape formation as well as increased precipitation, accelerating rates of erosion. Rivers leave markers of landscape evolution through terrace landforms, former river floodplains that are left behind when rivers incise into a valley. To better understand landscape response to uplift, this research investigated the initial linkages between uplift, hillslope erosion (mass wasting) and river incision. At some point, it is thought that these three will be in equilibrium. Taiwan is a young mountain range making it the ideal setting to capture landscape development in the initial stages of uplift. I compare rates of river incision to rates of hillslope erosion and timing of terrace deposition to understand the links between erosion, tectonics and climate in the beginning stages of mountain building.

This thesis uses luminescence to provide age control for the last time sediment was exposed to light to determine when river terraces formed. Field mapping and observations allowed us to measure the height between terraces to quantify the rate at which streams incised. The results from this study show that the rivers of southern Taiwan are incising on average at a rate of 2.4 ± 1.2 meters per thousand years (m/kyr)

with rates ranging from 6 ± 2.6to 0.2 ± 0.1 m/kyr. River incision rates and hillslope erosion (denudation) rates increase northward with drainage development suggesting that rates of erosion are primarily linked to tectonic forces on medium to longer-term scales (1,000-1,000,000 years) . Regional periods of terrace development occurred at 1, 11, 18, 28, and 40 ka. Periods of terrace development align with periods of increased East Asian Summer Monsoon (EASM) intensity chronicled in paleoclimate records. The EASM is the dominate weather pattern that delivers moisture to East Asia affecting 1/3 of global populations. Terrace deposits recording EASM intensity extends the record of landscape response to climate in Taiwan and reveals that climate signals can obscure tectonic forces on short-time scales ($10^0 – 10^3$ yrs).

ACKNOWLEDGMENTS

I would like to thank sincerely the National Science Foundation, Geological Society of America, and USU Geology Department for their generous funding and support of this research project. I would also like to acknowledge the enormous help of Carlie Ideker, Michelle Nelson, Harriet Cornachione, Natalie Tanski, and Maggie Erlick of the USU Luminescence Laboratory for their endless help and support. I am grateful for my committee members, Dr. Brian Yanites and Dr. Patrick Belmont for their advisement and time spent editing my thesis. I am grateful to Dr. Chia-Yu Chen, Dr. Bruce Shyu, Eva Yin, Clark DeLisle and others for their assistance in the field in southern Taiwan.

I am especially grateful to my advisor, Dr. Tammy Rittenour. She gave me the opportunity to attend USU and receive an advanced degree in Geology studying the fascinating landscape of Taiwan through a research assistantship and tuition waivers. She spent numerous hours editing my writing, discussing my data with me and writing references. I am so grateful for her patience through challenging times and working with me to finish my thesis after I began working in Montana.

In addition to scholarly support, I would like to give thanks to my friends and parents who helped me push through challenging times and finish my thesis. The numerous biking, skiing, and fishing breaks provided much-needed breaks. I cannot express how much the support of my parents, Jill Woodhouse, Jack McLaren, and Oscar S.S. Shore meant to me. Thank you all for you unwavering and constant support.

Dominique M. Shore

CONTENTS

LIST OF TABLES

Page

LIST OF FIGURES

Page

CHAPTER 1 - INTRODUCTION

Drainage development is often used to understand the underlying tectonics and mechanisms of uplift. Recent studies have shown that different processes have the ability to obscure the underlying tectonic mechanisms controlling river incision and topographic development. Due to the young nature of the island, Taiwan provides a 'natural lab' with fast rates of uplift and erosion, allowing the initial development of topo to be captured. Southward propagating uplift allows us to study a range of drainage evolution stages in response to modern, ongoing uplift. This research addresses questions about the role of tectonics and the influence of climate on drainage evolution by studying the rates and timing of river incision and aggradation in southern Taiwan. The results highlight a dynamic landscape controlled by tectonics and influenced by climate driven changed in sediment supply.

Chapter 2 investigates patterns of river incision through luminescence dating of terrace deposits and field mapping. This chronology was used to determine rates, timing, and spatial patterns of fluvial incision over a steep rise in topographic gradient. The results show that incision rates increase with distance northward with drainage development and hillslope steepness in response to southward propagating uplift. Incision rates mirror hillslope denudation rates supporting the linkages between hillslope and river erosion rates on which steady-state assumptions are built. This research suggests that the underlying drivers of uplift can be revealed through incision rates, although caution should be taken when comparting rates of Holocene landscape development to uplift rates average over millions of years.

Chapter 3 is a study of landscape response to the East Asian Summer Monsoon in southern Taiwan. I compared terrace deposition ages in the Holocene and late Pleistocene with paleoclimate records from Taiwan and China. Results show that periods of terrace deposition coincided of periods of increased monsoon intensity and hillslope activity. Results from this study reveal that variations in climate are capable of stalling the overall pattern of river incision controlled by tectonic uplift. Additionally, data introduced in this study extends the record of landscape response to East Asian Summer Monsoon intensity in Taiwan, which was previously constrained to the limits of radiocarbon dating.

Chapter 4 is a summary of these studies and their implications as well as recommendations for future work.

CHAPTER 2 - SPATIAL AND TEMPORAL PATTERNS OF RIVER INCISION IN SOUTHERN TAIWAN

2.1. ABSTRACT

Tectonics are often interpreted from the modern landscape, making the mechanisms driving landscape processes a long-asked question in the field of geomorphology. Research has shown difficulty in distinguishing if landscape response to uplift is controlled by detachment-limited or transport-limited fluvial processes, restraining our understanding of landscape evolution in response to climate and tectonics. Southern Taiwan provides an ideal natural laboratory to study landscape response to uplift. The island is characterized by ongoing, rapid uplift coupled with a warm, wet climate leading to accelerated rates of erosion. This research introduces incision rates in the southern 100 km of Taiwan to test the hypothesis that incision rates will increase northward across a steep gradient in topography until a critical hillslope steepness is met at which point sediment supply will blanket the river channel slowing rates of river incision. Calculated incision rates range from 6 ± 2.6 to 0.2 ± 0.1 m/kyr with an average of 2.4 ± 1.2 m/kyr. Incision rates increase northward with hillslope steepness and denudation rates until ~80 km from the southern tip of Taiwan, at which point denudation rates begin to decrease while incision rates continue to increase. Northward increasing uplift suggests that tectonics are the primary driver of landscape development on medium to longer-term scales (10^3-10^6 yrs). The presence of terraces representing unsteadiness in incision and variations between Holocene and Pleistocene incision rates show that other factors such as climate and seismicity can obscure tectonic signals on shorter timescales.

2.2. INTRODUCTION

Topography is often used to interpret underlying tectonic forcing making the mechanisms of landscape response to tectonics and climate a central question in the field of geomorphology (Beaumont et al., 1992; Howard, 1994; Willett, 1999; Kirby and Whipple, 2001; Lavé and Avouac, 2001; Wobus et al., 2006; Pazzaglia, 2013). Rates of bedrock river incision are often assumed to reflect underlying tectonics and control the pattern of landscape response to uplift (Whipple, 2004; Perron, 2017). However, it can be challenging to distinguish if rivers are steepening due to rock-uplift (Kirby and Whipple, 2001; Ouimet et al., 2009) or in response to increased sediment supply (Cowie et al., 2008; Yanites and Tucker, 2010). In many mountain ranges, the early stages of landscape response to tectonics have been erased by elapsed time making it difficult to understand what drives landscape evolution during the incipient stages of mountain building. This research investigates patterns of river incision in a developing orogen and the relationship between hillslope and fluvial processes to better the understanding of the limits of interpreting underlying tectonics from landscape processes.

Taiwan is an ideal location to study drainage-basin evolution because rapid uplift coupled with a warm, wet climate allows for rapid erosion and landscape development allowing the initial stages of landscape development to be captured within a resolvable timeframe (Hsieh and Knupfer, 2002; Dadson et al., 2003; Schaller et al., 2005; Yanites et al., 2009; Chen et al. 2020). Additionally, southward propagating uplift allows a range of uplift rates and durations to be investigated. While studies have calculated bedrock river incision rates in the foothills of Taiwan, few have quantified rates from the core of the Central Range, the large north-south oriented range spanning the island (Hsieh and

Knupfer, 2002; Dadson et al., 2003; Schaller et al., 2005; Yanites et al., 2009; Hsieh et al., 2014). Additionally, most of these studies focused on Holocene incision rates, precluding longer-term observations in this dynamic landscape. This study provides spatial and temporal assessment of incision rates from the southern Central Range of Taiwan to explore the relationship between hillslope denudation and river incision rates in an active orogen.

Incision rates from luminescence dated terraces of varying ages were calculated from drainages along a 100 km in transect in southern Taiwan to explore the relationship between hillslope and drainage development and river incision rates in this N-S transect. The study area captures a steep rise in topographic gradient and drainage development as maximum elevations rise ~2500 m in the north. The objective of this work is to test the hypothesis that river incision rates increase to the north with relief until a critical hillslope threshold is met. At this point, river incision rates are slowed by an influx of hillslope sediment blanketing the river channel. If the data does not reveal a northward increasing trend in incision rate, this would suggest that sediment supply plays a more significant role than tectonics in the drainage evolution of southern Taiwan.

2.3. BACKGROUND

2.3.1. STUDY AREA

The island of Taiwan is made up of an accretionary ridge created by the collision of the Luzon Arc with the Eurasian Plate that began 6.5 Ma (Figure 2.1, (Ching et al., 2011). The two plates are converging at an average rate of 82 mm/yr (Suppe, 1981). Data suggests that the central range is uplifting at a rate of 3-6 km/Myr with slower rates of

1.5-2.5 km/Myr in the foothills (Dadson et al., 2003). This uplift is thought to propagate southward due to the obliquity between the Chinese Continental Margin and the Luzon Arc (Suppe, 1981; Yu et al., 1997; Liu et al., 2001; Simoes and Avouac, 2006) at a rate of 30 to 90 km/Myr (Suppe, 1981; Liu et al., 2001; Simoes and Avouac, 2006). However, this apparent southward propagation of uplift may instead be driven by an acceleration of uplift in the last 0.5-1 Myr creating a steep north-south gradient in relief and basin evolution (Lee et al., 2015; Hsu et al., 2016). Either way, this tectonic gradient allows us to investigate patterns of river incision in southern Taiwan which provides the opportunity to observe drainage evolution across a transect in drainage development.

This research investigates a N-S transect of drainages in the southern 100 km of Taiwan paralleling the Chaochou Fault, the main thrust fault in the region. Within the study area, the mean elevation rises from sea level to ~2500 m asl along the axis of the north-south trending Central Range. This study exploits this natural gradient in topography to study drainage-basin evolution along the Central Range (Figure 2.1). Eight drainages from the western flank of the Central Range and five drainages from the eastern flank were included in this study. While there has been research into the modern slip rates using GPS data, little is known about the long-term slip rates that may explain the steep gradient in topography along the southern tip of the island (Hu et al., 2007; Wiltschko et al., 2010; Mesalles, 2014; Huang and Byrne, 2014). Much of the long-term evidence for varying uplift with latitude relies on the assumption that rivers are in steady state and the main control on incision rate is uplift (Wiltschko et al., 2010).

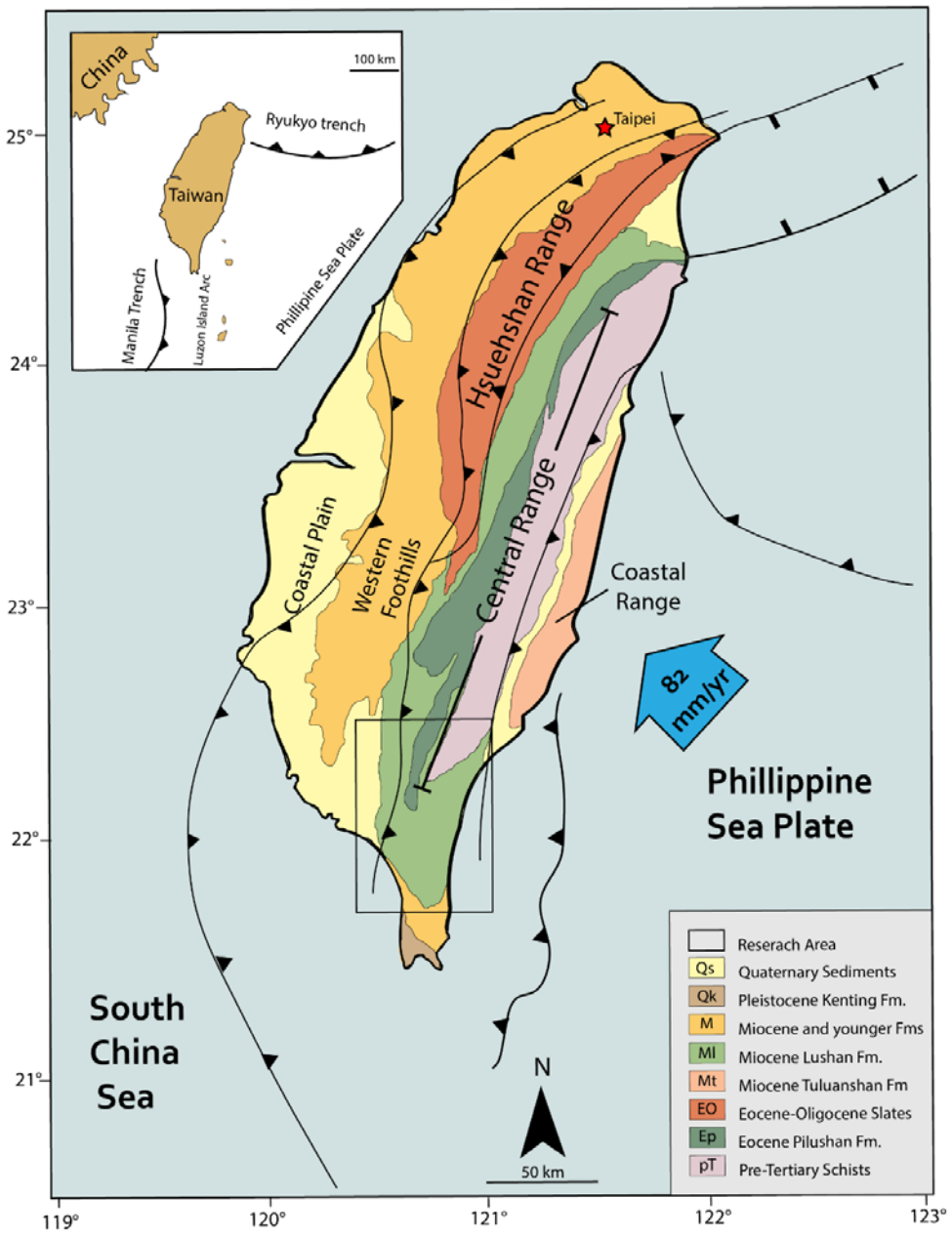

Figure 2.1 Geologic map of Taiwan after Ho (1986). The bedrock dominating the study area is the Miocene Lushan Formation, composed of easily erodible shales, slates, and sandstones.

The bedrock of the hanging wall of the Chaochou Fault is composed of low-grade Miocene slates with the metamorphic grade increasing to the north (Ho, 1986; Hu et al., 2007) (Figure 2.1). Relatively homogenous bedrock throughout the study area limits the role of lithology-dominate knickpoints in basin development. Weak, easily erodible bedrock in combination with a wet climate and active uplift produces high incision and denudation rates, allowing us to capture active landscape response to modern tectonic processes (last 5 Myr or less). The antiquity of most other orogens or slow rates of uplift/incision preclude assessment involving pre-steady state (equilibrium) conditions elsewhere and make Taiwan an ideal setting to capture the initial response of landscape to uplift and orogen formation.

2.3.2. GEOMORPHIC RESPONSE TO UPLIFT

Bedrock incision rates are often used as a proxy for uplift rates in active orogens because it is thought these rivers are in a ‘steady-state’ – rates of erosion equal rates of uplift (Ouimet et al., 2009; Cyr et al., 2010; DiBiase et al., 2015). Steady-state conditions evolve over time throughout the process of mountain building (Figure 2.2) (Burbank et al., 1996). Initially, uplift outpaces river incision, which allows net elevation to increase and topography to form (Burbank et al., 1996). Eventually, elevation rise leads to increasing slope and therefore the erosive power of rivers, which then begin to incise faster. As net elevation continues to rise due to uplift (Figure 2.2), hillslopes steepen until a critical threshold is met where hillslope process overload the fluvial system with sediment and slow vertical bedrock incision (Howard, 1994; Whipple and Tucker, 1999;

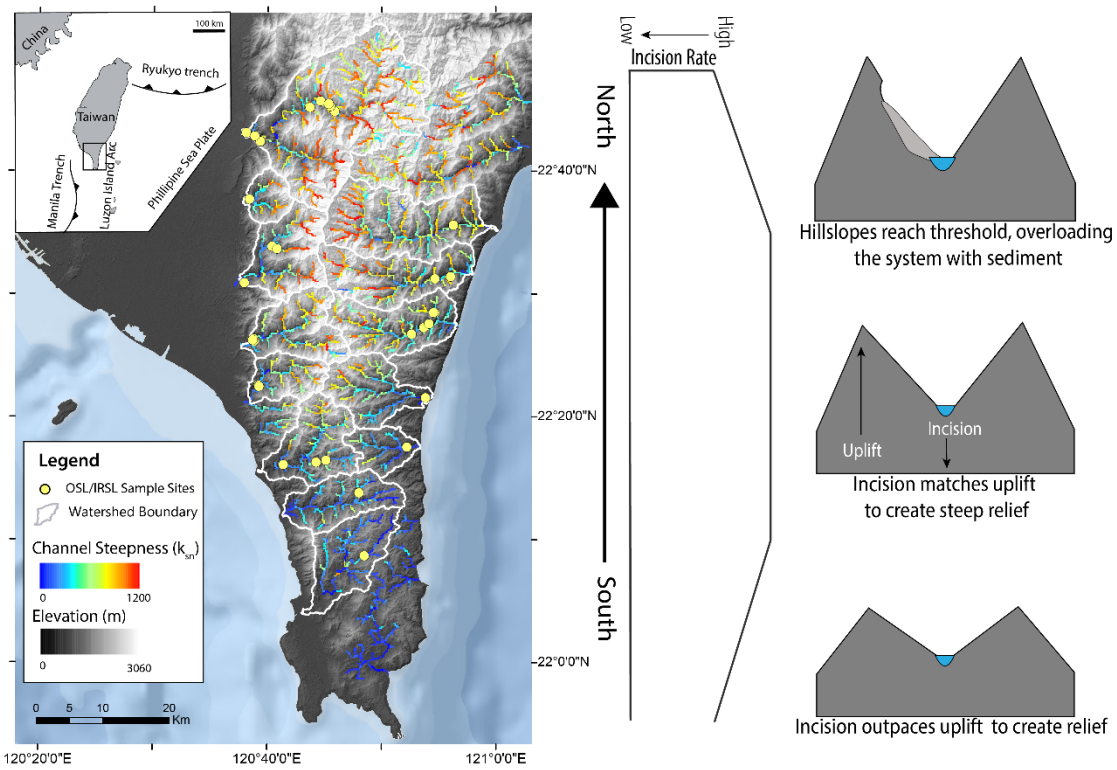

Figure 2.2 Conceptual model of drainage evolution in southern Taiwan.

Montgomery and Brandon, 2002; Tsou et al., 2014). At this point, hillslope processes mirror incision rates making it difficult to differentiate the response of hillslope and rivers to tectonic uplift. Studying incision rates in the young, actively developing landscape of Taiwan will allow us a rare opportunity to investigate drainage response to base-level fall across a transect of landscape development stages.

Bedrock incision is traditionally thought of as detachment limited where incision rates are controlled by the ability to entrain and erode bedrock (Seidl and Dietrich, 1992; Howard, 1994; Whipple and Tucker, 1999; Wobus et al., 2006; Royden and Perron, 2013). However, the sediment transport of a river system has also been shown to control

river dynamics (Duvall, 2004; Cowie et al., 2008; Yanites and Tucker, 2010). In systems with high sediment loads, sediment may armor bedrock channel, limiting the erosion potential causing rivers to steepen in order to evacuate sediment. In transport-limited systems, climate may obscure tectonic signals as increased precipitation will increase hillslope erosion rates and the system will respond by steepening in response to factor unrelated to uplift. Investigating the controls of river dynamics across different environments advances the understanding of landscape response to tectonics and climate.

Constraining rates of river incision can help us understand the role of tectonics, climate, and sediment supply on landscape development. This study investigates river incision rates in southern Taiwan by dating abandoned river terraces. Terraces record periods of unsteadiness in a river system as the river must remain at one elevation long enough for either aggradation or lateral widening to occur followed by a pulse of incision. Dating the sediment from terraces provides a time constraint on river elevation over time and is used to provide rates of river incision (e.g. Hsieh and Knupfer, 2002; Dadson et al., 2003; Pederson et al., 2006; Pazzaglia, 2013; Gallen et al., 2015; Yanites et al., 2018). Changes in climate can play a role in the timing of river aggradation and terrace formation (Peizhen et al., 2001; Hancock and Anderson, 2002; Hartshorn, 2002). A discussion of the role of past climate on terrace deposition in southern Taiwan can be found in Chapter 3.

2.3.3. MEASURING RATES OF EROSION

Mass balance equations use rates of erosion and uplift to predict changes in elevation. Uplift rates discussed in this paper are measured using apatite fission-track dating.

Apatite-fission track dating describes rates of uplift on million-year timescales and is noted in km/Myr. Erosion rates are discussed in this paper more specifically as rates of denudation and river incision. Denudation rates describe how quickly a parcel of sediment becomes exposed at the Earth's surface by erosive processes. This process can be measured using the concentration of cosmogenic radionuclides (CRN), as the concentration of CRN in a parcel of sediment is a function of how quickly it is brought to the surface by erosion. When sediment reaches the surface, it is transported into the fluvial system where it mixes with sediment from other contributing hillslopes representing the basin-wide denudation rate (Yanites et al., 2009). Measuring the concentration of CRN found in alluvial sediment can produce a catchment-averaged rate of denudation. Rates determined by CRN dating discussed in this study are averaged over centennial and millennial timescales and are best described in terms of m/kyr.

River incision is defined by the narrow erosion caused by rivers resulting in the elevation loss of a river channel. In this paper, river incision is calculated by dating terrace sediment and dividing terrace height by the age of terrace deposition. As the terraces sampled in this study range from Holocene to Pleistocene in age, the most appropriate way to describe these incision rates is by m/kyr. Observation and instrumental methods of calculating uplift, denudation, and incision integrate over only decal and centennial scales and are best noted in mm/yr.

Dimensional analysis shows that 1 mm/yr is equal to 1 m/kyr and 1 km/Myr. However, it can be problematic to view these units as equivalent and compare rates over vastly different timescales. It has been shown that rates averaged over shorter periods of time reveal much faster rates (Sadler, 1981; Finnegan et al., 2014; Sadler and Jerlomack,

2014; Donovan and Belmont, 2019). Instantaneous uplift rates in Taiwan can be as high as 20 mm/yr while uplift rates averaged over millions of years range from 1.5 – 6 km/Myr, resulting in an order of magnitude difference. The mechanisms driving rates of erosion and uplift can be very different on decal, centennial, millennial, and million-year timescales. Studies have shown that on decadal and centennial timescales, storm events and earthquakes play a dominant roles on controlling denudation rates in Taiwan (Dadson et al., 2003; Yanites et al., 2018), while other studies show tectonics are a primary driver of (Howard, 1994; Whipple and Tucker, 1999; Whipple, 2004). This study investigates the role of stochastic climate events and sediment supply versus underlying tectonics on landscape response to uplift in southern Taiwan.

2.3.4. PREVIOUS WORK

Previous studies quantifying river incision have found Holocene rates ranging from 4-20 m/kyr in the Western Foothills of Taiwan (Hsieh and Knupfer, 2002; Dadson et al., 2003; Schaller et al., 2005; Yanites et al., 2009). Dadson et al. (2003) used ^{14}C dating of organics in strath terraces to reveal incision rates ranging from 1.3->16 m/kyr in the western and eastern foothills of the Central Range. Studies using ^{14}C dating of organic material found in strath terraces along five rivers in south-central Taiwan show incision rates ranging from 2 – >20 m/kyr (Hsieh and Knupfer, 2002; Yanites et al., 2010). These incision rates appear to increase on the hanging wall of the thrust faults that form the Central Range (Yanites et al., 2010).

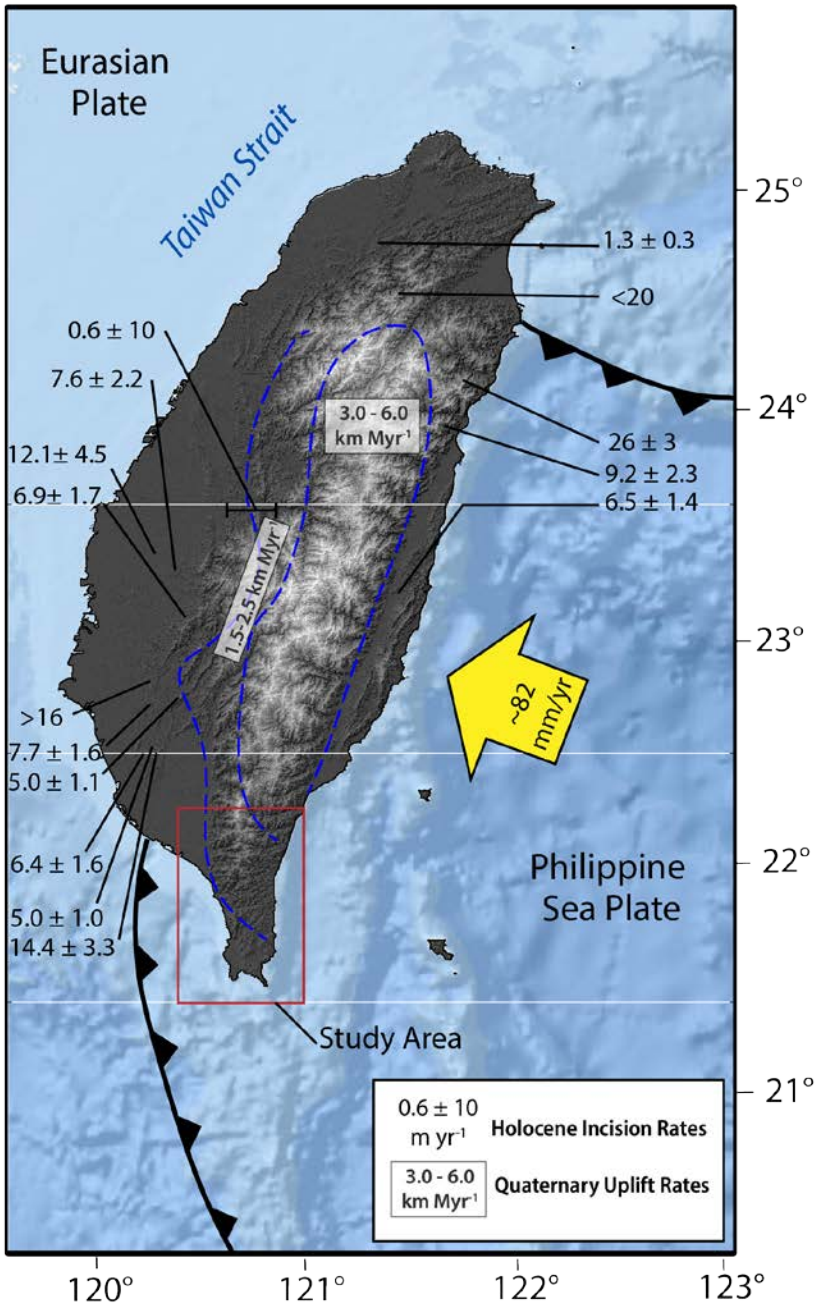

Figure 2.3 Map of incision rates from previous studies (Hsieh and Knupfer, 2002; Dadson et al., 2003; Schaller et al., 2005; Yanites et al., 2009). Uplift rates are from Dadson et al. (2003). Study area is outlined in red.

Numerous studies have been conducted to understand hillslope erosion in southern Taiwan using CRN dating (Derrieux et al., 2014; Fellin et al., 2017; Chen et al., 2020). A study conducted in the same area as this research showed CNR derived catchment average denudation rates ranging from 0.1 – 4 m/kyr with denudation rates increasing northward (Chen et al., 2020). This same pattern can be seen across a larger area with CRN-derived denudation rates increasing from 1 m/kyr in southern Taiwan to >4m/kyr in northern Taiwan as relief increases with maturity of the orogen (Fellin et al., 2017). Results for zircon and apatite fission-track dating found that exhumation rates increased one million years ago from 1 km/Myr to 4-10 km/Myr in the Southern Central Range of Taiwan supporting the hypothesis of southward propagating uplift (Willett et al., 2003; Lee et al., 2006, see Figure 2.3).

2.4. METHODS

In order to study temporal and spatial patterns of river incision, terrace samples were collected from thirteen drainages from both the eastern and western flank of the Central Range along a 100 km N-S transect (Figure 2.3). This was done in order to capture the variation in incision rates along the steep topographic gradient present in southern Taiwan. Research goals were to collect samples from at least three different terrace heights in each drainage when possible to understand spatial and temporal variations in incision rates (Figure 2.4). Age control to calculate incision rates was obtained using luminescence dating of terrace deposits.

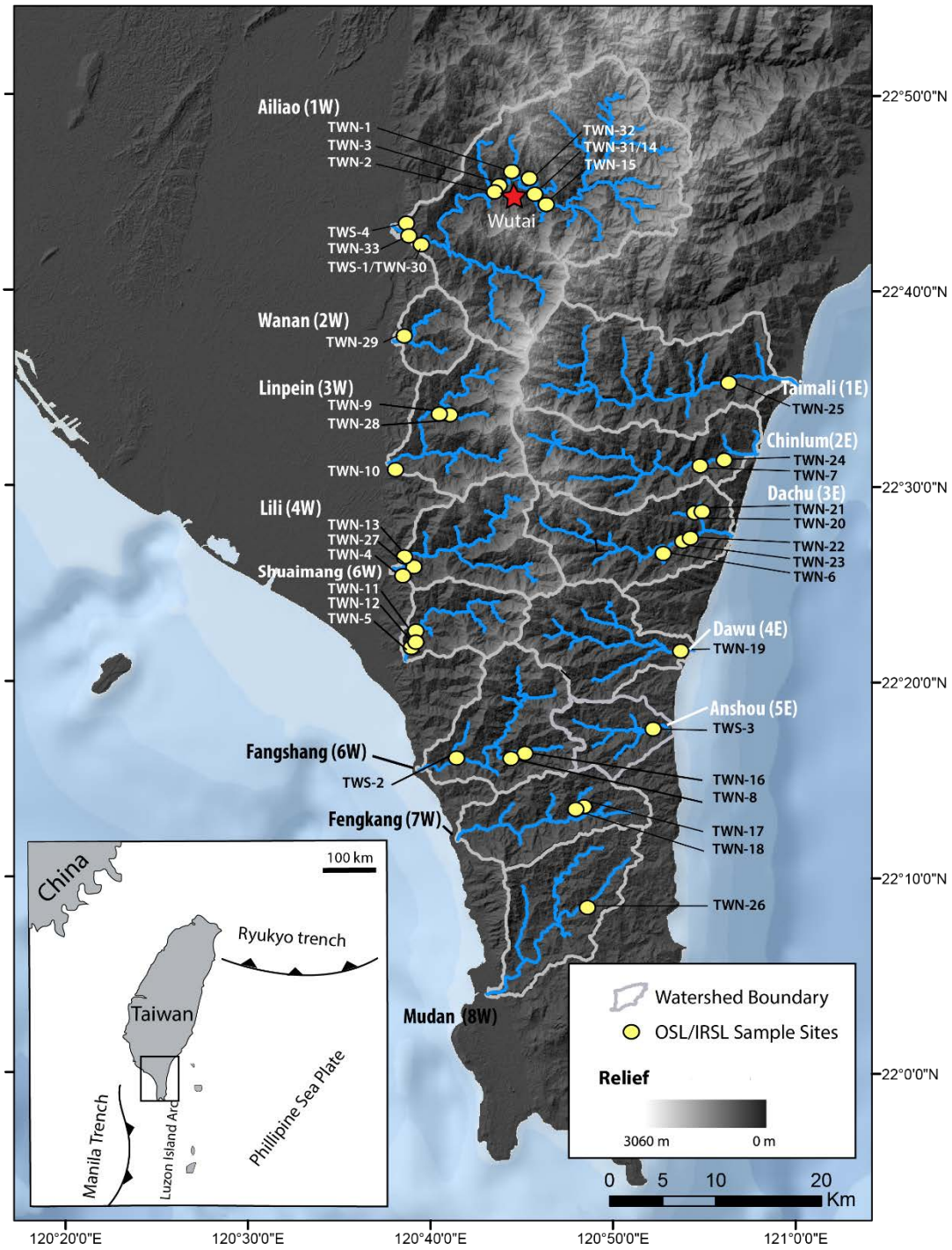

Figure 2.4 Map of sample sites. Thirty-seven samples were taken from thirteen drainages in Southern Taiwan. Yellow markers denote sample locations. Watersheds are outlined in grey.

2.4.1. LUMINESCENCE GEOCHRONOLOGY

Luminescence techniques have become a widely applied method of dating late-Quaternary sediment deposits (Rhodes, 2011). Optically stimulated luminescence (OSL) dating of quartz (Huntley et al., 1985), and infrared stimulated luminescence (IRSL) dating of potassium feldspar (Hütt et al., 1988) provide an age estimate for the last time that sediment was exposed to light, which resets the luminescence signal. Following deposition and removal from sunlight, the minerals re-acquire a luminescence signal due to exposure to ionizing radiation from K, Rb, Th, and U in the surrounding sediments, plus a small contribution from incident cosmic radiation. Free electrons produced from exposure to this ionizing radiation can be stored in defects (traps) in the crystal lattice over time. The amount of radiation the sediment was exposed to following deposition is known as the environmental dose rate (D_R). When sediment is then exposed to light or heat, there is sufficient energy to evict electrons from these traps and photon of light is emitted when the electron recombines at a lower energy state, producing luminescence. In a laboratory setting, the equivalent dose (D_E) of radiation required to replicate the natural luminescence signal is calculated. OSL/IRSL ages are determined by dividing the equivalent dose (D_E) by the environmental dose rate (D_R).

Quartz that has undergone multiple sedimentary cycles of transport and deposition generally have the best luminescence sensitivity. As quartz undergoes multiple cycles of dose accumulation and bleaching, the luminescence sensitivity (light intensity per unit mass per unit radiation) increases until a plateau is reached. Applying OSL dating in tectonically active landscapes such as Taiwan has proven problematic due to low luminescence sensitivity because of a short landscape history (Dörschner et al., 2012;

Tseng et al., 2016). Feldspar does not require multiple cycles of bleaching and transport to produce a high intensity luminescence signal which can make IRSL dating of feldspar more suitable in tectonically active landscapes (Godfrey-Smith et al., 1988; Preusser et al., 2006). However, OSL dating is often preferred over IRSL dating due to a faster time required to zero the luminescence signal during transport than feldspar. Additionally, anomalous fading of feldspar luminescence signals caused by electron leakage can lead to age underestimations (Godfrey-Smith et al., 1988; Wallinga, 2002; Lawson et al., 2012). The longer time required to bleach (reset) the luminescence signal in feldspar can be problematic for IRSL dating in landscapes like Taiwan that experience frequent flood events. Sediments are transported and deposited quickly in high sediment load and turbid flood events and may not be exposed to sunlight long enough for the luminescence signal to be completely reset leading partial bleaching and age over-estimation.

Thirty-seven samples were collected from terraces within 13 drainages in the southern 100 km of Taiwan. Terrace deposits were selected where fluvial bedding structures were present and there was little evidence of bioturbation. Samples were collected by pounding a metal pipe into sand lenses or collecting sediment from sandy matrixes while under a lightproof tarp for cases where sediment lenses were not present. Both methods included the collection of the surrounding sediment to measure the environmental dose rate and water content following the protocol laid out by Nelson et al. (2015).

Sample processing and analysis was completed at the Utah State University Luminescence Laboratory using the single-aliquot regenerative-dose (SAR) method for OSL dating of quartz (Murray and Wintle, 2000) and IRSL dating of potassium feldspar

(Wallinga et al., 2000). Samples collected from terraces <50 m in height were dated using OSL while samples collected from higher terraces were dated using IRSL. The choice of mineral analyzed was because the dose-response curve of feldspar can grow to much higher doses than those of quartz extending the dating range of feldspar by a factor of 4-5 compared to OSL dating of quartz (Buylaert et al., 2012). IRSL measurements were carried out at 50C and were corrected for anomalous fading, loss of signal with time (Huntley and Lamothe, 2001; Auclair et al., 2003). Dose rates were calculated using inductively coupled plasma mass spectrometry (ICP-MS) and inductively coupled plasma atomic emission spectra (ICP-AES) to determine the elemental concentration of radiogenic elements (U, Th, K, Rb) surrounding the sample site and convert to dose rate following the conversion factors of Guérin et al. (2011). The cosmic contribution to dose rate was determined following Prescott and Hutton (1994). The dose rate was then corrected for attenuation from water content and grain-size (Aitken, 1998; Brennan, 2003). Depositional ages were then calculated by dividing the equivalent dose by the dose rate.

2.4.2. INCISION RATE CALCULATIONS

Terraces and basal bedrock straths serve as a marker of past river position and can be used to calculate river incision over time, helping to understand river response to uplift (Hsieh and Knupfer, 2002; Dadson et al., 2003; Pederson et al., 2006; Yanites et al., 2010; Pazzaglia, 2013; Gallen et al., 2015). In order to calculate incision rates, I measured the height of the terrace surface above the river, depth of the sample within the fill, and, when possible, the height of the bedrock strath above the river at each site. Incision rate was calculated using the following formula,

$$Incision\ Rate\ = \frac{T}{A} \qquad \text{Eq. 2.1}$$

where *T* is the measured incision depth from the top of the terrace surface to the bottom of the modern river channel and *A* is the age of the terrace deposit, derived from luminescence dating. Error associated with the incision rate comes from the luminescence age and uncertainty in terrace-height measurement relative to the channel. The alluvial mantel of the channel is not preferred as a reference point for incision depth as it shifts over short time intervals (Gallen et al., 2015). Ideally, bedrock incision depth would be measured from top of basal bedrock strath under a terrace landform to the level of bedrock underlying the modern channel. However, we were not able to collect the basal bedrock strath height at most sites due to dense vegetation and anthropogenic reinforcement of hillslopes. Bedrock depth below the modern river was not visible in many of the modern channels due to Typhoon Morakot (2009), which caused widespread aggradation in southern Taiwan. Prior to Typhoon Morakot, it is believed that the rivers in our research area were incising into bedrock. Uncertainty of terrace height relative to the pre-Morakot channel elevation and the thickness of Morakot-triggered aggradation were both considered when calculating uncertainty in the incision rate. Error associated with luminescence ages and terrace height is propagated using the Eq. 2.1.

$$Incision\ Rate\ Error = \sqrt{\left(\frac{1\sigma_A}{A}\right)^2 + \left(\frac{\widehat{e_M}}{T + \widehat{M}}\right)^2 + \left(\frac{\widehat{e_M}}{\widehat{M}}\right)^2} \qquad \text{Eq. 2.2}$$

where σ_A is the 1σ error associated with luminescence ages and $\widehat{M}$ is projected Morakat aggradation. $\widehat{M}$ is produced from a linear fit of estimated Morakot-caused aggradation

and distance from the southern tip of the island (DeLisle 2020, unpublished data). Residual error from this linear fit (e_M) displays heteroscedastic behavior with residual error increasing with distance from the southern tip of the island (D) (Figure 2.5). Incision rate error must account for heteroscedasticity therefore, I produced a linear model of e_M and D producing a projected error of aggradation, $\widehat{e_M}$.

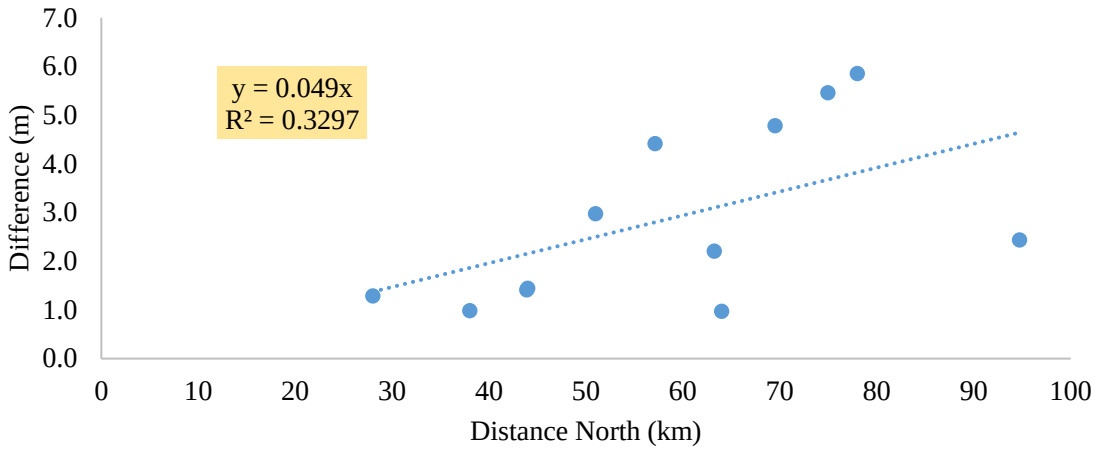

Figure 2.5 Projected error of aggradation

2.5. RESULTS

Thirty-four terraces from thirteen drainages were described, surveyed, and sampled for luminescence dating (Table 2.1). Samples were collected from eight drainages on the western flank of the Central Range and five drainages on the Eastern side (Figure 2.4). Drainages are identified by terrace name and drainage code, which represents its position

Table 2.1 Luminescence Results

Drainage	Sample ID	USU ID	Longitude (DD)	Latitude (DD)	Depth (m)	Method	Aliquots	Dose Rate (Gy/ky)	Equivalent dose (Gy)	Age ± 2σ (ka)
Western Drainages										
Ailiao (1W)										
	TWN-30	USU-3343	120.65556	22.70747	3.5	OSL	15(27)	3.48 ± 0.29	13.27 ± 3.38	3.8 ± 1.1
	TWN-1	USU-2825	120.74395	22.76206	17	OSL	15(30)	3.61 ± 0.31	16.86 ± 4.07	4.7 ± 1.2
	TWN-15	USU-2991	120.76467	22.74799	9.2	OSL	8(43)	3.19 ± 0.27	22.67 ± 2.44	7.1 ± 1.1
	TWN-32	USU-3345	120.75588	22.75811	5.5	IRSL	6(10)	4.84 ± 0.56	180.59 ± 48.88	50 ± 11
	TWN-33	USU-3346	120.6476	2271433	3	IRSL	4(10)	4.37 ± 0.43	145.84 ± 62.93	39 ± 18
	TWN-31	USU-3344	120.75836	22.75497	3.6	IRSL	9(12)	5.05 ± 0.62	206.72 ± 80.22	48 ± 20
	TWS-4	USU-2075	120.63539	22.719116		IRSL	11(19)	4.88 ± 0.81	515.58 ± 49.53	146 ± 32
	TWN-3	USU-2827	120.72827	22.75317	6.46	IRSL	12(22)	5.04 ± 0.54	334.06 ± 92.24	95 ± 29
	TWN-2	USU-2826	120.72693	22.75398	22.12	IRSL	15(19)	5.03 ± 0.56	304.02 ± 61.6	88 ± 21
Wanan (2W)										
	TWN-29	USU-3342	120.64016	22.62862	4.25	OSL	17(24)	3.58 ± 0.32	138.28 ± 21.22	39 ± 7.4
Linpien (3W)										
	TWN-9	USU-2985	120.67303	22.5648	5.3	OSL	19(30)	3.87 ± 0.33	18.83 ± 4.42	4.9 ± 1.3
	TWN-28	USU-3341	120.68063	22.56145	33	IRSL	11(12)	5.01 ± 0.52	101.44 ± 22.77	28 ± 7.2
	TWN-10	USU-2986	120.63266	22.5152	8	OSL	8(17)	3.47 ± 0.28	42.75 ± 14.04	12 ± 4.3
Lili (4W)										
	TWN-4	USU-2828	120.64659	22.43928	2	OSL	15(27)	3.44 ± 0.32	5.60 ± 3.07	1.6 ± 0.9
	TWN-13	USU-2989	120.64677	22.43598	10	OSL	10(16)	3.81 ± 0.38	96.30 ± 11.14	25 ± 4.2
	TWN-27	USU-3340	120.64533	22.43781	5.5	OSL	6(16)	3.48 ± 0.31	120.73 ± 54.66	35 ± 16
Shuaimang (5W)										
	TWN-11	USU-2987	120.65398	22.37425	3.5	OSL	14(17)	3.78 ± 0.37	42.36 ± 12.69	11 ± 3.6
	TWN-5	USU-2829	120.65369	22.37598	5.3	OSL	25(43)	3.68 ± 0.34	42.45 ± 11.82	12 ± 3.5
	TWN-12	USU-2988	120.6544	22.237457	1	OSL	13(16)	3.91 ± 0.36	29.36 ± 7.07	7.5 ± 2.1
Fengshang (6W)										
	TWN-8	USU-2832	120.73795	22.2719	3	OSL	6(35+6)	3.77 ± 0.35	14.55 ± 4.64	3.9 ± 1.3

Drainage	Sample ID	USU ID	Longitude (DD)	Latitude (DD)	Depth (m)	Method	Aliquots	Dose Rate (Gy/ky)	Equivalent dose (Gy)	Age ± 2σ (ka)
	TWN-16	USU-2992	120.75252	22.27466	12	OSL	12(34)	3.79 ± 0.37	45.58 ± 17.72	12 ± 4.9
	TWS-2	USU-2073	120.69016	22.26863	2	OSL	23(35+27)	3.66 ± 0.36	3.31 ± 1.61	0.90 ± 0.45
Fengkang (7W)										
	TWN-17	USU-2993	120.8005	22.23098	2	OSL	10(41)	3.88 ± 0.4	18.51 ± 5.53	4.8 ± 1.5
	TWN-18	USU-2994	120.80077	22.23055	2	OSL	17(41)	3.84 ± 0.37	45.83 ± 15.56	12 ± 4.3
Mudan (8W)										
	TWN-26	USU-3002	120.80852	22.14512	1	OSL	18(25)	3.94 ± 0.39	4.97 ± 2.16	1.3 ± 0.6
Eastern Drainages										
Taimali (1E)										
	TWN-25	USU-3001	120.93812	22.59372	15	OSL	12(21)	3.18 ± 0.26	26.26 ± 6.6	8.3 ± 2.3
Chinlum (2E)										
	TWN-24	USU-3000	120.91144	22.52086	15	OSL	8(16)	3.57 ± 0.32	148.99 ± 52.12	42 ± 15
	TWN-7	USU-2831	120.93414	22.52385	25	IRSL	17(18)	5.11 ± 0.61	227.09 ± 37.57	58 ± 13
Dachu (3E)										
	TWN-22	USU-2998	120.90285	22.45969	3.7	OSL	16(18)	3.57 ± 0.30	64.26 ± 9.83	18 ± 3.4
	TWN-21	USU-2997	120.90941	22.47522	22.3	OSL	17(28)	3.21 ± 0.27	58.20 ± 10.16	18 ± 3.8
	TWN-23	USU-2999	120.87726	22.44588	1.4	OSL	12(15)	3.83 ± 0.15	44.05 ± 11.5	12 ± 3.2
	TWN-6	USU-2830	120.89513	22.45448	4	OSL	19(57)	3.45 ± 0.28	27.79 ± 8.39	8.1 ± 2.6
	TWN-20	USU-2996	120.91112	22.47485	8.4	OSL	10(15)	3.60 ± 0.30	36.95 ± 7.36	10 ± 2.3
Dawu (4E)										
	TWN-19	USU-2995	120.89748	22.35939	4.5	OSL	8(43)	3.48 ± 0.38	61.51 ± 9.07	18 ± 3.5
Anshuo (5E)										
	TWS-3	USU-2074	120.870417	22.2924	5	OSL	11(18)	3.79 ± 0.36	44.02 ± 11.92	12 ± 3.4

on the east (E) or west (W) side of the Central Range and position northward. The number preceding E or W is an indicator of their N-S position with the lowest numbers representing the drainages further to the north (Figure 2.6). For example, W1 represents the farthest north drainage on the west side, while E5 represents the farthest south drainage on the east side.

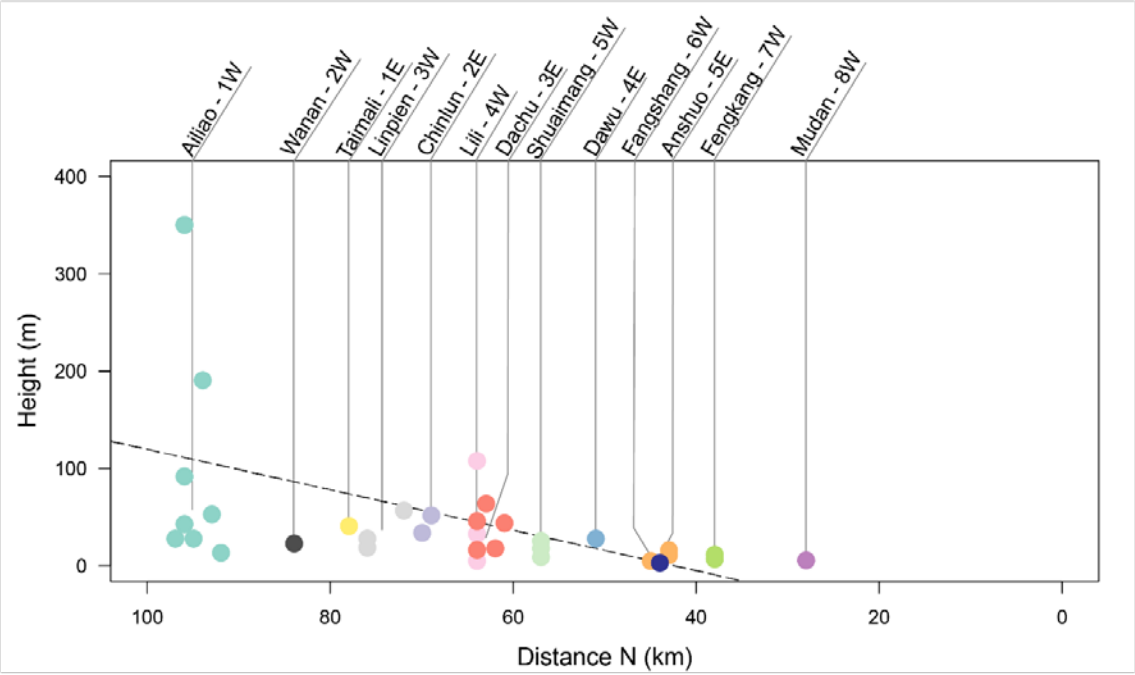

Figure 2.6 Terrace height (m) versus distance from the southern tip of Taiwan (km). Drainages from which samples were sampled is note by color and text.

Samples were collected based on access and selection criteria. Not all terraces had visible bedrock straths. In fact, most of the terraces with observed underlying bedrock were not strath terraces. Instead, many of the terraces had think alluvial fill packages that formed due to large aggradation events, as opposed to lateral planation and valley widening that would form a traditional strath terrace. Sediments in these fluvial deposits ranged from well to moderately stratified, but commonly lacked bedding structures such

as ripple or cross beds. The gravels were matrix and clast-supported and sediment size ranged from poorly sorted sands with lithic grains sands to sub-rounded pebbles and cobbles. Evidence for sediment weathering and soil development was dependent on terrace age, but older terraces typically had orangish-red lateritic soils and weathered profiles. The sediment lithology at most sites was predominately low-grade metamorphic shale and slate with occasional sandstone and resistant vein-quartz clasts.

2.5.1. WESTERN DRAINAGES

2.5.1.1. *Ailiao – 1W*

The Ailiao River basin is the farthest north in the study area and has the largest drainage area (414 km^2) and steepest hillslopes (Figure 2.2). Eleven samples were collected from eight terraces along the Ailiao River (Figure 2.7). Samples were taken from two main regions in the drainage: upstream near the village of Wutai and downstream where the Ailiao exits the mountain front. Seven samples (TWN-1, TWN-2, TWN-3, TWN-14, TWN-15, TWN-31, and TWN-32) were collected from the upstream area. TWN-3 and TWN-2 were both collected from a large alluvial fill package in a 350 m terrace. Contact with a bedrock strath was not visible, but the presence of alluvium along the roadway suggests the strath was at most 328 m above the channel. TWN-3 was collected closer to the top of the alluvial fill package than TWN-2 to measure how long it took for the package to be deposited. Preliminary IRSL results suggest ages of 88 ± 21 ka and 95 ± 29 ka, respectively (Table 2.1). Samples TWN-31 and TWN-14 were collected from the same 91-m terrace with a bedrock strath 87 m above the modern channel. Preliminary OSL results from TWN-14 yield an anomalously young age of 13 ka, so

TWN-31 was collected from the same terrace during the 2020 field season. IRSL dating of TWN-31 revealed a preliminary depositional age of 48 ± 20 ka (Table 2.1). TWN-32 was collected from a 42 m terrace. Contact with the bedrock strath was not visible due to roadwork, but observations of the alluvial fill thickness suggests that the basal strath was at most 36.5 m above the modern channel. Preliminary OSL dating of TWN-32 yields an age of 49 ± 11 ka (Table 2.1). TWN-1 was collected from a 27 m terrace with a maximum bedrock strath height of 10-m above the modern channel. Preliminary OSL

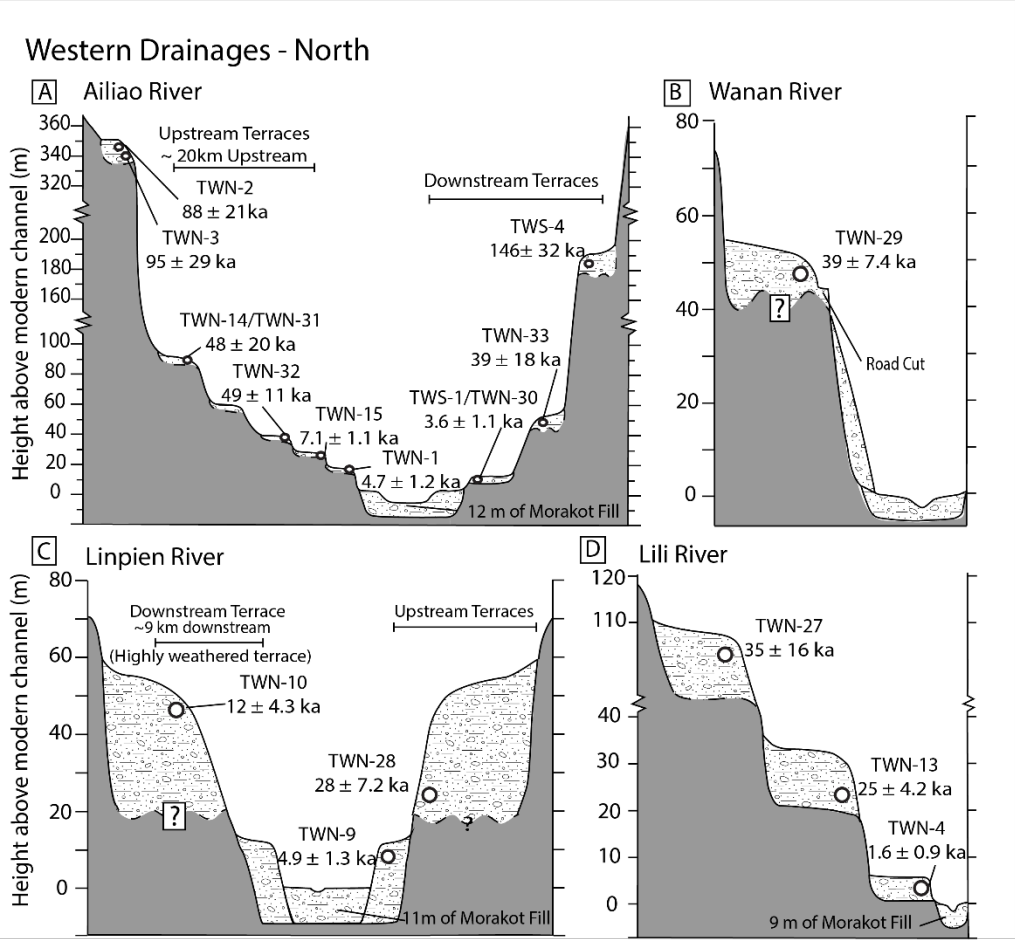

Figure 2.7 Drainage schematics of the four northern drainages on the western side of the Central Range.

results suggest an age of 4.7 ± 1.2 ka (Table 2.1). TWN-15 (7.1 ± 1.1 ka, Table 2.1) was collected upstream of TWN-1 from another 27-m terrace with a 13-m bedrock strath.

TWS-1, TWS-4, TWN-30 and TWN-33 were collected downstream near the mountain front. TWS-4 was taken from the 190-m terrace and yielded a preliminary IRSL age of 146 ± 32 ka (Table 2.1). While distance to bedrock from the terrace fill surface was not visible where the sample was collected, cutbank exposures along the river channel suggest that this surface is underlain by 80m of fill over a 110-m bedrock strath. TWN-33 (39 ± 18 ka, Table 2.1) was collected from a 52-m terrace at the mouth of the Ailiao drainage. Distance to bedrock was not visible due to anthropogenic reinforcement of the hillslope, but observations of alluvial fill near the sample site suggest the strath was at most 4 m above the modern river. TWN-30 and TWS-1 were collected from the same 12 m terrace with a 6-m bedrock strath. TWS-1 was collected in 2015, may not have been collected using best practice, so the terrace was resampled (TWN-30) during the 2020 field season. OSL dating TWN-30 reveals a preliminary age of 3.6 ± 1.1 ka (Table 2.1). This terrace is inset into a 27 m terrace, which was not able to be sampled. Across the channel and to the north of TWN-30/TWS-1 were terrace surfaces 190 m terrace above the modern channel and a 30 m terrace, likely correlative with terrace from which TWN-30 and TWS-1 were sampled.

2.5.1.2. ***Wanan – 2W***

The Wanan drainage, just south of the Ailiao River, is the smallest drainage (42 km^2) in this study area. TWN-29 was taken from a 22 m terrace with a maximum bedrock strath height of 17.5-m (Figure 2.7). OSL dating of this sample yields an age of 39 ± 7.4 ka (Table 2.1).

2.5.1.3. *Linpien – 3W*

Three samples were collected from the Linpien Drainage (125 km^2). Samples were taken from three terraces: two terraces 55-m above the modern channel and one 12-m terrace (Figure 2.7). TWN-10 (12 ± 4.3 ka, Table 2.1) was taken from a highly weathered 55-m terrace near the mountain front. No bedrock strath was observed due to roadwork, but observations of alluvial fill suggest the maximum strath height is 48-m. TWN-28 was sampled from another 55-m terrace with a maximum strath height of 33-m ~10 km upstream of TWN-10. Preliminary OSL dating of TWN-28 reveals an age of 28 ± 7.2 ka (Table 2.1). The alluvial deposits from which TWN-28 was taken appeared younger and showed less signs of weathering than the sediment from which TWN-10 was sampled. TWN-9 was taken from a 12 m terrace that was continuous along both sides of the modern channel. Bedrock was not exposed along the channel, suggesting that the bedrock strath is below the modern channel. Preliminary OSL results from TWN-9 suggests an age 4.9 ± 1.3 ka (Table 2.1). The fill package was likely deposited during a large flood event.

2.5.1.4. *Lili – 4W*

Three samples were collected from the Lili Drainage (116 km^2) from 107, 32, and 4 m terraces that were closely grouped at the mouth of the drainage (Figure 2.7). TWN-4 (1.6 ± 1.0 ka, Table 2.1) was collected from a 3 m terrace with crossbedding structures. Bedrock was not observed along the channel, suggesting that the bedrock strath is below the alluvium of the modern channel. TWN-13 was sampled from a 32 m terrace underlain by 12 m of highly weathered alluvium over a 20 m basal strath. Preliminary results yield an age of 25 ± 4.2 ka (Table 2.1). TWN-27 was collected from a 107-m terrace on a ridge

straddling the Lili and Chichia River and produced a preliminary OSL age of 35 ± 16 ka (Table 2.1). Contact with bedrock was not visible, but alluvial deposits suggest a maximum strath height of 100 m.

2.5.1.5. ***Shuaimang – 5W***

Three samples were collected from 25, 17, 10 m terraces in the Shuaimang drainage (68 km^2, Figure 2.8). The terraces were closely grouped at the mouth of the drainage. TWN-12 was taken from a 25 m terrace with a maximum strath height of 21.5 m. IRSL dating of TWN-12 yielded a preliminary age of 7.5 ± 2.0 ka (Table 2.1). TWN-11 (11 ±

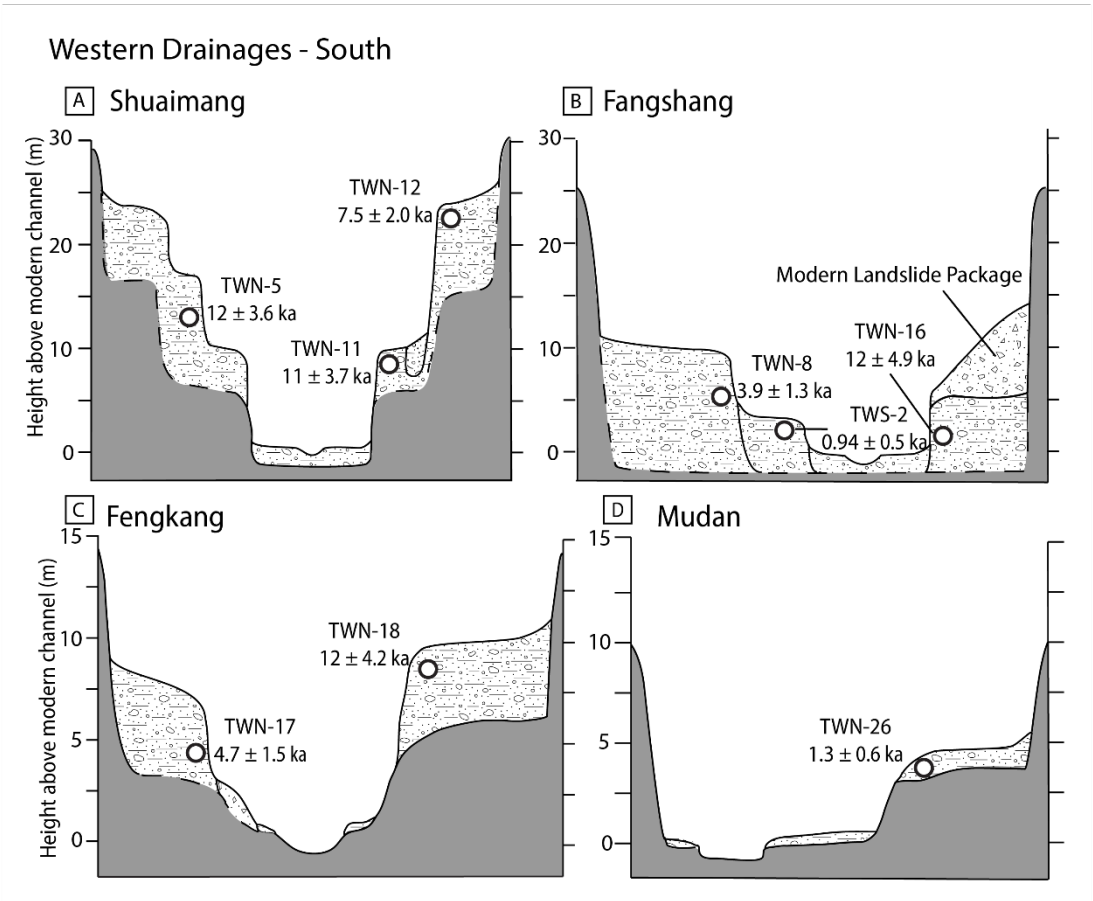

Figure 2.8 Drainage schematics of the four southern drainages on the western side of the Central Range.

3.7 ka, Table 2.1) was sampled from a 10-m terrace with intertounging colluvial deposits and an uneven bedrock strath. TWN-5 was sampled from a 17-m terrace adjacent from TWN-12 and TWN-11. The bedrock strath was not visible, but alluvial deposits suggest a maximum strath height of 12 m. OSL dating of TWN-5 yields a preliminary age of 12 ± 3.5 ka (Table 2.1)

2.5.1.6. *Fangshang – 6W*

We collected three samples from 10, ~6, and 4 m terraces in the Fangshang drainage (102 km^2, Figure 2.8). Alluvial sediment was visible from the top of all terrace surfaces to the modern channel. TWN-8 (3.8 ± 1.3 ka, Table 2.1) was sampled from a 10-m terrace near the terrace from which TWN-16 (12 ± 4.9 ka, Table 2.1) was taken. TWN-16 was taken from a terrace estimate to be ~6-m above the modern channel overlain by a large landslide package (see Figure 2.7). TWS-2 was collected further downstream from a 4-m terrace. Preliminary dating of TWS-2 suggests a depositional age of 0.9 ± 0.5 ka (Table 2.1). Large fill packages were observed along both sides of the channel from the mountain front the to headwaters, but samples from these terraces range from ~12-1 ka suggesting that the river has not incised into bedrock during the Holocene.

2.5.1.7. *Fengkang – 7W*

Two samples were collected in the Fengkang drainage (102 km^2) from 10.5 and 6 m terraces (Figure 2.8). TWN-18 was taken from a 10.5 m terrace with a bedrock strath height of 5 m. Preliminary OSL dating of this sample yields an age of 12 ± 4.3 ka (Table 2.1). TWN-17 (3.7 ± 1.6 ka, Table 2.1) was taken from a 6 m directly across the river from TWN-18. Modern colluvium obstructed the bedrock strath contact, but observations near the sample site suggest the bedrock strath was at most 3 m above the modern

channel. Bedrock was exposed in the modern channel, suggesting the river is actively incising into bedrock where TWN-17 and TWN-18 were sampled.

2.5.1.8. ***Mudan – 8W***

The Mudan drainage (124 km^2) is the most southern drainage with the lowest hillslope and channel steepness (Figure 2.2). One sample, TWN-26, was taken in this drainage from a 5 m terrace with a 3.7 m bedrock strath (Figure 2.8). Preliminary luminescence dating of TWN-26 reveals a depositional age of 1.3 ± 0.6 ka (Table 2.1). Bedrock was visible in the modern channel below TWN-26.

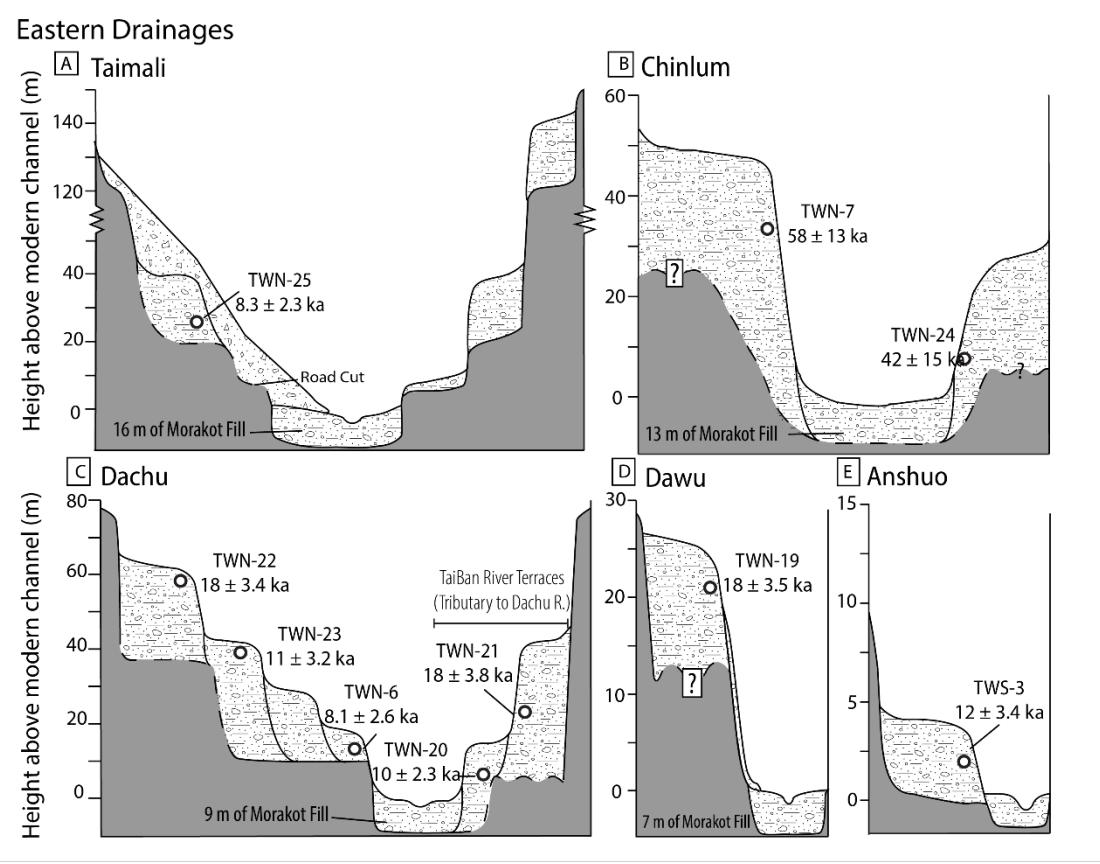

Figure 2.9 Drainage schematics of the five eastern drainages on the eastern side of the Central Range.

2.5.2. EASTERN DRAINAGES

2.5.2.1. *Taimali – 1E*

The Taimali drainage (212 km^2) is the most northern of the study drainages on the eastern flank of the central range. One sample, TWN-25, was collected from a 40 m terrace (Figure 2.9). Depth to bedrock was not visible underneath the terrace, but a paired terrace on the adjacent riverbank had a 20 m bedrock strath. Preliminary dating of this sample yields an age of 9.5 ± 2.6 ka (Table 2.1). This terrace was adjacent from a set of three terraces interpreted to be an abandoned scrolling meander with terraces at the following heights: a 144 m terrace with a 120 m bedrock strath, a 40 m terrace with a 20 m bedrock strath, and a 10 m terrace with a 4 m bedrock strath.

2.5.2.2. *Chinlum – 2E*

Two samples, TWN-24 and TWN-7, were taken from 51 and 33 m terraces (Figure 2.9), respectively, in the Chinlum drainage (150 km^2). Contact with a bedrock strath was not visible underneath TWN-24, but observations of alluvial fill suggest the strath was at most 36 m above the modern channel. Preliminary dating of TWN-24 reveals an age of ~18 ka (Table 2.1). TWN-7 (58 ± 13, Table 2.1) was sampled from a 33 m terrace with no bedrock strath.

2.5.2.3. *Dachu – 3E*

Five total samples were collected from the Dachu drainage (134 km^2). Three samples (TWN-22, TWN-23, and TWN-6) were collected along the main-stem Dachu River and two samples (TWN-20 and TWN-21) were collected along a tributary, the Taimali River (Figure 2.9). TWN-22 (18 ± 3.4 ka) was taken from a 63 m terrace with a maximum

bedrock strath height of 59 m. TWN-21 was taken from a 45 m terrace along the Taimali River with a maximum strath height of 14. Preliminary luminescence dating of TWN-21 yields a depositional age of 18 ± 3.8 ka, similar to that of TWN-22. Sample TWN-23 (12 ± 3.2 ka, Table 2.1) was taken from a 43 m terrace with a bedrock strath height of 9 m. TWN-6 (8.1 ± 2.6 ka, Table 2.1) was taken from a 17 m terrace upstream of TWN-23 that also had a bedrock strath height of 9 m. TWN-20 was taken from a 15 m terrace along the Taimali River. While contact with the bedrock strath was obscured, observations of the surrounding alluvial fill suggest a maximum strath height of 6.5 m. Preliminary dating of this sample yields an age of 14 ± 2.4 ka (Table 2.1)

2.5.2.4. *Dawu – 4E*

One sample, TWN-19, was collected in the Dawu drainage (110 km^2) from a 27-m terrace atop a ridge separating the Dawu River and a small, captured drainage (Figure 2.9) Preliminary OSL dating of this terrace yields an age of 11 ± 4.1 ka (Table 2.1).

2.5.2.5. *Anshuo – 5E*

The Anshuo drainage (55 km^2) is the farthest south of the eastern drainages with low hillslope and channel steepness (Figure 2.2). One sample, TWS-3 was collected from a low, 2-m terrace with no bedrock strath (Figure 2.9). Preliminary luminescence dating reveals an age of 12 ± 3.4 ka.

2.5.3. INCISION RATES

Preliminary incision rates calculated in this study range from 6 – 0.2 m/kyr with a mean incision rate of 2.4 ± 1.2 m/kyr (Table 2.1, Figure 2.11) and show a moderate trend with distance northward (r = 0.31, Figure 2.11). Average preliminary incision rates are

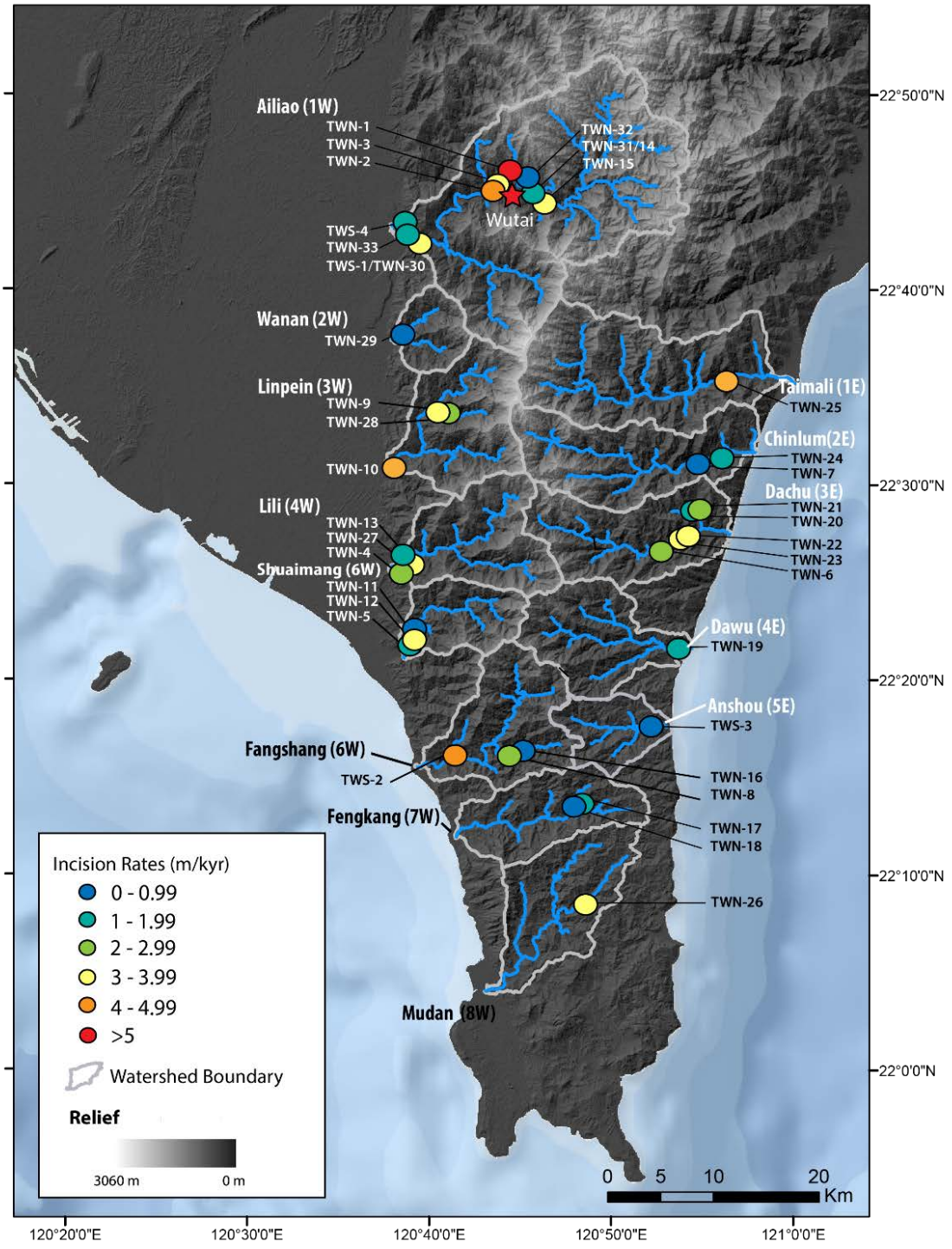

Figure 2.10 Map of incision rates.

1.9 ± 1.0 m/kyr (n=7) in the southern drainages (6W, 7W, 8W, and 5E), 2.3 ± 0.6 m/kyr (n=12) in the central drainages (4W, 5W, 3E and 4E), and 2.7 ± 0.8 m/kyr (n=16) in the northern drainages (1W, 2W, 3W, 1E, and 2E). Incision rates do not vary significantly between the eastern and western drainages with average incision rates of 2.2 ± 1.5 m/kyr and 2.4 ± 1.2 m/kyr, respectively (Figure 2.11). This is a common phenomenon as rates averaged over longer periods of time are generally slower than those averaged over shorter periods of time (Sadler, 1981). Incision rates averaged over the Pleistocene are, on average, 0.5 m/kyr slower than rates averaged over the Holocene.

Table 2.2 Incision rate data

Drainage	Sample ID	USU ID	Distance from S. tip of Island (km)	Terrace Height (m)	Height of Basal Strath	Age (ka)	Incision Rate (m/ka)
Western Drainages							
Ailiao (1W)							
	TWN-30	USU-3343	92	13	6	3.6 ± 1.1	3.5 ± 1.7
	TWN-1	USU-2825	97	27	3.5	4.7 ± 1.2	5.8 ± 2.6
	TWN-15	USU-2991	95	27	13	7.1 ± 1.1	3.8 ± 1.5
	TWN-32	USU-3345	96	42	<37	49 ± 11	0.9 ± 0.4
	TWN-33	USU-3346	93	52	<49	39 ± 18	1.3 ± 0.7
	TWN-31	USU-3344	96	91	88	48 ± 19	1.9 ± 1.0
	TWS-4	USU-2075	94	190	<110	146 ± 32	1.3 ± 0.5
	TWN-3	USU-2827	96	350	<328	95 ± 29	3.7 ± 1.7
	TWN-2	USU-2826	96	350	<328	88 ± 21	4.0 ± 1.6
Wanan (2W)							
	TWN-29	USU-3342	84	22	<18	39 ± 7.4	0.6 ± 0.2
Linpien (3W)							
	TWN-9	USU-2985	77	12	N/A	4.9 ± 1.3	3.6 ± 1.8
	TWN-28	USU-3341	76	55	N/A	28 ± 7.2	2.0 ± 1.0
	TWN-10	USU-2986	72	56	N/A	12 ± 4.3	4.5 ± 2.4
Lili (4W)							
	TWN-4	USU-2828	64	4	N/A	1.6 ± 1.0	2.5 ± 1.9

Drainage	Sample ID	USU ID	Distance from S. tip of Island (km)	Terrace Height (m)	Height of Basal Strath	Age (ka)	Incision Rate (m/ka)
	TWN-13	USU-2989	64	32	21	25 ± 4.3	1.3 ± 0.6
	TWN-27	USU-3340	64	107	<101	35 ± 24	3.1 ± 0.6
Shuaimang (5W)							
	TWN-11	USU-2987	57	10	<4.5	11 ± 3.7	0.7 ± 0.3
	TWN-5	USU-2829	57	17	<10	12 ± 3.5	1.5 ± 0.5
	TWN-12	USU-2988	57	25	21.5	7.6 ± 2.1	3.3 ± 0.5
Fengshang (6W)							
	TWN-8	USU-2832	44	10	N/A	3.9 ± 1.4	2.6 ± 1.0
	TWN-16	USU-2992	43	6	N/A	12 ± 4.9	0.5 ± 0.2
	TWS-2	USU-2073	45	4	N/A	0.9 ± 0.5	4.4 ± 2.7
Fengkang (7W)							
	TWN-17	USU-2993	38	6	<3	4.8 ± 1.5	1.3 ± 0.5
	TWN-18	USU-2994	38	11	5.3	12 ± 4.3	0.9 ± 0.3
Mudan (8W)							
	TWN-26	USU-3002	28	5	3.7	1.3 ± 0.6	3.7 ± 1.7
Eastern Drainages							
Taimali (1E)							
	TWN-25	USU-3001	78	40	<25	8.3 ± 2.3	4.8 ± 2.3
Chinlum (2E)							
	TWN-24	USU-3000	69	51	<36	42 ± 15	1.2 ± 0.7
	TWN-7	USU-2831	70	33	N/A	58 ± 13	0.6 ± 0.3
Dachu (3E)							
	TWN-22	USU-2998	63	63	<59	18 ± 3.4	3.5 ± 1.8
	TWN-21	USU-2997	64	45	<14	18 ± 3.8	2.5 ± 1.2
	TWN-23	USU-2999	61	43	9	12 ± 3.2	3.7 ± 1.1
	TWN-6	USU-2830	62	17	9	8.1 ± 2.6	2.1 ± 1.2
	TWN-20	USU-2996	64	15	<6.5	10 ± 2.3	1.5 ± 0.8
Dawu (4E)							
	TWN-19	USU-2995	51	27	<22.5	18 ± 3.5	1.5 ± 1.0
Anshuo (5E)							
	TWS-3	USU-2074	44	2	N/A	12 ± 3.4	0.2 ± 0.1

2.6. DISCUSSION

To investigate spatial and temporal variations in river incision in response to active tectonics, I calculated incision rates from thirty-four terraces in southern Taiwan. Rapid

uplift in Taiwan is propagating southward resulting in a steep topographic gradient in landscape development within the southern 100 km of the island (see Figure 2.2). Measuring the spatial and temporal variation of incision rates reveals controls on river dynamics in response to active uplift in the beginning stages of mountain building. Research tests the hypothesis that incision rates increase northward with relief as a reflection of the underlying tectonics until a critical hillslope threshold is met. At the critical hillslope threshold, hillslope processes will overwhelm the fluvial system with sediment, thereby disconnecting river incision from underlying tectonics. Failure to observe a northward increasing trend in incision rates would suggest that sediment supply controls patterns of incision rates in southern Taiwan.

2.6.1. SOURCES OF UNCERTAINTY

Incision rates in this study are calculated by dividing terrace height above the modern channel by the age calculated from luminescence ages of sediment deposition. Both of these measurements introduce error into the incision-rate calculation. Luminescence measurements used in this study as age control can be more difficult to apply in quickly eroding landscapes with short tectonic histories, as partial bleaching and low luminescence sensitivity can be problematic. Previous studies have been able to successfully apply this method in Taiwan despite the challenges of poor luminescence sensitivity in tectonically active landscapes (Dörschner et al., 2012; Tseng et al., 2013, 2016) .

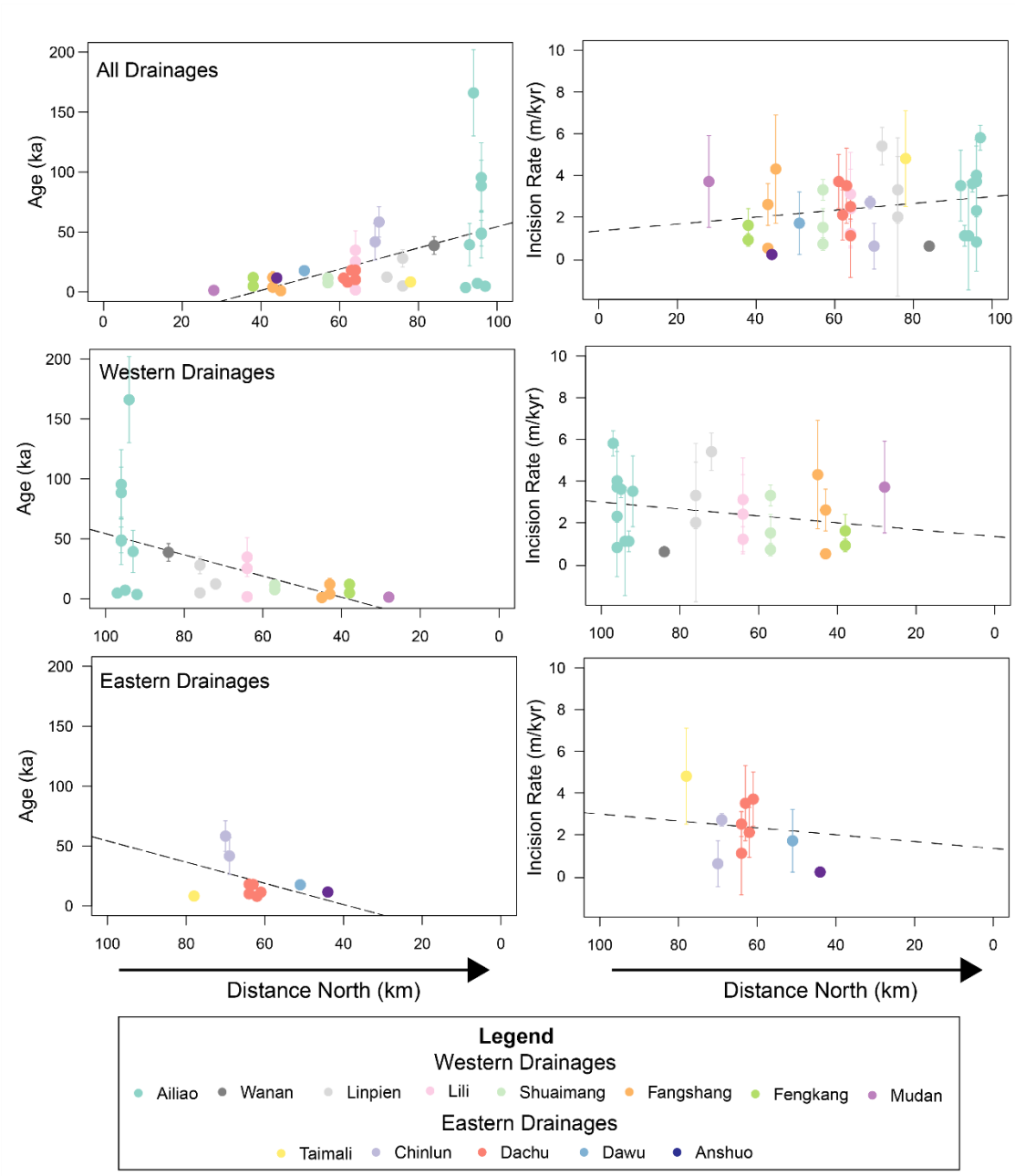

Figure 2.11 Incision rates and terrace age plotted versus distance northward. A) Age (ka) versus distance from the southern tip of Taiwan. All drainages, western drainages, and eastern drainages are plotted separately. B) Incision rate versus distance from the southern tip of Taiwan. All drainages, western drainages, and eastern drainages are plotted separately. Samples are plotted different colors based on the drainage from which they were sampled (see legend). Trend line is representative of all drainages combined.

I addressed low quartz sensitivity by rejecting aliquots that do not meet criteria for SAR protocol (Murray and Wintle, 2000). Partial bleaching is more likely to influence samples from late Holocene sediments and samples dated using IRSL dating of feldspar which requires longer light exposure to bleach the luminescence signal than quartz (Jaiswal et al., 2009). For this reason, IRSL dating was only applied to samples collected from terraces >50 m which were estimated to be older in age. Preliminary luminescence ages presented here are based on aliquot measurements that have passed rejection, however more analyses are required to meet statistical requirements for final age reporting. Uncertainty associated with luminescence ages is included in the incision-rate error calculation (Table 2.2).

Error is also introduced into incision-rate calculation through the measurement of terrace height. In the quickly eroding, dynamic landscape of southern Taiwan, strath terraces rarely form, as the rivers do not stay at a constant elevation long enough for lateral planation and valley widening necessary for bedrock strath formation to occur. The bedrock outcroppings observed underneath terrace surfaces showed topography, suggesting terraces form through valley-filling events. Large aggradation events bury the landscape and stall bedrock incision temporarily. Therefore, the method of calculating river grade change from the top of the terrace tread to the modern channel does not reflect a bedrock incision rate, but an incision rate from a period of incision unsteadiness between terrace aggradation and subsequent return to channel degradation. However, the preliminary incision rates presented here do reflect incision over time, although this rate is influenced by climate and sediment supply in addition to stream response to uplift (see Chapter 3).

Aggradation caused by Typhoon Morakot also complicates the calculation of meaningful incision rates. The change in modern channel reference position affects lower terraces more than higher ones. For example, 10 m of aggradation decreases the incision depth of a terrace surface 20 m above the modern strath by 50% whereas the incision depth from a 350 m terrace only changes 3%. The aggradation caused by Morakot and uncertainty of these measurements was accounted for in calculations of incision rate error (Section 2.4.2). Although incision rates presented here may not represent direct bedrock incision rates, they do represent the rate at which the river shifted in elevation from a remnant river surface to its current position.

2.6.2. TRENDS IN TERRACE PRESERVATION, AGE, AND INCISION RATES

Results show seventeen terraces deposited during the Holocene and seventeen deposited in the late-Pleistocene ranging from <1 ka to ~170 ka. This study provides new context by averaging terrace ages and incision rates over longer periods of time—into the Pleistocene—than the Holocene-age terraces previously studied (Hsieh and Knupfer, 2002; Dadson et al., 2003; Schaller et al., 2005; Yanites et al., 2009). Terrace age increases with distance northward in the study area with the oldest terraces in the Ailiao drainage (1W) (Figure 2.11). This may be a result of limited of terrace formation and preservation in the southern drainages, which are in wider valleys with gentler hillslope gradients (Figure 2.2). The primary mechanism for terrace development in southern Taiwan is large aggradation pulses causing valleys to fill with sediment. In southern drainages with gentler hillslope gradients, shallower hillslope gradients decrease the likely hood of slope failure causing large pulses of aggradation, which fill the valley

bottoms and leave behind terrace deposits when incision resumes. The age gradient with distance north shows that unsteadiness of river incision over long time periods is more likely to be recorded in the steeper landscape to the north.

Preliminary incision rates range from 6 – 0.2 m/kyr (Table 2.2) and show a moderate correlation with distance from the southern tip of the island (r = 0.31, Figure 2.11). Average incision rates for the southern, central, and northern drainages are 1.6 ± 1.6 m/kyr (n=7), 2.3 ± 1.0 m/kyr (n=12), 2.6 ± 1.6 m/kyr (n=16), respectively. The average incision rates within the three regions are within error of each other, demonstrating the variability and uncertainty of incision rates and influence of other potential controlling factors such as localized tectonics, duration of time over which the rate is averaged, and individual basin characteristics. However, the trend of increasing incision rates with

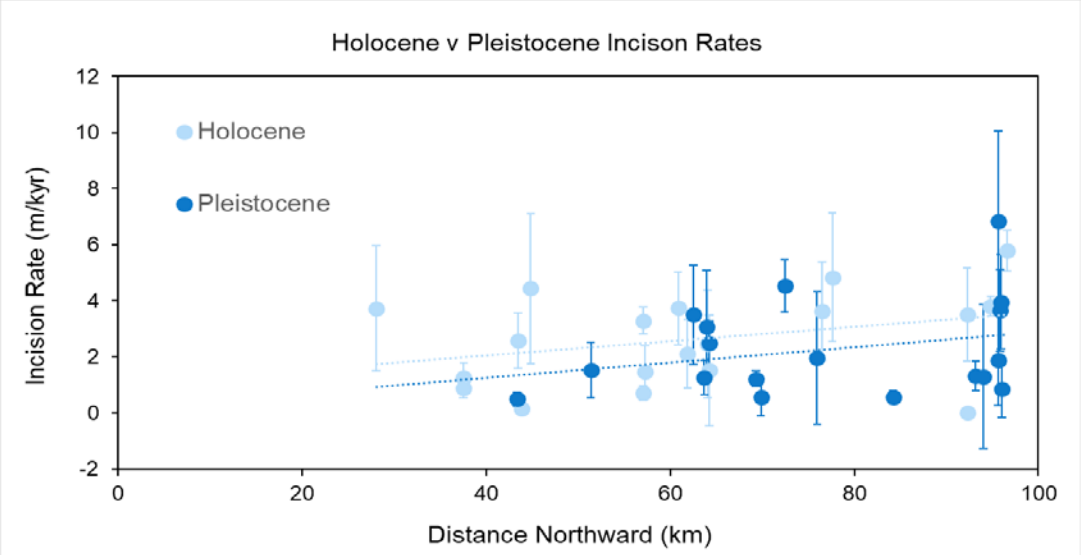

Figure 2.12 Holocene and Pleistocene incision rates plotted versus distance northward.

distance northward supports the expected relationship between increasing relief and tectonic uplift.

Incision rates averaged over the Pleistocene are slower than those averaged over the Holocene are (Figure 2.12). However, the relationship between incision rate and distance from the southern tip of the island does not appear to have shifted from the Pleistocene to the Holocene. Rates averaged over longer periods of time are often slower than those averaged over shorter periods of time (Sadler, 1981, Figure 2.13). While caution should be used when interpreting tectonics from short-term incision rates, Holocene and Pleistocene incision rates show a similar trend with distance northward suggesting that orogen growth is a primary driver of river incision over millennial-time scales. While climate controls rates of erosion on decadal and centennial time scales (Dadson et al.,

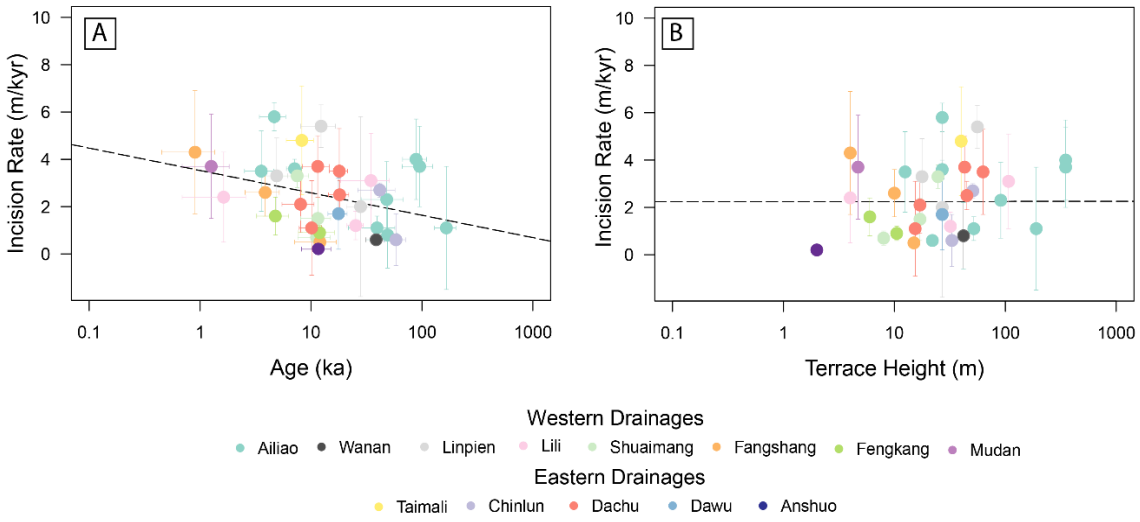

Figure 2.13 Incision rates compared with terrace age and terrace height. A) Incision rate (m/kyr) versus terrace height (m) B) Incision rate (m/kyr) versus age (ka)

2003; Yanites et al., 2018), it does not appear to be the main driver of incision rates in the longer-term record in southern Taiwan.

I expected faster incision rates from the interior of the Central Range of Taiwan than the foothills due to faster uplift in the Central Range (Dadson et al., 2003). We observed an opposite trend. Holocene incision rates from the foothills of the Central Range vary from 4 - >20 m/kyr, which is, on average, faster than those calculated in this study (Hsieh and Knupfer, 2002; Dadson et al., 2003; Schaller et al., 2005; Yanites et al., 2009). This suggests that incision-rate patterns are decoupled from uplift on centennial and millennial timescales, suggesting that caution is advised when using short-term incision rates to interpret underlying tectonics.

2.6.3. IMPLICATIONS FOR LANDSCAPE RESPONSE TO TECTONICS

The relationship between hillslope denudation rates, uplift rates, and rates of river incision is often used to interpret how a landscape is adapting to tectonic forces. Modern catchment averaged denudation rates within the study area show hillslope denudation rates increasing from ~1 m/kyr in the south to ~4 m/kyr to the north along with hillslope steepness (Yanites et al. 2018; Chen et al., 2020, see Figure 2.14). Incision rates and denudation rates averaged over decadal to millennial timescales occur at roughly equivalent rates and are within the same order of magnitude (Chen et al., 2020). Thermochronology data shows that the Central Range of Taiwan is uplifting 3-6 km/Myr (Dadson et al., 2003). While uplift rates derived from thermochronology data are averaged over much longer periods than incision and denudation rates discussed in this paper, it is worth noting that uplift rates roughly equal rates of erosion within the study

area supporting the theory that uplift is driving erosion processes on timescales greater than 10^3 yr.

This research tests the hypothesis that incision rates will increase northward until a critical hillslope threshold is met at which point hillslope processes will overwhelm the fluvial system with sediment stalling river incision. Preliminary incision rates show a moderate correlation with distance northward (r = 0.31), suggesting that as topographic relief increases, so too do incision rates. Figure 2.14 shows catchment-averaged denudation rates increase northward until a plateau is reached ~80 km from the southern tip of Taiwan suggesting that a critical threshold for hillslope processes has been reached (Yanites et al., 2019; Chen et al., 2020). However, it is less clear if incision rates show a

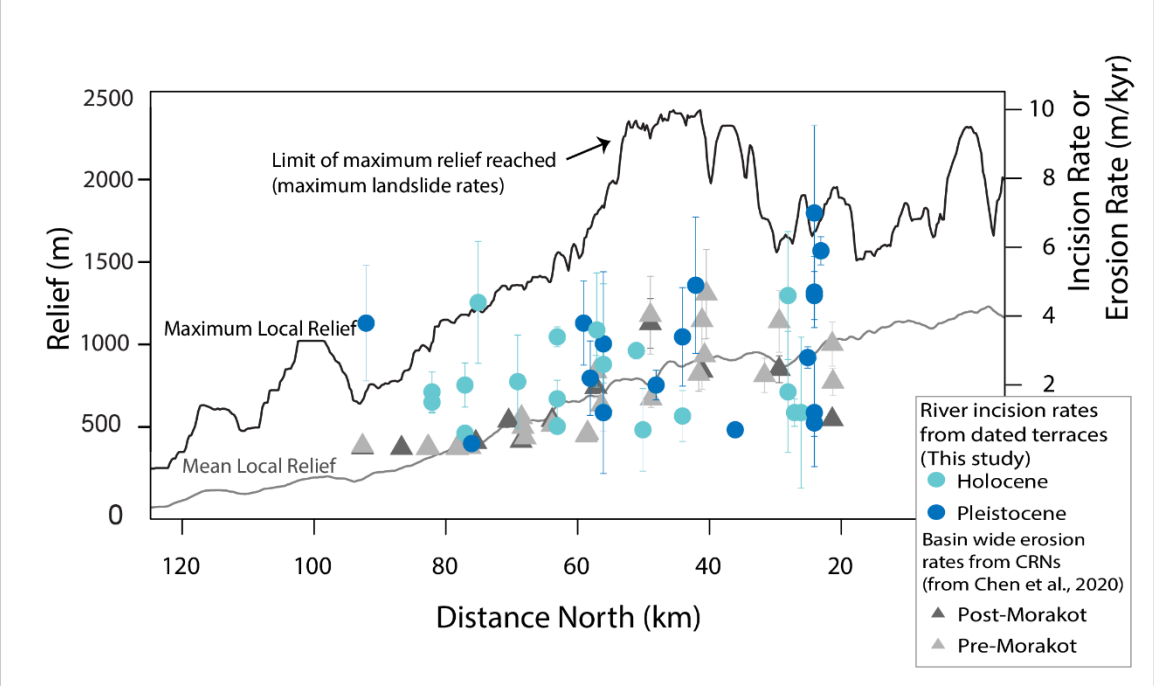

Figure 2.14 Incision rates and catchment averaged denudation rates relative to distance northward. Incision rates averaged over the Holocene (light blue) and Pleistocene (dark blue) are denoted by triangles. Catchment average denudation rates measured pre-Typhoon Morakot (light gray) and post-Typhoon Morakot are denoted by triangles (Chen et al., 2020). Black and gray lines note maximum and mean local relief, respectively.

similar pattern due to the larger spread incision rates in the data and higher rates of uncertainty (Figure 2.14).

Incision rates increasing with distance northward supports the hypothesis that underlying tectonics-drive drainage development in the beginning stages of mountain building. While denudation rates plateau at ~80 km north, incision rates continue to increase, suggesting that incision rates are not linked to denudation rates at this point, as suggested by previous studies (Hsieh et al. 2014; Tsou et al., 2014, 2015; Yanites et al. 2018).

It is possible that incision rates do plateau at this point but the variability and error associated with incision rate calculations obscure this trend. As the incision rates calculated in this study are generally averaged over longer periods of time than modern catchment-averaged erosion rates, it is expected that more variation may be expected due to climatic and tectonic forcing. If incision rates plateau ~80 km northward along with hillslope erosion rates, this would support the hypothesis a critical hillslope will be met at which point incision rates slow due to increased hillslope activity. This trend is not observed; instead, we see incision rates continue to increase along with channel steepness (Figure 2.2) while denudation rates begin to decrease in the northern drainages of the study area. This suggests that hillslope erosion rates are limited by slope stability while channel steepness and river incision do not reach a threshold within the study area. A similar trend has been observed along the actively evolving eastern margin of the Tibetan Plateau (Ouimet et al., 2009).

Steady-state conditions are often assumed in bedrock rivers as linkages have been shown between hillslope denudation, river incision and rock-uplift (Ouimet et al., 2009; DiBiase et al., 2010; Cyr et al., 2010). It is difficult to distinguish if a detachment or transport-limited model is the most appropriate for understanding landscape response to climate or tectonics. We are able to capture drainage response to ongoing tectonics occurring at accelerated rates in the quickly eroding and uplifting landscape of southern Taiwan. Incision rates and denudation rates increasing with relief to the north suggest a detachment-limited erosion model reflects landscape development in southern Taiwan on 10^3-10^5 timescales. However, the presence of terraces throughout southern Taiwan represents unsteadiness in patterns of river incision driven by climate and stochastic triggers such as extreme weather events and seismicity. Caution should be used inferring mechanisms of uplift from short-term incision and denudation rates, as these rates may be heavily influenced by factors unrelated to tectonics.

2.7. CONCLUSIONS

Results from this study are used to calculate rates of incision from thirty-four terraces along a ~100 km transect in southern Taiwan with a steep gradient in topography and drainage development due to southward propagating uplift. We test the hypothesis that incision rates will increase with distance northward due to increasing relief until critical hillslope threshold is met. At this point, surplus sediment supply entering the river system from increased hillslope processes will slow incision. Incision rates calculated ranged from 6 ± 2.6to 0.2 ± 0.1 m/kyr with an average incision rate of 2.4 ± 1.2 m/kyr. Incision rates increase northward with hillslope denudation rates until ~80km at which point denudation rates begin to decrease and incision rates continue to increase. Increasing

incision rates northward suggest a detachment-limited model for drainage development is appropriate for understanding how the landscape of southern Taiwan responds to active, southward propagating uplift. Variations in incision rates from the Holocene to the Pleistocene suggests caution should be used when applying short-term erosion rates (10-10^3) to interpret rates of uplift in Taiwan.

2.8. REFERENCES

Aitken, M.J., 1998, An Introduction to Optical Dating: The dating of Quaternary sediments by the use of photon-stimulated luminscence: New York, Oxford University Press, 267 p.

Auclair, M., Lamothe, M., and Huot, S., 2003, Measurements of anomalous fading for feldspar IRSL using SAR: Radiation Measurements, v. 37, p. 487–492.

Beaumont, C., Fullsack, P., and Hamilton, J., 1992, Erosional control of active compressional orogens: Thrust Tectonics, p. 1–18.

Brennan, B.J., 2003, Beta doses to spherical grains: Radiation Measurements, v. 37, p. 299–303.

Burbank, D.W., Leland, J., Fielding, E., Anderson, R.S., Brozovic, N., Reid, M.R., and Duncan, C., 1996, Bedrock incision, rock uplift and threshold hillslopes in the northwestern Himalayas: Nature, v. 379, p. 505–511.

Buylaert, J.P., Jain, M., Murray, A.S., Thomsen, K.J., Thiel, C., and Sohbati, R., 2012, A robust feldspar luminescence dating method for Middle and Late Pleistocene sediments: Boreas, v. 41, p. 435–451.

Chen, C., Willett, S.D., West, A.J., Dadson, S., Hovius, N., Christl, M., and Shyu, J.B.H., 2020, The impact of storm-triggered landslides on sediment dynamics and catchment-wide denudation rates in the southern Central Range of Taiwan following the extreme rainfall event of Typhoon Morakot: Earth Surface Processes and Landforms, v. 45, p. 548–564, doi:10.1002/esp.4753.

Ching, K.-E., Hsieh, M.-L., Johnson, K.M., Chen, K.-H., Rau, R.-J., and Yang, M., 2011, Modern vertical deformation rates and mountain building in Taiwan from precise leveling and continuous GPS observations, 2000–2008: Journal of Geophysical Research, v. 116, p. B08406, doi:10.1029/2011JB008242.

Cowie, P.A., Whittaker, A.C., Attal, M., Roberts, G., Tucker, G.E., and Ganas, A., 2008, New constraints on sediment-flux–dependent river incision: Implications for extracting tectonic signals from river profiles: Geology, v. 36, p. 535, doi:10.1130/G24681A.1.

Cyr, A.J., Granger, D.E., Olivetti, V., and Molin, P., 2010, Quantifying rock uplift rates using channel steepness and cosmogenic nuclide–determined erosion rates: Examples from northern and southern Italy: Lithosphere, v. 2, p. 188–198, doi:10.1130/L96.1.

Dadson, S.J. et al., 2003, Links between erosion, runoff variability and seismicity in the Taiwan orogen: Nature, v. 426, p. 648–651, doi:10.1038/nature02150.

Derrieux, F., Siame, L.L., Bourlès, D.L., Chen, R.-F., Braucher, R., Léanni, L., Lee, J.-C., Chu, H.-T., and Byrne, T.B., 2014, How fast is the denudation of the Taiwan mountain belt? Perspectives from in situ cosmogenic 10Be: Journal of Asian Earth Sciences, v. 88, p. 230–245, doi:10.1016/j.jseaes.2014.03.012.

DiBiase, R.A., Whipple, K.X., Heimsath, A.M., and Ouimet, W.B., 2010, Landscape form and millennial erosion rates in the San Gabriel Mountains, CA: Earth and Planetary Science Letters, v. 289, p. 134–144, doi:10.1016/j.epsl.2009.10.036.

DiBiase, R.A., Whipple, K.X., Lamb, M.P., and Heimsath, A.M., 2015, The role of waterfalls and knickzones in controlling the style and pace of landscape adjustment in the western San Gabriel Mountains, California: Geological Society of America Bulletin, v. 127, p. 539–559, doi:10.1130/B31113.1.

Donovan, M., and Belmont, P., 2019, Timescale dependence in river channel migration measurements: Earth Surface Processes and Landforms, v. 44, p. 1530–1541.

Dörschner, N., Reimann, T., Wenske, D., Lüthgens, C., Tsukamoto, S., Frechen, M., and Böse, M., 2012, Reconstruction of the Holocene coastal development at Fulong Beach in north-eastern Taiwan using optically stimulated luminescence (OSL) dating: Quaternary International, v. 263, p. 3–13, doi:10.1016/j.quaint.2011.12.009.

Duvall, A., 2004, Tectonic and lithologic controls on bedrock channel profiles and processes in coastal California: Journal of Geophysical Research, v. 109, p. F03002, doi:10.1029/2003JF000086.

Fellin, M.G., Chen, C.-Y., Willett, S.D., Christl, M., and Chen, Y.-G., 2017, Erosion rates across space and timescales from a multi-proxy study of rivers of eastern Taiwan: Global and Planetary Change, v. 157, p. 174–193, doi:10.1016/j.gloplacha.2017.07.012.

Finnegan, N.J., Pazzaglia, F.J., and Finnegan, S., 2014, A signature of transience in bedrock river incision rates over timescales of 10^4–10^7 years: Nature, v. 505, p. 391–394.

Gallen, S.F., Pazzaglia, F.J., Wegmann, K.W., Pederson, J.L., and Gardner, T.W., 2015, The dynamic reference frame of rivers and apparent transience in incision rates: Geology, v. 43, p. 623–626, doi:10.1130/G36692.1.

Godfrey-Smith, D.I., Huntley, D.J., and Chen, W.-H., 1988, Optical dating studies of quartz and feldspar sediment extracts: Quaternary Science Reviews, v. 7, p. 373–380, doi:10.1016/0277-3791(88)90032-7.

Guérin, G., Mercier, N., and Adamiec, G., 2011, Dose-rate conversion factors: update: v. 29, p. 4.

Hancock, G.S., and Anderson, R.S., 2002, Numerical modeling of fluvial strath-terrace formation in response to osciallting climate: Geological Society of America Bulletin, v. 114, p. 1131–1142.

Hartshorn, K., 2002, Climate-Driven Bedrock Incision in an Active Mountain Belt: Science, v. 297, p. 2036–2038, doi:10.1126/science.1075078.

Ho, C.S., 1986, A synthesis of the geologic evolution of Taiwan: Memoir of the Geological Society of China, v. 7, p. 15–29.

Howard, A.D., 1994, A detachment-limited model of drainage basin evolution: Water Resources Research, v. 30, p. 2261–2286.

Hsieh, M.-L., and Knupfer, P.L.K., 2002, Synchroneity and morphology of Holocene river terraces in the southern Western Foothill, Taiwan: A guide to interpreting and correlation erosional river terraces across growing anticlines, *in* Geology and Geophysics of an Arc-Continent Collision, Taiwan, GSA Special Paper 358, p. 55–74.

Hsu, W.H., Byrne, T.B., Ouimet, W., Lee, Y.H., Chen, Y.G., van Soest, M., and Hodges, K., 2016, Pleistocene onset of rapid, punctuated exhumation in the eastern Central Range of the Taiwan orogenic belt: Geology, v. 44, p. 719–722.

Hu, J.-C. et al., 2007, Fault activity and lateral extrusion inferred from velocity field revealed by GPS measurements in the Pingtung area of southwestern Taiwan: Journal of Asian Earth Sciences, v. 31, p. 287–302, doi:10.1016/j.jseaes.2006.07.020.

Huang, C., and Byrne, T.B., 2014, Tectonic evolution of an active tectonostratigraphic boundary in accretionary wedge: An example from the Tulungwan-Chaochou Fault system, southern Taiwan: Journal of Structural Geology, v. 69, p. 320–333, doi:10.1016/j.jsg.2014.06.007.

Huntley, D.J., Godfrey-Smith, D.I., and Thewalt, M.L.W., 1985, Optical dating of sediments: Nature, v. 313, p. 105–107.

Huntley, D.J., and Lamothe, M., 2001, Ubiquity of anomalous fading in K-feldspars and teh measurements and correction for it in optical dating: Canadian Journal of Earth Sciences, v. 38, p. 1093–1106.

Hütt, G., Jaek, I., and Tchonka, J., 1988, Optical dating: K-feldspars optical response stimulation spectra: Quaternary Science Reviews, v. 7, p. 381–385.

Jaiswal, M.K., Chen, Y.G., Kale, V.S., and Achyuthan, H., 2009, Residual Luminescence in Quartz from Slack Water Deposits in Kaveri Basin, South India: A Single Sliquot Approach: Geochronometria, p. 1–8.

Kirby, E., and Whipple, K., 2001, Quantifying differential rock-uplift rates via stream profile analysis: , p. 4.

Lavé, J., and Avouac, J.P., 2001, Fluvial incision and tectonic uplift across the Himalayas of central Nepal: Journal of Geophysical Research: Solid Earth, v. 106, p. 26561–26591, doi:10.1029/2001JB000359.

Lawson, M.J., Roder, B.J., Stang, D.M., and Rhodes, E.J., 2012, OSL and IRSL Characteristics of Quartz and Feldspar from Southern California: Radiation Measurements, p. 830–836.

Lee, Y.-H., Byrne, T., Wang, W.-H., Lo, W., Rau, R.-J., and Lu, H.-Y., 2015, Simultaneous mountain building in the Taiwan orogenic belt: Geology, v. 43, p. 451–454, doi:10.1130/G36373.1.

Lee, Y.-H., Chen, C.-C., Liu, T.-K., Ho, H.-C., Lu, H.-Y., and Lo, W., 2006, Mountain building mechanisms in the Southern Central Range of the Taiwan Orogenic Belt — From accretionary wedge deformation to arc–continental collision: Earth and Planetary Science Letters, v. 252, p. 413–422, doi:10.1016/j.epsl.2006.09.047.

Liu, T.-K., Hsieh, S., Chen, Y.-G., and Chen, W.-S., 2001, Thermo-kinematic evolution of the Taiwan oblique-collision mountain belt as revealed by zircon ¢ssion track dating: Earth and Planetary Science Letters, v. 186, p. 45–56.

Mesalles, L., 2014, Mountain building at a subduction-collision transition zone, Taiwan: Insights from morphostructural analysis and thermochronological dating [Doctorate Thesis]: Université Pierre et Marie Curie.

Montgomery, D.R., and Brandon, M.T., 2002, Topographic controls on erosion rates in tectonically active mountain ranges: Earth and Planetary Science Letters, v. 201, p. 481–489, doi:10.1016/S0012-821X(02)00725-2.

Murray, A.S., and Wintle, A.G., 2000, Dating quartz using an improved single-aliquot regenerative-dose (SAR) protocol: Radiation Measurements, v. 32, p. 57–73.

Ouimet, W.B., Whipple, K.X., and Granger, D.E., 2009, Beyond threshold hillslopes: Channel adjustment to base-level fall in tectonically active mountain ranges: Geology, v. 37, p. 579–582, doi:10.1130/G30013A.1.

Pazzaglia, F.J., 2013, Fluvial Terraces, *in* Schroder, J.F. and Wohl, E. eds., Treatise on Geomorphology, Academic Press, v. 9, p. 379–412.

Pederson, J.L., Anders, M.D., Rittenhour, T.M., Sharp, W.D., Gosse, J.C., and Karlstrom, K.E., 2006, Using fill terraces to understand incision rates and evolution of the Colorado River in eastern Grand Canyon, Arizona: Journal of Geophysical Research: Earth Surface, v. 111, doi:10.1029/2004JF000201.

Peizhen, Z., Molnar, P., and Downs, W.R., 2001, Increased sedimentation rates and grain sizes 2-4 Myr ago due to the influence of climate change on erosion rates: Nature, v. 410, p. 891–897.

Perron, J.T., 2017, Climate and the Pace of Erosional Landscape Evolution: Annual Review of Earth and Planetary Science, v. 45, p. 561–591.

Prescott, J.R., and Hutton, J.T., 1994, Cosmic ray contributions to dose rates for luminescence and ESR dating: Large depths and long-term time variations: Radiation Measurements, v. 23, p. 497–500, doi:10.1016/1350-4487(94)90086-8.

Preusser, F., Ramseyer, K., and Schlüchter, C., 2006, Characterization of Low OSL Intensity Quartz from the New Zealand Alps: Radiation Measurements, p. 871–877.

Rhodes, E.J., 2011, Optically Stimulated Luminescence Dating of Sediments over the Past 200,000 Years: Annual Review of Earth and Planetary Science, v. 39, p. 461–488.

Royden, L., and Perron, J.T., 2013, Solutions of the stream power equation and application to the evolution of river longitudinal profiles: SOLUTIONS OF THE STREAM POWER EQUATION: Journal of Geophysical Research: Earth Surface, v. 118, p. 497–518, doi:10.1002/jgrf.20031.

Sadler, P.M., 1981, Sediment Accumulation Rates and the Completeness of Stratigraphic Sections: The Journal of Geology, v. 89, p. 569–584, doi:10.1086/628623.

Sadler, P.M., and Jerlomack, D.J., 2014, Scaling laws for aggradation, denudation and progradation rates: the case for time-scale invariance at sediment sources and sinks, *in* Strata and Time: Probing the Gaps in Our Understanding, London, Geological Society, Special Publications 404, http://dx.doi.org/10.1144/SP404.7.

Schaller, M., Hovius, N., Willett, S.D., Ivy-Ochs, S., Synal, H.-A., and Chen, M.-C., 2005, Fluvial bedrock incision in the active mountain belt of Taiwan fromin situ-produced cosmogenic nuclides: Earth Surface Processes and Landforms, v. 30, p. 955–971, doi:10.1002/esp.1256.

Seidl, M.A., and Dietrich, W.E., 1992, The problem of channel erosion into bedrock: Functional geomorphology: landform analysis and models, v. 23.

Simoes, M., and Avouac, J.P., 2006, Investigating the kinematics of mountain building in Taiwan from the spatiotemporal evolution of the foreland basin and western foothills: Journal of Geophysical Research, v. 111, p. B10401, doi:10.1029/2005JB004209.

Suppe, J., 1981, Mechanics of mountain building and metamorphism in Taiwan: Memoir of the Geological Society of China, v. 4, p. 67–89.

Tseng, C.-H., Lüthgens, C., Tsukamoto, S., Reimann, T., Frechen, M., and Böse, M., 2016, Late Pleistocene to Holocene alluvial tableland formation in an intra-mountainous basin in a tectonically active mountain belt — A case study in the

Puli Basin, central Taiwan: Quaternary Science Reviews, v. 132, p. 26–39, doi:10.1016/j.quascirev.2015.11.006.

Tseng, C.-H., Wenske, D., Böse, M., Reimann, T., Lüthgens, C., and Frechen, M., 2013, Sedimentary features and ages of fluvial terraces and their implications for geomorphic evolution of the Taomi River catchment: A case study in the Puli Basin, central Taiwan: Journal of Asian Earth Sciences, v. 62, p. 759–768, doi:10.1016/j.jseaes.2012.11.028.

Tsou, C.-Y., Chigira, M., Matsushi, Y., and Chen, S.-C., 2014, Fluvial incision history that controlled the distribution of landslides in the Central Range of Taiwan: Geomorphology, v. 226, p. 175–192, doi:10.1016/j.geomorph.2014.08.015.

Wallinga, J., 2002, Optically stimulated luminescence dating of fluvial deposits: a review: Boreas, p. 303–322.

Wallinga, J., Murray, A.S., and Wintle, A.G., 2000, The single-aliquot regenerative-dose (SAR) protocol applied to coarse-grain feldspar: , p. 529–533.

Whipple, K.X., 2004, Bedrock rivers and the geomorphology of active orogens: Annual Review of Earth and Planetary Science, v. 32, p. 151–185.

Whipple, K.X., and Tucker, G.E., 1999, Dynamics of the stream-power river incision model: Implications for height limits of mountain ranges, landscape response timescales, and research needs: Journal of Geophysical Research: Solid Earth, v. 104, p. 17661–17674, doi:10.1029/1999JB900120.

Willett, S.D., 1999, Orogeny and orography: The effects of erosion on the structure of mountain belts: Journal of Geophysical Research: Solid Earth, v. 104, p. 28957–28981, doi:10.1029/1999JB900248.

Willett, S.D., Fisher, D., Fuller, C., En-Chao, Y., and Chia-Yu, L., 2003, Erosion rates and orogenic-wedge kinematics in Taiwan inferred from fission-track thermochronometry: Geology, v. 31, p. 945–948, doi:10.1130/G19702.1.

Wiltschko, D.V., Hassler, L., Hung, J.-H., and Liao, H.-S., 2010, From accretion to collision: Motion and evolution of the Chaochou Fault, southern Taiwan: CHAOCHOU FAULT, TAIWAN: Tectonics, v. 29, p. n/a-n/a, doi:10.1029/2008TC002398.

Wobus, C.W., Whipple, K.X., Kirby, E., Snyder, N.P., Johnson, J., Spyropolou, K., Crosby, B., and Sheehan, D., 2006, Tectonics from topography: Procedures, promise, and pitfalls, *in* Tectonics, climate, and landscape evolution, GSA Special Paper 398, p. 55–74.

Yanites, B.J., Mitchell, N.A., Bregy, J.C., Carlson, G.A., Cataldo, K., Holahan, M., Johnston, G.H., Nelson, A., Valenza, J., and Wanker, M., 2018, Landslides control the spatial and temporal variation of channel width in southern Taiwan: Implications for landscape evolution and cascading hazards in steep, tectonically active landscapes: Variation in channel morphology controlled by landslides in s.

Taiwan: Earth Surface Processes and Landforms, v. 43, p. 1782–1797, doi:10.1002/esp.4353.

Yanites, B.J., and Tucker, G.E., 2010, Controls and limits on bedrock channel geometry: Journal of Geophysical Research, v. 115, p. n/a-n/a, doi:10.1029/2009JF001601.

Yanites, B.J., Tucker, G.E., and Anderson, R.S., 2009, Numerical and analytical models of cosmogenic radionuclide dynamics in landslide-dominated drainage basins: Journal of Geophysical Research, v. 114, p. n/a-n/a, doi:10.1029/2008JF001088.

Yanites, B.J., Tucker, G.E., Mueller, K.J., Chen, Y.-G., Wilcox, T., Huang, S.-Y., and Shi, K.-W., 2010, Incision and channel morphology across active structures along the Peikang River, central Taiwan: Implications for the importance of channel width: Geological Society of America Bulletin, v. 122, p. 1192–1208, doi:10.1130/B30035.1.

Yu, S.-B., Chen, H.-Y., and Kuo, L.-C., 1997, Velocity field of GPS stations in the Taiwan area: Tectonophysics, v. 274, p. 41–59, doi:10.1016/S0040-1951(96)00297-1.

CHAPTER 3 - TERRACE FORMATION IN RESPONSE TO CLIMATE CHANGE IN SOUTHERN TAIWAN

3.1. ABSTRACT

Taiwan is a young island undergoing rapid, southward propagating uplift resulting from the oblique collision of the Philippine Sea Plate and Eurasian Plate. The topography is sculpted by high rates of erosion due to rapid uplift coupled with a warm, wet climate and weak bedrock. Incision of bedrock rivers is often thought of as detachment-limited systems reflecting the underlying tectonics. This research investigates the influences of climate on sediment supply from hillslope, which can interrupt patters of river incision. This research provides age control for terrace deposits left behind as geomorphic markers of paused river incision to understand how climate effects river dynamics in southern Taiwan. Thirty-four terraces from thirteen drainages were dated throughout the southern 100 km of Taiwan. Ages span the last 170 kyr and record four periods of regional terrace deposition during the Holocene around 1, 4-5, 8, and 11 ka and at least three periods during the late-Pleistocene at 18, 28, and 40 ka. Periods of deposition during the Holocene at 1 ka and 11 ka correspond with times of increased East Asian Summer Monsoon (EASM) intensity and records of increased mass-wasting in Taiwan. Regional terrace deposition during the Pleistocene around 18, 28, and 40 ka correspond with the precessional cycles of solar insolation and EASM intensity. Results from this study extend the record of landscape response to EASM monsoon intensity in Taiwan into the late-Pleistocene. Changes in climate can interrupt the overarching pattern of river incision driven by underlying tectonics revealing that, on short (10^0-10^3 yr) timescales, climate signals may obscure tectonic drivers of erosion.

3.2. INTRODUCTION

Incision of bedrock rivers is a significant driver of regional topography in active orogens, controlling rates and patterns of denudation (Whipple, 2004). Terraces are abandoned river floodplains and record the style and pace of bedrock incision over time. Terraces represent the unsteadiness of a river system because terrace formation requires periods of valley-widening and deposition followed by vertical incision (Whipple, 2004; Pazzaglia, 2013). Shifts in river erosion can be caused by a variety of external perturbations including tectonic activity (Burbank et al., 1996), drainage reorganization (Finnegan and Dietrich, 2011; Yang et al., 2015) or climate (Hancock and Anderson, 2002; Pan et al., 2003). Climatic variability can cause variability in sediment supply and transport capacity which controls the ability of rivers to incise or aggrade (Pan et al., 2003).

Rapid denudation and incision rates coupled with active uplift in Taiwan make it possible to study landscape response to climate (Suppe, 1981; Chen et al., 2020, see Chapter 2). Researchers have investigated the correlation between mass-wasting deposits and past climate in Taiwan (Hsieh and Chyi, 2010a; Hsieh et al., 2011, 2012, 2014). Hillslope activity has been shown to increase during periods of increased East Asian Summer Monsoon (EASM) intensity, as increased precipitation rates increase hillslope denudation rates (Langbein and Schumm, 1958; Hsieh and Chyi, 2010a; Hsieh et al., 2011, 2012, 2014). The EASM system dominates the climate of Taiwan, influencing the frequency and magnitude of storms. EASM intensity waxed and waned throughout the Holocene and Pleistocene (Cheng et al., 2009; Lee and Liew, 2010; Li et al., 2013). Individual large storm events in Taiwan can have long-lasting landscape-scale impact.

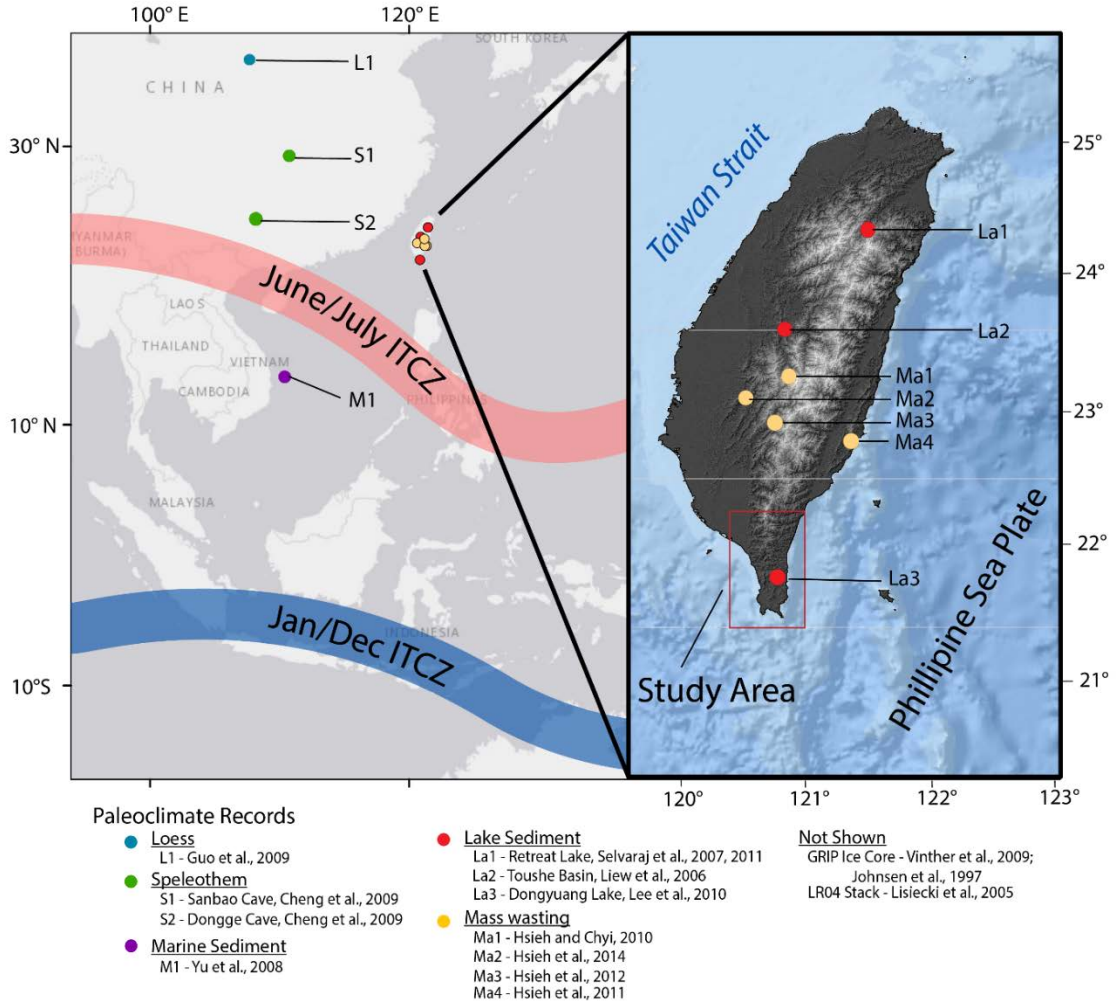

Figure 3.1 ITCZ position relative to Taiwan and paleoclimate records from the South China Sea. (A) Map showing locations of paleoclimate records synthesized in this study. The position the ITCZ during the summer (red) and winter (blue) are noted. (B) Inset map shows geologic setting of Taiwan. The research area from this study is marked in red.

Storm events can trigger widespread mass-wasting events that blanket stream channels with sediment, stalling incision into bedrock (Yanites et al., 2018). These studies show that individual storm events can trigger widespread mass-wasting events that blanket the channel with sediment and stall bedrock incision. Few studies have investigated terrace

development in response to climate in southern Taiwan to test the predicted link between hillslope erosion and stream incision. It is predicted that stronger EASM intensity will lead to increased hillslope erosion blanketing river bottoms with sediment and stall bedrock incision (see Chapter 2). To understand the relationship between climate and river incision in southern Taiwan, we used luminescence dating of terraces from catchments draining the southern Central Range in Taiwan (Figure 2.4).

Thirty-seven luminescence geochronology samples were collected from alluvial terrace deposits in thirteen drainages throughout the southern 90 km of Taiwan (Figure 2.4). Samples were collected from drainages along the east and west sides of the Central Range, the large mountain range that runs from north to south in Taiwan (Figure 2.3). Terraces sampled ranged from 4-350 m in elevation above the modern channel in order to represent a range of terrace deposits spanning the late Pleistocene to Holocene. It is expected that during times of increased precipitation when then strength of the EASM system was enhanced, mass wasting from landslides and debris flows would have similarly or disproportionately increased. At a certain threshold, the additional influx of sediment into the valley bottoms would have paused river incision. During periods of weaker EASM, river incision driven by continued tectonic uplift would resume and terraces would form as the former valley bottoms were abandoned due to channel incision. Because of the dynamic nature of Taiwan, terraces are not generally formed by lateral planation followed by rapid incision, which requires the river to remain at a constant position for long time periods. Instead, terraces are formed by periods of aggradation interrupting the overall pattern of incision, which are linked to high rates of sediment supply due to in part to EASM intensity and the tectonic uplift setting.

Luminescence ages from terraces provide an age estimate of the time of sediment deposition. This work tests the hypothesis that terrace ages will align with periods of increased EASM intensity during which river incision was stalled due to increased sediment supply to the river systems from increased hillslope activity (landslides, debris flows).

3.3. BACKGROUND

3.3.1. CLIMATE SETTING

The EASM system is a major component of the global climate system, affecting the lives of one fourth of the world's population (Goldsmith et al., 2017). Seasonal shifts in landmass and ocean pressure gradients and resultant wind directions drive the EASM and lead to changes in precipitation in the region. As insolation intensity increases in the summer, the land surface becomes warmer than the ocean creating an area of low pressure. Air saturated with moisture from the oceans moves from high pressure to low pressure zones delivering moisture to the continents. The opposite occurs in the winter as land surfaces cool and moisture is delivered to areas of low pressure over the ocean (An et al., 2015). The EASM is caused by low pressure over mainland China driving moisture from the Pacific Ocean and South China Sea north along the eastern flank of Asia. In the winter, high pressure forms over the mainland and fuels the East Asian Winter Monsoon (EAWM), which produces cold, dry winds from Siberia (An, 2000; Ding and Chan, 2005). These seasonal changes are driven by the annual variations in insolation due to the tilt of the Earth's axis (Ding and Chan, 2005). During strong periods of stronger EASM intensity, the climate of Taiwan is wetter and warmer and the island receives more

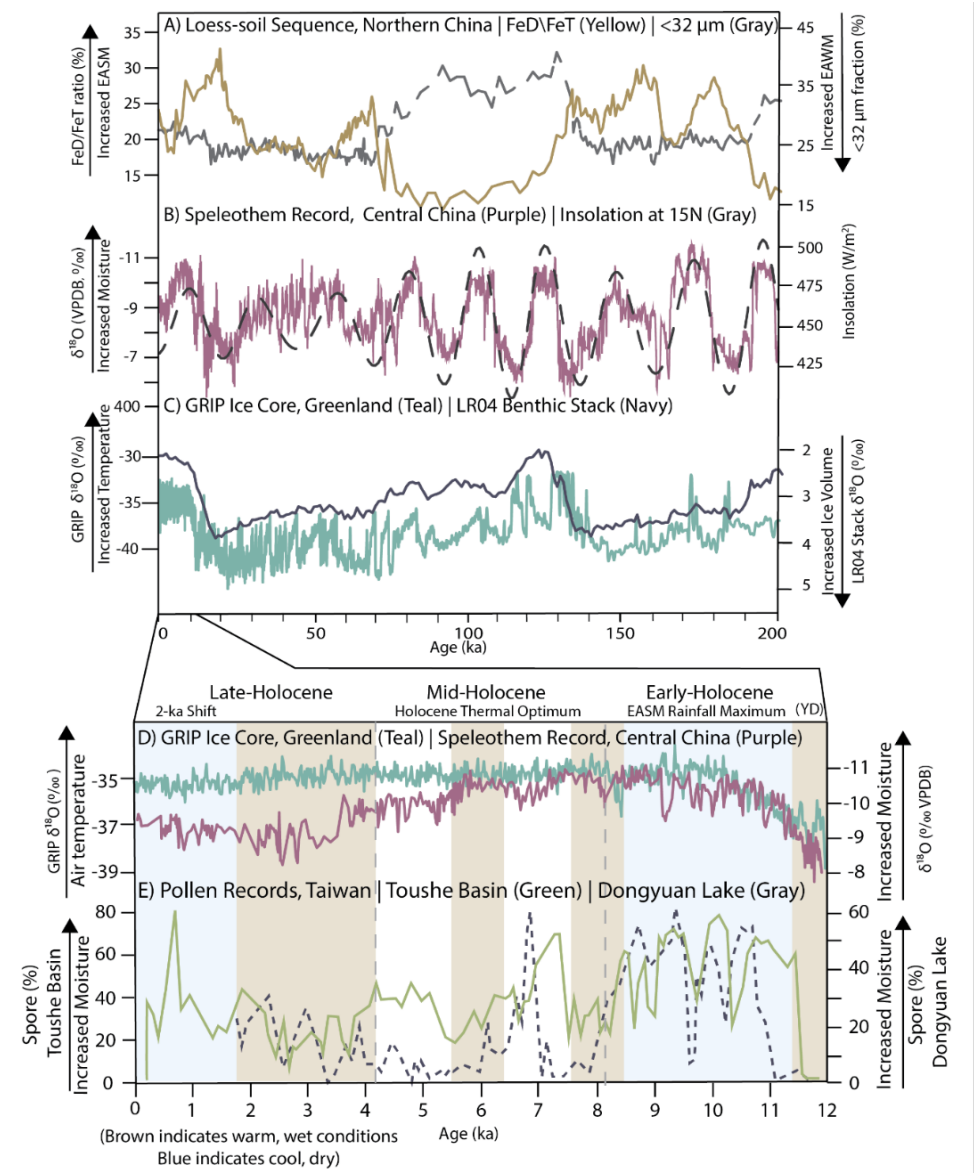

Figure 3.2 Holocene and Pleistocene climate records. (A) Loess Plateau records from Xifeng (Guo et al., 2000, 2009). Chemical weathering index (FeD/FeT) ratio (grey dashed) which is an indicator of EASM monsoon strength and content of >32µm fraction (%) (yellow), an East Asian Winter Monsoon (EAWM) indicator. (B) Mid-month July insolation (W/m2) at 15N (dashed silver) (Rachmayani et al., 2016). Speleothem records (purple) from the Dongge and Sanbao caves in Central China (Cheng et al., 2009). (C) Temperature Proxy (δ18O (0/00)) records from the GRIP Ice Core, Greenland (blue) (Johnsen et al., 1997). Ice volume proxy (δ18O (0/00)) from the LR04 Stack (Lisiecki and Raymo, 2005). (D) Temperature Proxy ($\delta^{18}O$ ($^{0}/_{00}$)) records from the GRIP Ice Core, Greenland (blue) (Vinther et al., 2009) and Speleothem precipitation proxy records ($\delta^{18}O$ ($^{0}/_{00}$ VPDB)) records (purple) (Cheng et al., 2009). (E) Percentage of spores indicating wet conditions from the Toushe Basin (green) (Liew et al., 2006) and Dongyuan Lake (dashed grey) (Lee and Liew, 2010). Brown shading indicates cool, dry periods and blue shading indicated warm, wet climate conditions from Ding et al. (2020).

frequent and intense storm event such as typhoons (Ding et al., 2020).

EASM intensity has been linked to Northern Hemisphere insolation on orbital timescales (Wang et al., 2008; Kutzbach et al., 2008; Zhang et al., 2019) and the climate of the North Atlantic on millennial timescales (Wang, 2001; Wang et al., 2008; Cheng et al., 2009, Figure 3.1). Speleothem records show that the 23 kyr precision cycle and Northern Hemisphere summer insolation are the primary driver of EASM strength through the Pleistocene (Wang, 2001; Wang et al., 2008; Cheng et al., 2016; Zhang et al., 2019, Figure 3.2). The Intertropical Convergence Zone (ITCZ) is pushed southward when northern hemisphere insolation is weaker reducing the intensity of EASM (Cheng et al., 2009, Figure 3.1). During periods of greater Northern Hemisphere glaciation in marine isotope stages (MIS) 2-4 and 6, EASM strength was reduced (Cheng et al., 2009, 2016). North Atlantic climate events that disrupt oceanic circulation patterns such as Heinrich events and increased ice rafted debris also have been observed to weaken the EASM strength. (Wang, 2001; Yu et al., 2008; Wang et al., 2008; Cheng et al., 2009; Zhang et al., 2019). Periods of weakened monsoon have been observed following the last four glacial terminations as meltwater from ice sheets disrupts oceanic circulation patterns (Cheng et al., 2009, 2016). The paleoclimate of Taiwan can be more complicated, as Taiwan has been connected to mainland China during glacial when sea level was 115-130 m lower removing the Taiwan Strait as a moisture source (Liu et al., 1997; Bintanja et al., 2005).

The variability of the EASM has been recorded in numerous paleoclimate proxy records including loess-paleosol sequences (An et al., 1991, 2015; Huang et al., 2000; Sun et al., 2006), lake and peat sediments (Lee et al., 2010; Li et al., 2013; Chen et al., 2015b),

Table 3.1 Paleoclimate records utilized in this study.

Site Name	Location	Time span	Type of Record	Proxies Used	Record Length	References
Retreat Lake	Northern, Taiwan 24°29'N, 121°26'E	10.3 kyr	Lake Core	TOC	1.7 m	(Selvaraj et al., 2007, 2011)
Toushe Basin	Central, Taiwan 23°49'N, 120°53'E	96 kyr	Lake Core	Spores, TOC, and n-alkane-δD	39.5 m	(Liew et al., 2006; Li et al., 2013)
Dongyuan Lake	Southern, Taiwan 22°10'N, 120°50'E	22 kyr	Lake Core	Spores	15 m	(Lee and Liew, 2010; Lee et al., 2010)
Vietnam Margin	South China Sea 13°47.54'N, 110°15.56'E	135 kyr	Foraminifer Record	$\delta^{18}O$ analysis	36.9 m	(Yu et al., 2008)
Xifeng	Central China 35.7° N, 107.6° E	800 kyr	Loess Record	FeD/FeT ($^{0}/_{00}$) >32 μm fraction (%)	109.4 m	(Guo et al., 2000, 2009)
Composite Sanbao & Dongge	Central China 31°40'N, 110°26' E; 25.28°N, 108°.08 E	640 kyr	Speleothem Record	$\delta^{18}O$		(Cheng et al., 2016)
Vostok	East Antarctica 78° S, 106° E	420 kyr	Ice Core	$\delta^{18}O_{atm}$	3,623 m	(Petit et al., 1999)
GRIP	Greenland 72°35 N; 37°34 E	~100 kyr	Ice Core	$\delta^{18}O_{atm}$	3,029 m	(Vinther et al., 2009)

marine sediments (Yu et al., 2008; Li et al., 2015), stalagmite records (Wang, 2001, 2005; Wang et al., 2008; Cheng et al., 2009, 2016; Zhang et al., 2019), and dune records (Ho et al., 2017). Records from Taiwan indicated that the climate of Taiwan experienced the EASM rainfall maximum in the early-Holocene (11.6 – 8.1 ka) due to strong Northern Hemisphere insolation and warm sea-surface temperatures in the Western Pacific Warm Pool (Ding et al., 2020). The mid-Holocene (8.2 – 4.1 ka) was marked by warm, dry conditions corresponding with the Holocene thermal optimum (Lee et al., 2010). The climate of late-Holocene (4.1 ka – present) began with a period of weak EASM intensity

from 4 – 2 ka followed by an intensification of EASM strength during the last 2 kyr driven by decreases of interhemispheric temperature gradients (Lee et al., 2010; Ding et al., 2020).

3.3.2. FLUVIAL TERRACES AS GEOMORPHIC MARKERS

The formation of terrace deposits represent the unsteadiness of a river system, as terrace development requires a period of valley-widening and aggradation followed by incision to create a terrace (Burbank et al., 1996; Pan et al., 2003; Pazzaglia, 2013; Bender et al., 2020). Unsteadiness in river incision has been linked to tectonic uplift (Burbank et al., 1996; Pan et al., 2003), drainage reorganization (Yang et al., 2015; Whipple et al., 2017), mass wasting events (Finnegan et al., 2014), and changes in climate (Peizhen et al., 2001; Hancock and Anderson, 2002; Hartshorn, 2002). Terraces are often grouped into two categories: strath and fill. Fill terraces reflect periods of aggradation filling valley bottoms with sediment followed by incision into the deposits and abandonment of the former floodplain due to a shift in stream flow, sediment supply, or base level. Strath terraces are formed by the lateral plantation and valley widening followed by a pulse of incision into bedrock, which requires uplift and incision rates, would need to be roughly equal as well as sediment supply and transport capacity for a significant duration of time. In the rapidly uplifting and incising landscape of Taiwan (7 – 0.5 m/kyr, see Chapter 2), it is unlikely that there is enough time for the valley widening events necessary to form strath terraces.

Increases in storm activity and precipitation associated with climate change have been linked to increasing mass-wasting activities, which could lead to aggradation events interrupting long-term tectonic-uplift driven river incision resulting in terrace

development (Trauth et al., 2003; Chen et al., 2015a). Studies from Taiwan (Hsieh et al., 2014; Tsou et al., 2014, 2015) have shown that terrace deposition in Taiwan has been linked to periods of increased hillslope activity. Increased precipitation and seismic activity have driven mass wasting events which blanket the channel with sediment stalling bedrock erosion (Howard, 1994; Sklar and Dietrich, 1998). When incision resumes after an aggradation event, terraces are left behind recording periods of aggradation interrupting overall river incision (Finnegan et al., 2014; Bender et al., 2020). Multiple studies have used ^{14}C dating of organics in mass-wasting deposits to study correlations between hillslope processes and climate (Hsieh and Chyi, 2010; Hsieh et al., 2011, 2012, 2014, 2017) see Table 3.2).

Table 3.2 Mass-wasting records used in this study

Site Name	Location	Time Span	Dating Method	Number of Dates	Proxies Used	References
Pa-Chang River	Southwestern Taiwan	14.8 kyr	^{14}C	55	Number of ^{14}C dates	(Hsieh et al., 2014)
Huang-tung Coast	Eastern Taiwan	17 kyr	^{14}C	34	Number of ^{14}C dates	(Hsieh et al., 2011)
Trunk Cho-Shui River and Chen-yeo-lan River	Central-south Taiwan	~40 kyr	^{14}C	25	Number of ^{14}C dates	(Hsieh and Chyi, 2010b)
Lao-nung River	Central-south Taiwan	18.5 kyr	^{14}C	22	Number of ^{14}C dates	(Hsieh and Chyi, 2010b)
Nan-tzu-hsien River	Southwestern Taiwan	21 kyr	^{14}C	7	Number of ^{14}C dates	(Hsieh et al., 2012)

3.3.3. STUDY AREA

Taiwan is a young tectonically active island (5 Ma) formed by the collision of the Philippine Sea Plate with the Eurasian Plate at a rate of ~80 mm/kyr (Suppe, 1981).

Uplift is rapid (3-6 km/Myr) and propagating southward due to an oblique collision between the two plates, causing a steep gradient in topography (Liu et al., 2001). Thermochrology data indicates that detrital zircon and apatite grains are reset in the north, but not in the south, suggesting a N-S gradient in exhumation (Hsu et al., 2016). Weak, Miocene slates and shales dominate the bedrock of southern Taiwan (Ho, 1986, Figure 2.1). Taiwan has a subtropical climate influenced by the EASM, receiving a mean annual precipitation of 2.5 m/yr and an average of four typhoons per year ("Central Weather Bureau," 2020). Active seismicity coupled with frequent rain events lead to frequent mass-wasting and rapid fluvial bedrock incision (Hovius et al., 2000; Hartshorn, 2002).

This study investigates periods of terrace deposition in the southern 100 km of the island. The study area captures a steep topographic gradient with maximum elevations rising 3- km from the southern tip of the island to the northern extent of the study area (Figure 2.4). Denudation and incision rates within the study area increase northward with denudation rates increasing from ~ 1 – 4 m/kyr and incision rates increasing from ~ 1.5 – 2.5 m/kyr (Chen et al., 2020, see Chapter 2). The Central Range of Taiwan runs north to south along the length of the island transecting the study area. Samples were collected from thirteen drainages: eight on the western side of the Central Range and five on the eastern side. Thirty-four terraces ranging in height from 350 – 4 m were included in this study spanning a wide temporal range.

3.4. METHODS

In order to understand linkages between climate and terrace deposition, I collected thirty-seven luminescence samples from thirteen drainages in southern Taiwan along the eastern and western side of the Central Range. Luminescence dating provides the age

sediment was last exposed to sunlight and therefore, luminescence dating of terrace deposits represents the age of terrace deposition rather than terrace formation, or abandonment caused by river incision. Either aggradation or valley widening forms terraces, both of which signal unsteadiness in an overall pattern of river incision. Terraces sampled in this study appear to be fill terraces likely caused by increased sediment supply, so ages derived for terrace sediment correspond with periods of increased sediment supply. Research test the hypothesis that increased EASM intensity triggers increased hillslope denudation resulting in aggradation and terrace deposition.

Terraces sampled ranged from 350 – 4 m in height with sampling skewed towards lower, younger terraces due to accessibility and likelihood of preservation. Lower terraces were often more accessible than higher terraces that were unable to be sampled due to either anthropogenic reinforcement or dense vegetation. Higher, and likely older, terraces are less common on the landscape, as older landscape features are less likely to preserved (Sadler, 1981). It is interpreted that the widespread preservation of similar aged terraces reflects a widespread terrace deposition event.

3.4.1. LUMINESCENCE DATING

Terrace deposits were dated using luminescence dating, a widely applied method for dating Quaternary sediment deposits (Rhodes, 2011). Optically stimulated luminescence (OSL) dating of quartz (Huntley et al., 1985) and infrared stimulated luminescence (IRSL) dating of potassium feldspar (Hütt et al., 1988) provide an age estimate for the last time sediment was exposed to sunlight. Following deposition, the minerals acquire a luminescence signal due to exposure of ionizing radiation from K, Rb,

Th, and U in the surrounding sediments, plus a small contribution from incident cosmic radiation. Electrons produced from ionizing radiation can be stored in defects (traps) in the crystal lattice. The radioactivity of the sounding sediments is known as the environmental dose rate (D_R). When the sediment is exposed to sunlight, there is sufficient energy to evict electrons from these traps and a photon of light is emitted when the electron recombines at a lower energy state, producing luminescence. In a laboratory setting, the equivalent dose (D_E) is calculated by measuring the amount of radiation required to replicate the natural luminescence signal. OSL/IRSL ages are determined by dividing the equivalent dose (D_E) by the environmental dose rate (D_R).

IRSL dating of feldspar can often be favored over OSL dating of quartz in tectonically active landscapes. Quartz requires more cycles of deposition, dose accumulation, and bleaching than feldspar in order to acquire a strong luminescence signal necessary to calculate accurate luminescence ages (Preusser et al., 2006; Pietsch et al., 2009). IRSL dating of feldspar can be more suitable in younger, tectonically active landscapes because it does not require a long sedimentary history of bleaching and transport to produce a high intensity signal (Godfrey-Smith et al., 1988; Preusser et al., 2006). However, OSL dating is often preferred over IRSL dating as quartz bleaches faster than feldspar and is not subject to anomalous fading, or signal loss with time, which can produce age underestimates (Godfrey-Smith et al., 1988; Wallinga, 2002; Lawson et al., 2012).

Drainages from both east and west side of the Central Range were sampled. Deposits with fluvial bedding structures and limited bioturbation were preferentially sampled. Samples were collected by pounding a steel pipe into sand lenses when

possible. In the case where no sand lens was present, samples were taken from a sandy matrix underneath a lightproof tarp. In both cases, the sediment around the sample was collected to measure the environmental dose rate. Water content samples were collected in an airtight container where possible. At some locations, the sediments were too coarse to collect water content sample, in those locations, an average water content value was used.

Samples were processed and analyzed at the Utah State University Luminescence Laboratory using the single-aliquot regenerative-dose (SAR) protocol for OSL quartz (Murray and Wintle, 2000) and IRSL dating of potassium feldspar (Wallinga, 2002). Samples collected from terraces <50 m above the channel were dated using OSL, while samples from terraces >50 m were dated using IRSL. The dose-response curve of feldspar can grow to much higher doses than those of quartz extending the dating range of feldspar by a factor of 4-5 compared to OSL dating of quartz (Buylaert et al., 2012). IRSL measurements were carried out at 50C and were corrected for anomalous fading, loss of signal with time (Huntley and Lamothe, 2001; Auclair et al., 2003). Dose rates were calculated using inductively coupled plasma mass spectrometry (ICP-MS) and inductively coupled plasma atomic emission spectra (ICP-AES) to determine the elemental concentration of radiogenic elements (U, Th, K, Rb) surrounding the sample and convert to dose rate following the conversion factors of Guérin et al. (2011). The cosmic contribution to dose rate was determined following Prescott and Hutton (1994). The dose rate was then corrected for attenuation from water content and grain-size (Aitken, 1998; Brennan, 2003). Depositional ages were calculated by dividing the equivalent dose by the dose rate.

3.5. RESULTS

In order to test for temporal and spatial patterns in the terrace deposition, terraces age were classified into similar-age groups that represent regional periods of terrace deposition. Of the thirty-four terraces sampled in this study, nineteen terraces were determined to be Holocene in age, and fifteen were late Pleistocene in age. Periods of regional terrace deposition were defined as at least two terraces from separate drainages that overlap in age within 1σ error. Many Pleistocene terrace groupings are based on two terraces while Holocene groupings are based 3-8 terraces. While Pleistocene groupings have a smaller population number than Holocene groupings, Pleistocene groupings are still considered to be significant because their preservation on the landscape. Pleistocene deposits were likely part of a widespread sediment deposition period, which time has erased as they were deposited much earlier than Holocene deposits. Additionally, terrace sampling was opportunistic, biased towards samples accessible by road cuts and from the modern channel, which often did not include higher, and likely older, terraces

Table 3.3 Periods of regional terrace deposition

Grouping	Sample ID	USU ID	Age* (ka)			Terrace Height	Basin ID	Basin Name
1 ka Period								
	TWS-2	2073	0.94	±	0.24	4	6W	Fengshang
	TWN-4	2828	1.7	±	0.5	5	4W	Lili
	TWN-26	3002	1.3	±	0.3	4	8W	Mudan
5 ka Period								
	TWN-17	2993	4.8	±	1	6	7W	Fengkang
	TWN-30	3343	3.6	±	0.7	13	1W	Ailiao
	TWN-9	2985	4.9	±	0.8	18	3W	Linpien
	TWN-8	2832	3.9	±	0.8	10	6W	Fengshang
	TWN-1	2825	4.7	±	0.8	27	1W	Ailiao
8 ka Period								
	TWN-25	3001	8.3	±	1.1	40	1E	Taimali
	TWN-6	2830	8.1	±	1.5	17	3E	Dachu
	TWN-12	2988	7.5	±	1.3	25	5W	Shauimang
	TWN-15	2991	7.1	±	0.9	27	1W	Ailiao
11 ka Period								
	TWN-11	2987	11	±	1.8	8	5W	Shauimang
	TWN-5	2829	11.5	±	1.7	17	5W	Shauimang
	TWS-3	2074	11.6	±	1.8	2	5E	Anshuo
	TWN-23	2999	11.5	±	1.7	43	3E	Dachu
	TWN-18	2994	11.9	±	4.3	11	7W	Fengkang
	TWN-16	2992	12	±	2.4	6	6W	Fengshang
	TWN-20	2996	10.1	±	1.5	15	3E	Dachu
	TWN-10	2986	12.3	±	2.4	56	3W	Linpien
18 ka Period								
	TWN-22	2998	18	±	2.4	63	3E	Dachu
	TWN-21	2997	18	±	2.4	45	3E	Dachu
	TWN-19	2995	18	±	2.7	27	4E	Dawu
28 ka Period								
	TWN-13	2989	25.9	±	3.4	32	4W	Lili
	TWN-28	3341	28	±	4.1	27	3W	Linpien

Grouping	Sample ID	USU ID	Age* (ka)			Terrace Height	Basin ID	Basin Name
~40 ka								
	TWN-29	3342	39	±	3.7	22	2W	Wanan
	TWN-27	3340	35	±	8.8	107	4W	Lili
	TWN-24	3000	41	±	7.7	51	2E	Chinlum
	TWN-33	3346	39	±	9.7	52	1W	Ailiao
50 ka								
	TWN-32	3345	49	±	7.9	42	1W	Ailiao
	TWN-31	3344	48	±	12	91	1W	Ailiao
60 ka Period								
	TWN-7	2831	58	±	6	33	2E	Chinlum
~ 90 ka								
	TWN-2*	2826	88	±	11	350	1W	Ailiao
	TWN-3*	2827	95	±	15	350	1W	Ailiao
~ 170 ka								
	TWS-4	2075	166	±	18	190	1W	Ailiao

Samples were collected from thirteen drainages, which have been assigned a basin ID based on their geographic position (Figure 3.3). Samples are identified as E or W, representing their position on the east or west side of the Central Range, respectively. The number preceding E or W is an indicator of their N-S position with the lowest numbers representing the drainages farthest to the north. For example, W1 represents the farthest north drainage on the west side, while E5 represents the farthest south drainage on the east side.

3.5.1. HOLOCENE TERRACES

Terraces were deposited in the Holocene during four main regional periods at ~1, 4-5, ~8, and 11 ka. The youngest terraces (TWN-4, TWN-26, TWS-2, see Table 3.3)

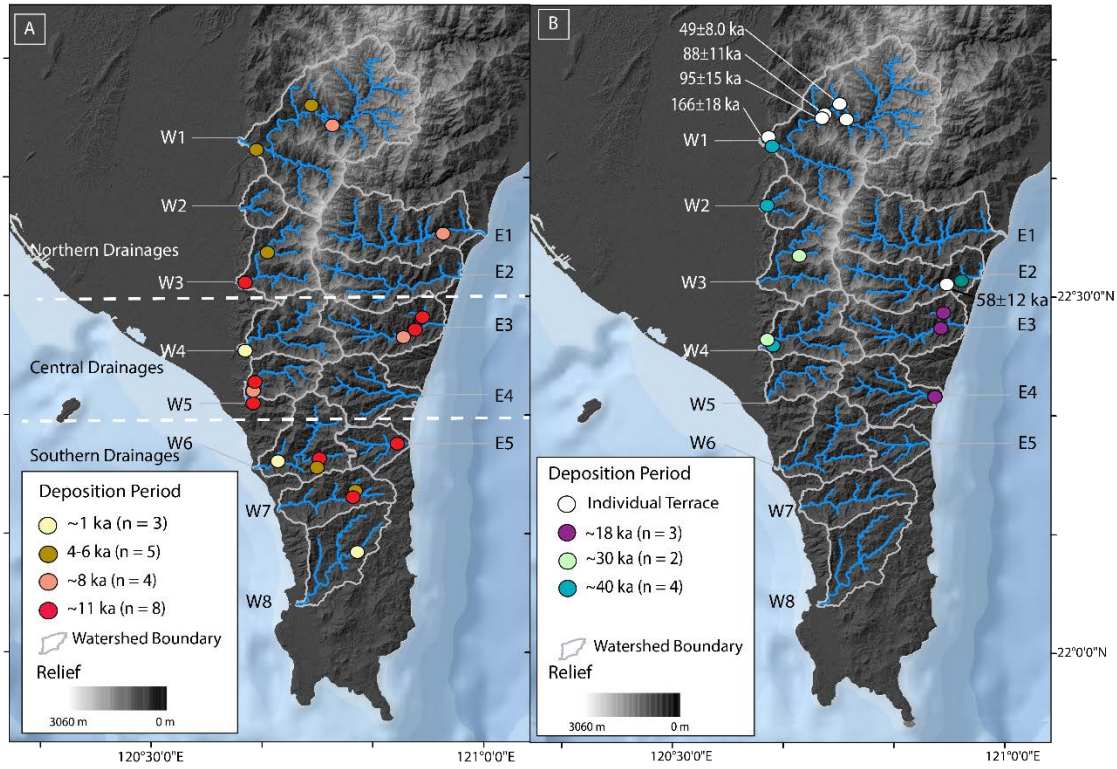

Figure 3.3 Map of regional periods of terrace deposition. (A) Locations of terraces sampled in this study dated to the Holocene. (B). Sample site locations dating to the Pleistocene

were deposited at ~ 1 ka in the Lili (4W), Fengshang (6W) and Mudan (8W) drainages. These terraces ranged in height from 4 – 5 m above the modern channel with no bedrock exposed below the terrace alluvium or under the modern valley fill, suggesting no bedrock incision since terrace formation. Five terrace deposits were dated between 4 - 5 ka (TWN-17, TWN-1, TWN-30, TWN-9, TWN-8, see Table 3.3). These samples were collected from four different drainages with three of the samples coming from the Ailiao (1W) drainage from terraces 13 –27 m above the modern channel. The remaining samples in the 4 – 5 ka grouping were collected in the Fengkang (7W), Fengshang (6W), and Linpien (3W) drainages from 6, 10, and 18 m terraces, respectively. Four terraces (TWN-

12, TWN-25, TWN-15 and TWN-6) were dated to ~8 ka (see Table 3.3). These samples were collected from the Dachu (3E), Shauimang (5W), Ailiao (1W), and Taimali (1E), drainages from 17, 25, 27, and 40 m terraces, respectively. Seven terraces (TWN-16, TWN-11, TWN-5, TWS-3, TWN-23, TWN-18, TWN-10 and TWN-20) date to the Holocene-Pleistocene transition around ~11 ka (Table 3.3). These samples were taken from seven different drainages on the east and west side of the Central Range. Samples were collected from the Ailiao (1W), Linpein (3W), Shaimang (5W), Fengshang (6W) and Fengkang (7W) drainages on the western side of the Central Range and Dachu (3E) and Anshou (5E) drainages on the eastern side of the Central Range. Terrace heights ranged from 2 – 43 m. The 2 m terrace yielding an age of 11.5 ± 3.4 ka was taken from the southern-most drainage in the study area, the Anshou. The period of terrace development at the Holocene-Pleistocene transition has the largest population of terrace deposits.

3.5.2. PLEISTOCENE TERRACES

This study found three periods of regional periods of terrace development during the late-Pleistocene. Three terraces (TWN-22, TWN-21, and TWN-19) with ages of deposition at 18 ka were sampled along the Dawu (4E) and Dachu (3E) rivers, adjacent drainages on the eastern side of the Central Range. TWN-19 was sampled in the Dawu drainages from a 27 m terrace, TWN-22 and TWN-21 were both taken in the Dachu drainage from 63 and 45 m terraces. Two samples (TWN-13 and TWN-28) were collected from terrace deposits dated to 28 ka. These terraces were located in the Linpien (3W) and Lili (4W) drainages from a 27 m terrace and a 32 m terrace, respectively. Four terraces (TWN-29, TWN-27, TWN-24, and TWN-33) collected from the Wanan (2W),

Lili (4W), Chinlum (2E), and Ailiao (1W) date to ~ 40 ka. These samples were taken from terraces ranging from 22 – 107 m in elevation above the modern channel.

There are no periods of regional terrace deposition recorded in terraces that date >40ka. Two terraces were deposited in the Ailiao drainage around 50 ka, but this grouping does not qualify as a regional period of terrace deposition, as samples were collected from only one drainage, the Ailiao. TWN-2 and TWN-3 were collected from the same 350 m terrace in the Ailiao (1W) drainage. The oldest terrace sampled in this study is a 190 m terrace in the Ailiao drainage. IRSL dating of this terrace yields an age of 166 ± 32 ka. There is only one sample collected outside of the Ailiao drainage (1W) that produced an age outside of a regional period of terrace development. TWN-29 was collected in the Wanan drainage (2W) from a 22 m terrace and yields an age of 39 ± 7.4 ka.

3.6. DISCUSSION

Thirty-four terraces were dated to determine periods of regional terrace deposition to test for the role of climate and sediment supply in drainage development in southern Taiwan. The identified periods of terrace deposition were compared to other mass-wasting and climate records to test if increased hillslope denudation due to strong EASM intensity can be recorded in river terrace formation. These data were used to test the hypothesis that terrace deposition in southern Taiwan is linked to periods of enhanced EASM rainfall due to linkage with increased hillslope erosion and channel aggradation. If EASM cycles control terrace deposition, terrace deposition periods would coincide with 20 kyr cycles of EASM intensity driven by precession in Earth's orbit. If there is no

linkage between EASM intensity, terraces could have been deposited stochastically as a result of other processes that stall river incision such as increased seismicity or singular storm events.

3.6.1. HOLOCENE CLIMATE AND TERRACES

Terraces yielding Holocene ages appear to have been deposited in four distinct regional periods of terrace deposition at 1, 4-5, 8, and 11 ka. Pollen records show the late-Holocene climate of Taiwan was defined by a dry period from 2-4 ka followed by increased in EASM precipitation in last 2 kyr (Liew et al., 2006). Luminescence ages from TWN-4, TWN-26 and TWS-2 show terrace deposition around 1 ka. Mass-wasting events dated with ^{14}C show increased hillslope activity around 1.3 ka BP in the Pa-Chang River, Huangtung Coast and Chen-yeo-lan River (Hsieh and Chyi, 2010; Hsieh et al., 2011, 2014). Paleoclimate records from Taiwan show increased precipitation in the past 2 kyr suggesting increased precipitation is linked with this period of terrace aggradation (Ding et al., 2020).

Regional periods of terrace deposition at 4-5 ka and 8 ka are not coincident with periods of strengthened EASM activity, as the climate of the mid-Holocene was marked by a weak EASM interval (Hsieh et al., 2014). Mass-wasting studies do not show increased hillslope activity around 4-5 ka (Hsieh and Chyi, 2010; Hsieh et al., 2011, 2014; Figure 3.4). Landslide deposits yielding ages of 8.9-9.5 cal ka BP in the Chen-yeo-lan River in central-south Taiwan and 8.7-9.4 cal ka BP in the Pa-Chang River in southwestern Taiwan suggest that hillslope activity did increase around the 8 ka period of regional terrace deposition (Hsieh and Chyi, 2010; Hsieh et al., 2011, 2014). Mass-

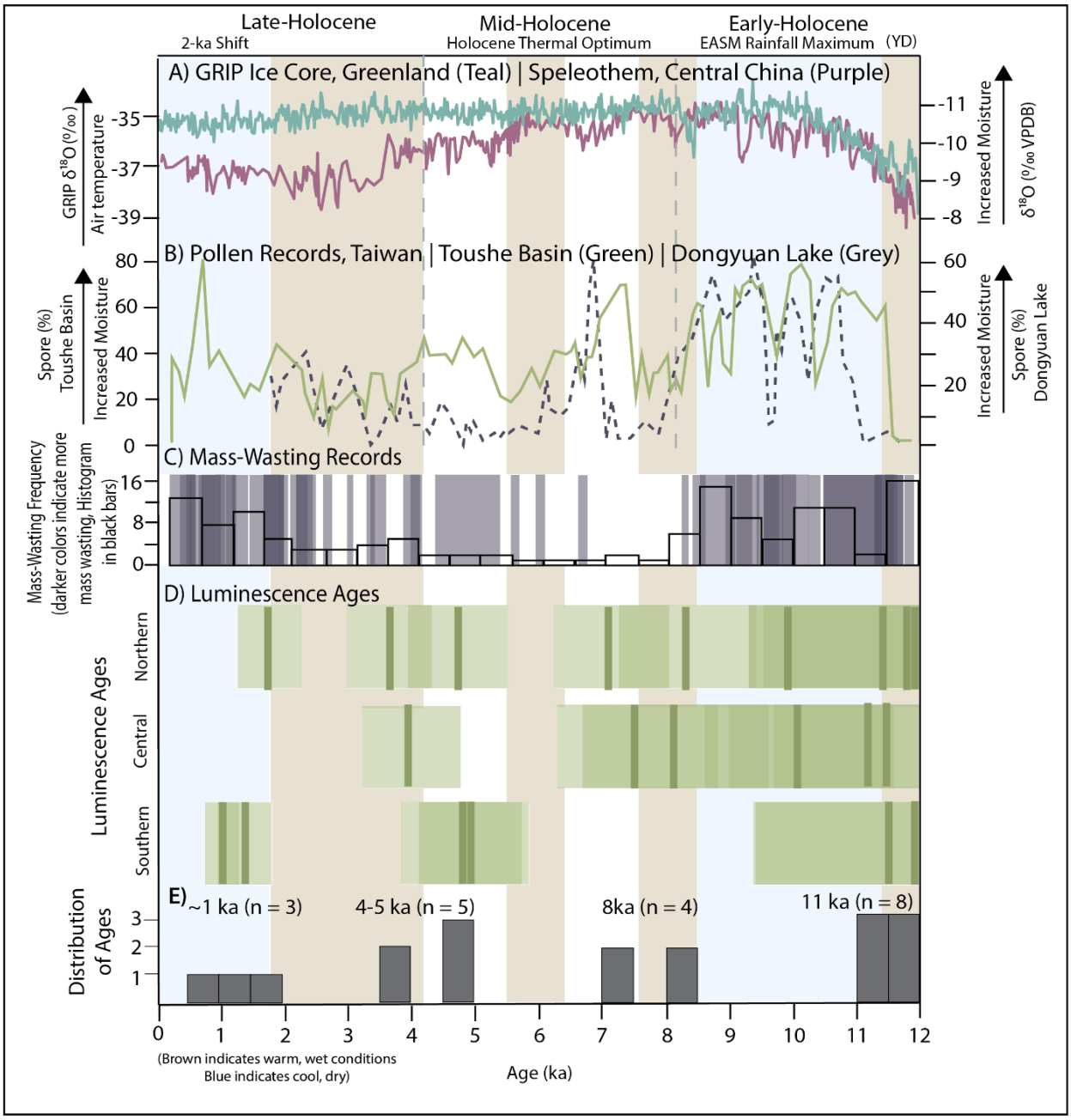

Figure 3.4 Holocene terrace deposition compared with paleoclimate records. A) Temperature Proxy (δ18O (0/00)) records from the GRIP Ice Core, Greenland (blue) (Vinther et al., 2009) and Speleothem precipitation proxy records (δ18O (0/00 VPDB)) records (purple) (Cheng et al., 2009). B) Percentage of spores indicating wet conditions from the Toushe Basin (green) (Liew et al., 2006) and Dongyuan Lake (dashed grey) (Lee and Liew, 2010). C) Mass Wasting records derived from 14C dating (Hsieh and Chyi, 2010; Hsieh et al., 2011, 2012, 2014) D) Luminescence ages from this study. Results are separated into northern drainages (Ailiao, Wanan, Linpien, Taimali, Linpien), middle drainages (Lili, Shuaimang, Dachu, Dawu), and southern drainages (Fangshang, Fengkang, Mudan, Anshuo). E) Histogram of the central point of age distribution displayed in dark grey.

wasting events can be triggered by large precipitation events (Trauth et al., 2003; Hsieh et al., 2012) but can also be caused by non-climatic processes such as seismicity (Hsieh and Chyi, 2010; Hsieh et al., 2011, 2014). The widespread spatial extent of terrace deposition during both of these time periods suggest that the mechanism triggering aggradation affected a large (50 – 70 km) transect of southern Taiwan.

The largest grouping of terraces identified in this study were deposited at 11 ka. Seven terraces from five different drainages yielded ages corresponding with the Holocene-Pleistocene boundary. Paleoclimate records show the Holocene EASM rainfall maximum occurred during the early Holocene. Records from Taiwan show increased mass-wasting events during the Holocene EASM rainfall maximum corresponding with increased terrace development during this period. Periods of regional terrace formation that align with periods of increased mass-wasting and strong EASM intensity, indicate hillslope denudation resulting from high precipitation rates can leave lasting landforms (Lee et al., 2010; Hsieh et al., 2014; Ding et al., 2020). Evidence from recent typhoon Morakot (2009) suggests that, while water supply also increases during periods of intensified precipitation, the increase in sediment supply from mass-wasting events exceeds the capacity of the increased precipitation to remove the sediment, resulting in large aggradation events. Terrace deposition around 4-5 ka and 8 ka does not correlate with periods of increased precipitation suggesting that climate is not the only factor causing widespread aggradation.

3.6.2. PLEISTOCENE CLIMATE AND TERRACES

Periods of regional terrace deposition linked to climate are also evident during the Pleistocene expanding the current record or landscape response the Holocene which has been limited by the time constraints of radiocarbon dating (~40 ka) (Figure 3.5). Seventeen terraces sampled in this study were deposited during the Pleistocene, revealing periods of regional terrace deposition at 18, 28, and 40 ka. Regional periods of terrace deposition appear to coincide with the rising and falling limbs of EASM intensity. Terrace deposition at 18 ka correlates with a period of increased mass-wasting observed in central Taiwan (Hsieh and Chyi, 2010a). Terraces deposited at 18 ka were in adjacent drainages suggesting that they may have been deposited due to a localized storm event or earthquake. However, speleothem and loess records from China do show increased moisture and EASM intensity around 18 ka, indicating that terrace deposition around 18 ka corresponds with increased moisture (Guo et al., 2000, 2009; Cheng et al., 2009). Periods of deposition at 28 and 40 ka exceed mass-wasting records, but correlate with periods of intermediate EASM intensity (Guo et al., 2000, 2009; Cheng et al., 2009).

One terrace deposited at ~60 ka was deposited in the Chinlum drainage (2E) and terraces were deposited in the Ailiao drainage (1W) at ~50, ~90, and ~166. These terrace deposition periods do not meet the criteria for a period of regional terrace deposition, because they do not correlate with terraces found in other drainages. It is possible that they were part of a widespread period of terrace deposition that has since been removed from the landscape or was not captured by samples collected in this study. Another explanation for terrace preservation in the northern drainages is the valley geometry, which is more conducive to both the formation and preservation of terraces. Steeper

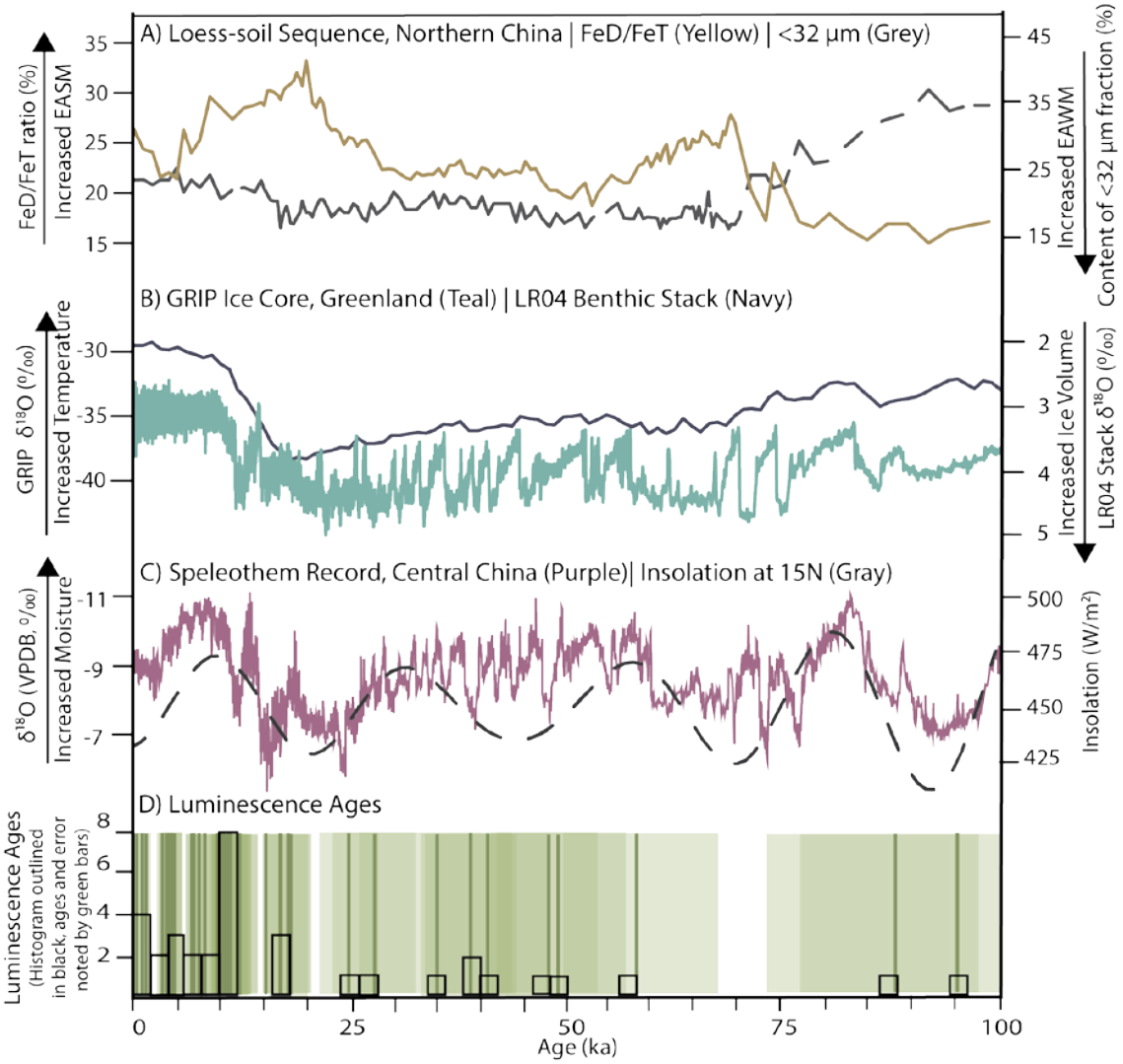

Figure 3.5 Pleistocene terrace deposition compared to paleoclimate records. A) Loess Plateau records from Xifeng (Guo et al., 2000, 2009). Chemical weathering index (FeD/FeT) ratio (grey dashed) which is an indicator of EASM monsoon strength and content of >32µm fraction (%) (yellow), an East Asian Winter Monsoon (EAWM) indicator. B) Temperature Proxy (δ18O (0/00)) records from the GRIP Ice Core, Greenland (blue) (Johnsen et al., 1997). Ice volume proxy (δ18O (0/00)) from the LR04 Stack (Lisiecki and Raymo, 2005). C) Mid-month July insolation (W/m2) at 15N (dashed silver) (Rachmayani et al., 2016). Speleothem records (purple) from the Dongge and Sanbao caves in Central China (Cheng et al., 2009). D) Luminescence results from this study. Ages with 1σ error reported in green boxes. Overlapping ages appear darker. Histogram of age distribution displayed in dark grey.

hillslopes are more prone mass-wasting events, causing large aggradation events and leaving behind terraces as the river begins to incise back into the valley fill.

Regional periods of terrace deposition aligned with periods of intermediate EASM intensity at 18, 28, and 40 ka the cyclicity of EASM intensity does play a role in terrace deposition. The initial hypothesis of this study was periods of terrace deposition would correlate with 20 kyr cycles of maximum EASM intensity. However, we see terrace deposition occurring during transitional periods of solar insolation and EASM intensity during the Pleistocene. This could be because the ITCZ is positioned north of Taiwan during maximums in solar insolation and therefore EASM intensity. Speleothem and Loess records showing precipitation maximized during peak insolation levels reflect the climate at latitudes farther north than Taiwan. The most rainfall may be delivered to Taiwan during intermediate insolation periods as the ITCZ shifts over Taiwan as it moves northward when insolation intensifies and southward again as wanes. While terrace deposition periods recorded in this study do not correlated with EASM maximums as predicted, they do appear to correlate with cyclic insolation levels. This may suggest that increased precipitation caused by the ITCZ shifting over Taiwan accelerates hillslope activity causing regional aggradation, which interrupts river incision. When hillslope activity slows as the climate dries, rivers begin incising again leaving behind markers of past climate.

3.6.3. IMPLICATIONS FOR LANDSCAPE RESPONSE TO CLIMATE

Large mass-wasting events triggered by stochastic events such as typhoons and earthquakes have the potential to leave lasting impacts on the landscape (Dadson et al.,

2003; Yanites et al., 2018). The Chi-Chi earthquake (M_w7.6, 1999) caused 9,272 landslides, the majority of which were within a ~20 km radius of the epicenter, but landslides occurred as far as 60-70 km away (Khazai and Sitar, 2004). Paleoseismic records from southern Taiwan suggest that earthquakes of a similar magnitude occur with a recurrence intervals reported in centuries (Chen et al., 2007; Yen et al., 2008). Holocene terrace deposition periods at 1 ka and 11 ka align with periods of increased EASM intensity, but periods at 4-5 and 8 ka appear to occur during drier periods. It is possible that deposition periods at 4-5 ka and 8 ka are the result of large aggradation events triggered by large landslides. Large earthquake events can cause widespread aggradation, but the spatial distribution of Holocene terrace deposits is larger than would be expected because of seismicity, as mass-wasting rates decrease steeply away from the epicenter. The magnitude of aggradation necessary to cause a regional terrace deposition event suggests that regional mechanisms like climate are a more likely trigger than more localized events such as seismicity.

Individual precipitation events like Typhoon Morakot (2009) can also cause widespread aggradation. Typhoon Morakot triggered 22,705 landslides along a ~70 km transect of southern Taiwan. Sediment deposited by Morakot-induced landslides is estimated to take centuries to evacuate (DeLisle, unpublished). Typhoon intensity increases with EASM intensity. Terrace deposition events introduced in this study may be the result of singular storm events, the frequency of which increase during of strong EASM. Aggradation may also be the be the result of increased denudation rates region-wide due to increased precipitation during periods of EASM intensity. In either case,

correlation between EASM intensity and terrace deposition shows that climate is a dominant factor controlling patterns of river incision in southern Taiwan.

In contrast to the assumption that bedrock rivers in active orogens such as Taiwan meet ‘steady-state’ conditions (Ouimet et al., 2009; Cyr et al., 2010; DiBiase et al., 2015), the presence of terraces in southern Taiwan represents unsteadiness in river incision implying that uplift is not the only factor controlling incision rates. Research results suggest that climate heavily influences rates of river incision in southern Taiwan. Periods of regional terrace deposition at 1, 11, 18, 28, and 40 ka align with paleoclimate records showing increased moisture and EASM intensity supporting the hypothesis that terrace deposition in Taiwan is linked to climate (Figure 3.4 and Figure 3.5). However, regional terrace deposition at 4-5 and 8 ka during periods of weak EASM intensity reveal that other mechanisms, such as seismicity, may also play a role in widespread aggradation events.

3.7. CONCLUSION

In this study, terrace deposits throughout the Central Range in southern Taiwan were dated to test the linkage between terrace deposition and climate. Periods of regional terrace deposition coinciding with periods of increased EASM intensity suggest there is a strong linkage between increased precipitation and river aggradation. Widespread terrace deposition corresponding with EASM intensity occurred at 1 ka and 11 ka during the Holocene and 18, 28, and 40 ka during the Pleistocene. Results from this study show that climate-caused aggradation is temporarily able to interrupt tectonic-driven river incision. Pollen and mass-wasting deposits have been used to construct paleoclimate records in

Taiwan, but are limited to the 40 ka limit of radiocarbon dating. Results of this study provide a new record of landscape response to EASM intensity extending past 40 ka. While hillslope activity in Taiwan has been shown to increase during periods of increased EASM intensity, this study shows that EASM intensity is also recorded in terrace formations.

3.8. REFERENCES

Aitken, M.J., 1998, An Introduction to Optical Dating: The dating of Quaternary sediments by the use of photon-stimulated luminscence: New York, Oxford University Press, 267 p.

An, Z. et al., 2015, Global Monsoon Dynamics and Climate Change: Annual Review of Earth and Planetary Sciences, v. 43, p. 29–77, doi:10.1146/annurev-earth-060313-054623.

An, Z., 2000, The history and variability of the East Asian paleomonsoon climate: Quaternary Science Reviews, v. 19, p. 171–187, doi:10.1016/S0277-3791(99)00060-8.

An, Z., Kukla, G.J., Porter, S.C., and Xiao, J., 1991, Magnetic susceptibility evidence of monsoon variation on the Loess Plateau of central China during the last 130,000 years: Quaternary Research, v. 36, p. 29–36, doi:10.1016/0033-5894(91)90015-W.

Auclair, M., Lamothe, M., and Huot, S., 2003, Measurements of anomalous fading for feldspar IRSL using SAR: Radiation Measurements, v. 37, p. 487–492.

Beaumont, C., Fullsack, P., and Hamilton, J., 1992, Erosional control of active compressional orogens: Thrust Tectonics, p. 1–18.

Bender, A.M., Lease, R.O., Corbett, L.B., Bierman, P.R., Caffee, M.W., and Rittenour, T.M., 2020, Late Cenozoic climate change paces landscape adjustments to Yukon River capture: Nature Geoscience, v. 13, p. 571–575, doi:10.1038/s41561-020-0611-4.

Bintanja, R., van de Wal, R.S.W., and Oerlemans, J., 2005, Modelled atmospheric temperatures and global sea levels over the past million years: Nature, v. 437, p. 125–128.

Brennan, B.J., 2003, Beta doses to spherical grains: Radiation Measurements, v. 37, p. 299–303.

Burbank, D.W., Leland, J., Fielding, E., Anderson, R.S., Brozovic, N., Reid, M.R., and Duncan, C., 1996, Bedrock incision, rock uplift and threshold hillslopes in the northwestern Himalayas: Nature, v. 379, p. 505–511.

Buylaert, J.P., Jain, M., Murray, A.S., Thomsen, K.J., Thiel, C., and Sohbati, R., 2012, A robust feldspar luminescence dating method for Middle and Late Pleistocene sediments: Boreas, v. 41, p. 435–451.

Central Weather Bureau, 2020, Climate Statistics, https://www.cwb.gov.tw/V8/C/C/Taiwan/index.html (accessed August 2020).

Chen, W.-S. et al., 2007, Late Holocene Paleoseismicity of the Southern Part of the Chelungpu Fault in Central Taiwan: Evidence from the Chushan Excavation Site: Bulletin of the Seismological Society of America, v. 97, p. 1–13, doi:10.1785/0120050161.

Chen, C.W., Saito, H., and Oguchi, T., 2015a, Rainfall intensity - duration conditions for mass movements in Taiwan: Progress in Earth and Planetary Science, v. 2, doi:https://doi.org/10.1186/s40645-015-0049-2.

Chen, R., Shen, J., Li, C., Zhang, E., Sun, W., and Ji, M., 2015b, Mid- to late-Holocene East Asian summer monsoon variability recorded in lacustrine sediments from Jingpo Lake, Northeastern China: The Holocene, v. 25, p. 454–468, doi:10.1177/0959683614561888.

Chen, C., Willett, S.D., West, A.J., Dadson, S., Hovius, N., Christl, M., and Shyu, J.B.H., 2020, The impact of storm-triggered landslides on sediment dynamics and catchment-wide denudation rates in the southern Central Range of Taiwan following the extreme rainfall event of Typhoon Morakot: Earth Surface Processes and Landforms, v. 45, p. 548–564, doi:10.1002/esp.4753.

Cheng, H. et al., 2016, The Asian monsoon over the past 640,000 years and ice age terminations: Nature, v. 534, p. 640–646, doi:10.1038/nature18591.

Cheng, H., Edwards, R.L., Broecker, W.S., Denton, G.H., Kong, X., Wang, Y., Zhang, R., and Wang, X., 2009, Ice Age Terminations: Science, v. 326, p. 248–252, doi:10.1126/science.1177840.

Ching, K.-E., Hsieh, M.-L., Johnson, K.M., Chen, K.-H., Rau, R.-J., and Yang, M., 2011, Modern vertical deformation rates and mountain building in Taiwan from precise leveling and continuous GPS observations, 2000–2008: Journal of Geophysical Research, v. 116, p. B08406, doi:10.1029/2011JB008242.

Cowie, P.A., Whittaker, A.C., Attal, M., Roberts, G., Tucker, G.E., and Ganas, A., 2008, New constraints on sediment-flux–dependent river incision: Implications for extracting tectonic signals from river profiles: Geology, v. 36, p. 535, doi:10.1130/G24681A.1.

Cyr, A.J., Granger, D.E., Olivetti, V., and Molin, P., 2010, Quantifying rock uplift rates using channel steepness and cosmogenic nuclide–determined erosion rates:

Examples from northern and southern Italy: Lithosphere, v. 2, p. 188–198, doi:10.1130/L96.1.

Dadson, S.J. et al., 2003, Links between erosion, runoff variability and seismicity in the Taiwan orogen: Nature, v. 426, p. 648–651, doi:10.1038/nature02150.

Derrieux, F., Siame, L.L., Bourlès, D.L., Chen, R.-F., Braucher, R., Léanni, L., Lee, J.-C., Chu, H.-T., and Byrne, T.B., 2014, How fast is the denudation of the Taiwan mountain belt? Perspectives from in situ cosmogenic 10Be: Journal of Asian Earth Sciences, v. 88, p. 230–245, doi:10.1016/j.jseaes.2014.03.012.

DiBiase, R.A., Whipple, K.X., Heimsath, A.M., and Ouimet, W.B., 2010, Landscape form and millennial erosion rates in the San Gabriel Mountains, CA: Earth and Planetary Science Letters, v. 289, p. 134–144, doi:10.1016/j.epsl.2009.10.036.

DiBiase, R.A., Whipple, K.X., Lamb, M.P., and Heimsath, A.M., 2015, The role of waterfalls and knickzones in controlling the style and pace of landscape adjustment in the western San Gabriel Mountains, California: Geological Society of America Bulletin, v. 127, p. 539–559, doi:10.1130/B31113.1.

Dietrich, W.E., Bellugi, D.G., Sklar, L.S., Stock, J.D., Heimsath, A.M., and Roering, J.J., 2003, Geomorphic Transport Laws for Predicting Landscape form and Dynamics, *in* Wilcock, P.R. and Iverson, R.M. eds., Geophysical Monograph Series, Washington, D. C, American Geophysical Union, p. 103–132, doi:10.1029/135GM09.

Ding, Y., and Chan, J.C.L., 2005, The East Asian summer monsoon: an overview: Meterology and Atmospheric Physics, v. 89, p. 117–142.

Ding, X., Zheng, L., Zheng, X., and Kao, S.J., 2020, Holocene East Asian Monsoon Rainfall Variability in Taiwan: Frontiers in Earth Science, v. 8, doi:doi: 10.3389/feart.2020.00234.

Dörschner, N., Reimann, T., Wenske, D., Lüthgens, C., Tsukamoto, S., Frechen, M., and Böse, M., 2012, Reconstruction of the Holocene coastal development at Fulong Beach in north-eastern Taiwan using optically stimulated luminescence (OSL) dating: Quaternary International, v. 263, p. 3–13, doi:10.1016/j.quaint.2011.12.009.

Duvall, A., 2004, Tectonic and lithologic controls on bedrock channel profiles and processes in coastal California: Journal of Geophysical Research, v. 109, p. F03002, doi:10.1029/2003JF000086.

Fellin, M.G., Chen, C.-Y., Willett, S.D., Christl, M., and Chen, Y.-G., 2017, Erosion rates across space and timescales from a multi-proxy study of rivers of eastern Taiwan: Global and Planetary Change, v. 157, p. 174–193, doi:10.1016/j.gloplacha.2017.07.012.

Finnegan, N.J., and Dietrich, W.E., 2011, Episodic bedrock strath terrace formation due to meander migration and cutoff: Geology, v. 39, p. 143–146, doi:10.1130/G31716.1.

Finnegan, N.J., Pazzaglia, F.J., and Finnegan, S., 2014, A signature of transience in bedrock river incision rates over timescales of 10^4–10^7 years: Nature, v. 505, p. 391–394.

Gallen, S.F., Pazzaglia, F.J., Wegmann, K.W., Pederson, J.L., and Gardner, T.W., 2015, The dynamic reference frame of rivers and apparent transience in incision rates: Geology, v. 43, p. 623–626, doi:10.1130/G36692.1.

Godfrey-Smith, D.I., Huntley, D.J., and Chen, W.-H., 1988, Optical dating studies of quartz and feldspar sediment extracts: Quaternary Science Reviews, v. 7, p. 373–380, doi:10.1016/0277-3791(88)90032-7.

Goldsmith, Y., Broecker, W.S., Xu, H., Polissar, P.J., deMenocal, P.B., Porat, N., Lan, J., Cheng, P., Zhou, W., and An, Z., 2017, Northward extent of East Asian monsoon covaries with intensity on orbital and millennial timescales: Proceedings of the National Academy of Sciences, v. 114, p. 1817–1821, doi:10.1073/pnas.1616708114.

Guérin, G., Mercier, N., and Adamiec, G., 2011, Dose-rate conversion factors: update: v. 29, p. 4.

Guo, Z., Berger, A., Yin, Q.Z., and Qin, L., 2009, Strong asymmetry of hemispheric climates during MIS-13 inferred from correlation Chine loess and Antartica ice records: Climate of the Past, v. 5, p. 21–31.

Guo, Z., Biscaye, P., Wei, L.Y., Chen, X.H., Peng, S.Z., and Liu, T.S., 2000, Summer monsoon variations over the last 1.2 Ma from the weathering of loess-soil sequences in China: Geophysical Research Letters, v. 27, p. 1751–1754.

Hancock, G.S., and Anderson, R.S., 2002, Numerical modeling of fluvial strath-terrace formation in response to osciallting climate: Geological Society of America Bulletin, v. 114, p. 1131–1142.

Hartshorn, K., 2002, Climate-Driven Bedrock Incision in an Active Mountain Belt: Science, v. 297, p. 2036–2038, doi:10.1126/science.1075078.

Ho, C.S., 1986, A synthesis of the geologic evolution of Taiwan: Memoir of the Geological Society of China, v. 7, p. 15–29.

Ho, L.-D., Lüthgens, C., Wong, Y.-C., Yen, J.-Y., and Chyi, S.-J., 2017, Late Holocene cliff-top dune evolution in the Hengchun Peninsula of Taiwan: Implications for palaeoenvironmental reconstruction: Journal of Asian Earth Sciences, v. 148, p. 13–30, doi:10.1016/j.jseaes.2017.08.024.

Hovius, N., Stark, C.P., Hao-Tsu, C., and Jiun-Chuan, L., 2000, Supply and Removal of Sediment in a Landslide-Dominated Mountain Belt: Central Range, Taiwan: The Journal of Geology, v. 108, p. 73–89, doi:10.1086/314387.

Howard, A.D., 1994, A detachment-limited model of drainage basin evolution: Water Resources Research, v. 30, p. 2261–2286.

Hsieh, M.-L., Ching, K.-E., Chyi, S.-J., Kang, S.-C., and Chou, C.-Y., 2014, Late Quaternary mass-wasting records in the actively uplifting Pa-chang catchment, southwestern Taiwan: Geomorphology, v. 216, p. 125–140, doi:10.1016/j.geomorph.2014.03.040.

Hsieh, M.-L., and Chyi, S.-J., 2010a, Late Quaternary mass-wasting records and formation of fan terraces in the Chen-yeo-lan and Lao-nung catchments, central-southern Taiwan: Quaternary Science Reviews, v. 29, p. 1399–1418, doi:10.1016/j.quascirev.2009.10.002.

Hsieh, M.-L., and Chyi, S.-J., 2010b, Late Quaternary mass-wasting records and formation of fan terraces in the Chen-yeo-lan and Lao-nung catchments, central-southern Taiwan: Quaternary Science Reviews, v. 29, p. 1399–1418, doi:10.1016/j.quascirev.2009.10.002.

Hsieh, M.-L., and Knupfer, P.L.K., 2002, Synchroneity and morphology of Holocene river terraces in the southern Western Foothill, Taiwan: A guide to interpreting and correlation erosional river terraces across growing anticlines, *in* Geology and Geophysics of an Arc-Continent Collision, Taiwan, GSA Special Paper 358, p. 55–74.

Hsieh, M.-L., Lai, L.S.-H., Lin, C.D.-J., and Shyu, J.B.H., 2012, Late Quaternary landscape evolution and genesis of the 2009 catastrophic landslide in the Hsiao-lin area, southwestern Taiwan: Geomorphology, v. 179, p. 225–239, doi:10.1016/j.geomorph.2012.08.014.

Hsieh, M.-L., Liew, P.-M., and Chen, H.-W., 2011, Early Holocene catastrophic mass-wasting event and fan-delta development on the Hua-tung coast, eastern Taiwan: Geomorphology, v. 134, p. 378–393, doi:10.1016/j.geomorph.2011.07.012.

Hsu, W.H., Byrne, T.B., Ouimet, W., Lee, Y.H., Chen, Y.G., van Soest, M., and Hodges, K., 2016, Pleistocene onset of rapid, punctuated exhumation in the eastern Central Range of the Taiwan orogenic belt: Geology, v. 44, p. 719–722.

Hu, J.-C. et al., 2007, Fault activity and lateral extrusion inferred from velocity field revealed by GPS measurements in the Pingtung area of southwestern Taiwan: Journal of Asian Earth Sciences, v. 31, p. 287–302, doi:10.1016/j.jseaes.2006.07.020.

Huang, C., and Byrne, T.B., 2014, Tectonic evolution of an active tectonostratigraphic boundary in accretionary wedge: An example from the Tulungwan-Chaochou Fault system, southern Taiwan: Journal of Structural Geology, v. 69, p. 320–333, doi:10.1016/j.jsg.2014.06.007.

Huang, C.C., Pang, J., and Zhao, J., 2000, Chinese loess and the evolution of the east Asian monsoon: Progress in Physical Geography, v. 24, p. 75–96.

Huntley, D.J., Godfrey-Smith, D.I., and Thewalt, M.L.W., 1985, Optical dating of sediments: Nature, v. 313, p. 105–107.

Huntley, D.J., and Lamothe, M., 2001, Ubiquity of anomalous fading in K-feldspars and teh measurements and correction for it in optical dating: Canadian Journal of Earth Sciences, v. 38, p. 1093–1106.

Hütt, G., Jaek, I., and Tchonka, J., 1988, Optical dating: K-feldspars optical response stimulation spectra: Quaternary Science Reviews, v. 7, p. 381–385.

Jaiswal, M.K., Chen, Y.G., Kale, V.S., and Achyuthan, H., 2009, Residual Luminescence in Quartz from Slack Water Deposits in Kaveri Basin, South India: A Single Sliquot Approach: Geochronometria, p. 1–8.

Johnsen, S.J. et al., 1997, The δ^{18} O record along the Greenland Ice Core Project deep ice core and the problem of possible Eemian climatic instability: Journal of Geophysical Research: Oceans, v. 102, p. 26397–26410, doi:10.1029/97JC00167.

Khazai, B., and Sitar, N., 2004, Evaluation of factors controlling earthquake-induced landslides caused by Chi-Chi earthquake and comparison with the Northridge and Loma Prieta events: Engineering Geology, v. 71, p. 79–95.

Kirby, E., and Whipple, K., 2001, Quantifying differential rock-uplift rates via stream profile analysis: , p. 4.

Kutzbach, J.E., Liu, X., Liu, Z., and Chen, G., 2008, Simulation of the evolutionary response of global summer monsoons to orbital forcing over the past 280,000 years: Climate Dynamics, v. 30, p. 567–579, doi:10.1007/s00382-007-0308-z.

Lavé, J., and Avouac, J.P., 2001, Fluvial incision and tectonic uplift across the Himalayas of central Nepal: Journal of Geophysical Research: Solid Earth, v. 106, p. 26561–26591, doi:10.1029/2001JB000359.

Lawson, M.J., Roder, B.J., Stang, D.M., and Rhodes, E.J., 2012, OSL and IRSL Characteristics of Quartz and Feldspar from Southern California: Radiation Measurements, p. 830–836.

Lee, Y.-H., Byrne, T., Wang, W.-H., Lo, W., Rau, R.-J., and Lu, H.-Y., 2015, Simultaneous mountain building in the Taiwan orogenic belt: Geology, v. 43, p. 451–454, doi:10.1130/G36373.1.

Lee, Y.-H., Chen, C.-C., Liu, T.-K., Ho, H.-C., Lu, H.-Y., and Lo, W., 2006, Mountain building mechanisms in the Southern Central Range of the Taiwan Orogenic Belt — From accretionary wedge deformation to arc–continental collision: Earth and Planetary Science Letters, v. 252, p. 413–422, doi:10.1016/j.epsl.2006.09.047.

Lee, C.-Y., and Liew, P.-M., 2010, Late Quaternary vegetation and climate changes inferred from a pollen record of Dongyuan Lake in southern Taiwan: Palaeogeography, Palaeoclimatology, Palaeoecology, v. 287, p. 58–66.

Lee, C.-Y., Liew, P.-M., and Lee, T.-Q., 2010, Pollen records from southern Taiwan: implications for East Asian summer monsoon variation during the Holocene: The Holocene, v. 20, p. 81–89, doi:10.1177/0959683609348859.

Li, D., Jiang, H., Knudsen, K.L., Björck, S., Olsen, J., Zhao, M., Li, T., and Li, J., 2015, A diatom record of mid- to late Holocene palaeoenvironmental changes in the southern Okinawa Trough: HOLOCENE PALAEOENVIRONMENTAL CHANGES IN THE OKINAWA TROUGH: Journal of Quaternary Science, v. 30, p. 32–43, doi:10.1002/jqs.2756.

Li, H.-C., Liew, P.-M., Seki, O., Kuo, T.-S., Kawamura, K., Wang, L.-C., and Lee, T.-Q., 2013, Paleoclimate variability in central Taiwan during the past 30Kyrs reflected by pollen, δ13CTOC, and n-alkane-δD records in a peat sequence from Toushe Basin: Journal of Asian Earth Sciences, v. 69, p. 166–176, doi:10.1016/j.jseaes.2012.12.005.

Liew, P.-M., Huang, S.-Y., and Kuo, C.-M., 2006, Pollen stratigraphy, vegetation and environment of the last glacial and Holocene—A record from Toushe Basin, central Taiwan: Quaternary International, v. 147, p. 16–33.

Liu, T.-K., Hsieh, S., Chen, Y.-G., and Chen, W.-S., 2001, Thermo-kinematic evolution of the Taiwan oblique-collision mountain belt as revealed by zircon ¢ssion track dating: Earth and Planetary Science Letters, v. 186, p. 45–56.

Liu, C.S., Huang, I.L., and Teng, L.S., 1997, Structural features off southwestern Taiwan: Marine Geology, v. 137, p. 305–316.

Mesalles, L., 2014, Mountain building at a subduction-collision transition zone, Taiwan: Insights from morphostructural analysis and thermochronological dating [Doctorate Thesis]: Université Pierre et Marie Curie.

Montgomery, D.R., and Brandon, M.T., 2002, Topographic controls on erosion rates in tectonically active mountain ranges: Earth and Planetary Science Letters, v. 201, p. 481–489, doi:10.1016/S0012-821X(02)00725-2.

Murray, A.S., and Wintle, A.G., 2000, Dating quartz using an improved single-aliquot regenerative-dose (SAR) protocol: Radiation Measurements, v. 32, p. 57–73.

Ouimet, W.B., Whipple, K.X., and Granger, D.E., 2009, Beyond threshold hillslopes: Channel adjustment to base-level fall in tectonically active mountain ranges: Geology, v. 37, p. 579–582, doi:10.1130/G30013A.1.

Pan, B., Burbank, D., Wang, Y., Wu, G., Li, J., and Guan, Q., 2003, A 900 ky record of strath terrace formation during glacial-interglacial transitions in northwest China: Geology, v. 31, p. 957–960.

Pazzaglia, F.J., 2013, Fluvial Terraces, *in* Schroder, J.F. and Wohl, E. eds., Treatise on Geomorphology, Academic Press, v. 9, p. 379–412.

Pederson, J.L., Anders, M.D., Rittenhour, T.M., Sharp, W.D., Gosse, J.C., and Karlstrom, K.E., 2006, Using fill terraces to understand incision rates and evolution of the

Colorado River in eastern Grand Canyon, Arizona: Journal of Geophysical Research: Earth Surface, v. 111, doi:10.1029/2004JF000201.

Peizhen, Z., Molnar, P., and Downs, W.R., 2001, Increased sedimentation rates and grain sizes 2-4 Myr ago due to the influence of climate change on erosion rates: Nature, v. 410, p. 891–897.

Petit, J.R. et al., 1999, Climate and atmospheric history of the past 420,000 years from the Vostok ice core, Antarctica: Nature, v. 399, p. 429–436, doi:10.1038/20859.

Pietsch, T.L., Olley, J.M., and Nanson, G.C., 2009, Fluvial transport as a natural luminescence sensitiser of quartz: Quaternary Geochronology, v. 3, p. 365–376.

Prescott, J.R., and Hutton, J.T., 1994, Cosmic ray contributions to dose rates for luminescence and ESR dating: Large depths and long-term time variations: Radiation Measurements, v. 23, p. 497–500, doi:10.1016/1350-4487(94)90086-8.

Preusser, F., Ramseyer, K., and Schlüchter, C., 2006, Characterization of Low OSL Intensity Quartz from the New Zealand Alps: Radiation Measurements, p. 871–877.

Rachmayani, R., Prange, M., and Schulz, M., 2016, Intra-interglacial climate variability: model simulations of Marine Isotope Stages 1, 5, 11, 13, and 15: Climate of the Past, v. 12, p. 677–695, doi:https://doi.org/10.5194/cp-12-677-2016, 2016.

Rhodes, E.J., 2011, Optically Stimulated Luminescence Dating of Sediments over the Past 200,000 Years: Annual Review of Earth and Planetary Science, v. 39, p. 461–488.

Royden, L., and Perron, J.T., 2013, Solutions of the stream power equation and application to the evolution of river longitudinal profiles: SOLUTIONS OF THE STREAM POWER EQUATION: Journal of Geophysical Research: Earth Surface, v. 118, p. 497–518, doi:10.1002/jgrf.20031.

Sadler, P.M., 1981, Sediment Accumulation Rates and the Completeness of Stratigraphic Sections: The Journal of Geology, v. 89, p. 569–584, doi:10.1086/628623.

Schaller, M., Hovius, N., Willett, S.D., Ivy-Ochs, S., Synal, H.-A., and Chen, M.-C., 2005, Fluvial bedrock incision in the active mountain belt of Taiwan fromin situ-produced cosmogenic nuclides: Earth Surface Processes and Landforms, v. 30, p. 955–971, doi:10.1002/esp.1256.

Seidl, M.A., and Dietrich, W.E., 1992, The problem of channel erosion into bedrock: Functional geomorphology: landform analysis and models, v. 23.

Selvaraj, K., Chen, C.T.A., and Lou, J.Y., 2007, Holocene East Asian monsoon variability: links to solar and tropical Pacific forcing: Geophysical Research Letters, v. 34, doi:doi:10.1029/2006GL028155.

Selvaraj, K., Chen, C.T.A., Lou, J.Y., and Kotlia, B.S., 2011, Holocene weak summer East Asian monsoon intervals in Taiwan and plausible mechanisms: Quaternary International, v. 229, p. 57–66, doi:doi: 10.1016/j.quaint.2010.01.015.

Simoes, M., and Avouac, J.P., 2006, Investigating the kinematics of mountain building in Taiwan from the spatiotemporal evolution of the foreland basin and western foothills: Journal of Geophysical Research, v. 111, p. B10401, doi:10.1029/2005JB004209.

Sklar, L., and Dietrich, W.E., 1998, River Longitudinal Profiles and Bedrock Incision Models: Stream Power and the Influence of Sediment Supply, *in* Rivers Over Rock: Fluvial Processes in Bedrock Channels, American Geophysical Union (AGU), Geophysical Monograph, v. 107, p. 237–260, doi:10.1029/GM107p0237.

Snyder, N.P., 2000, Landscape response to tectonic forcing: Digital elevation model analysis of stream profiles in the Mendocino triple junction region, northern California: Geological Society of America Bulletin, v. 112, p. 1250–1263.

Sun, Y., Chen, J., Clemens, S.C., Liu, Q., Li, J., and Tada, R., 2006, East Asian monsoon variability over the last seven glacial cycles recorded by a loess sequence from the northwest Chinese Loess Plateau: Geochemistry, Geophysics, Geosystems, v. 7, p. 525–535.

Suppe, J., 1981, Mechanics of mountain building and metamorphism in Taiwan: Memoir of the Geological Society of China, v. 4, p. 67–89.

Trauth, M.H., Bookhagen, B., Marwan, N., and Strecker, M.R., 2003, Multiple landslide clusters record Quaternary climate changes in the northwestern Argentine Andes: Palaeogeography, Palaeoclimatology, Palaeoecology, v. 194, p. 109–121.

Tseng, C.-H., Lüthgens, C., Tsukamoto, S., Reimann, T., Frechen, M., and Böse, M., 2016, Late Pleistocene to Holocene alluvial tableland formation in an intra-mountainous basin in a tectonically active mountain belt — A case study in the Puli Basin, central Taiwan: Quaternary Science Reviews, v. 132, p. 26–39, doi:10.1016/j.quascirev.2015.11.006.

Tseng, C.-H., Wenske, D., Böse, M., Reimann, T., Lüthgens, C., and Frechen, M., 2013, Sedimentary features and ages of fluvial terraces and their implications for geomorphic evolution of the Taomi River catchment: A case study in the Puli Basin, central Taiwan: Journal of Asian Earth Sciences, v. 62, p. 759–768, doi:10.1016/j.jseaes.2012.11.028.

Tsou, C.-Y., Chigira, M., Matsushi, Y., and Chen, S.-C., 2015, Deep-seated gravitational deformation of mountain slopes caused by river incision in the Central Range, Taiwan: Spatial distribution and geological characteristics: Engineering Geology, v. 196, p. 126–138, doi:10.1016/j.enggeo.2015.07.005.

Tsou, C.-Y., Chigira, M., Matsushi, Y., and Chen, S.-C., 2014, Fluvial incision history that controlled the distribution of landslides in the Central Range of Taiwan: Geomorphology, v. 226, p. 175–192, doi:10.1016/j.geomorph.2014.08.015.

Vinther, B.M. et al., 2009, Holocene thinning of the Greenland ice sheet: Nature, v. 461, p. 385–388, doi:10.1038/nature08355.

Wallinga, J., 2002, Optically stimulated luminescence dating of fluvial deposits: a review: Boreas, p. 303–322.

Wallinga, J., Murray, A.S., and Wintle, A.G., 2000, The single-aliquot regenerative-dose (SAR) protocol applied to coarse-grain feldspar: , p. 529–533.

Wang, Y.J., 2001, A High-Resolution Absolute-Dated Late Pleistocene Monsoon Record from Hulu Cave, China: Science, v. 294, p. 2345–2348, doi:10.1126/science.1064618.

Wang, Y., 2005, The Holocene Asian Monsoon: Links to Solar Changes and North Atlantic Climate: Science, v. 308, p. 854–857, doi:10.1126/science.1106296.

Wang, Y.J., Cheng, H., Edwards, R.L., Kong, X., Shao, X., Chen, S., Wu, J., Jiang, X., Wang, X., and An, Z., 2008, Millennial- and orbital-scale changes in the East Asian monsoon over the past 224,000 years: Nature, v. 451, p. 1090–1093, doi:10.1038/nature06692.

Whipple, K.X., 2004, Bedrock rivers and the geomorphology of active orogens: Annual Review of Earth and Planetary Science, v. 32, p. 151–185.

Whipple, K.X., Forte, A.M., DiBiase, R.A., Gasparini, N.M., and Ouimet, W.B., 2017, Timescales of landscape response to divide migration and drainage capture: Implications for the role of divide mobility in landscape evolution: Landscape Response to Divide Mobility: Journal of Geophysical Research: Earth Surface, v. 122, p. 248–273, doi:10.1002/2016JF003973.

Whipple, K.X., and Tucker, G.E., 1999, Dynamics of the stream-power river incision model: Implications for height limits of mountain ranges, landscape response timescales, and research needs: Journal of Geophysical Research: Solid Earth, v. 104, p. 17661–17674, doi:10.1029/1999JB900120.

Willett, S.D., 1999, Orogeny and orography: The effects of erosion on the structure of mountain belts: Journal of Geophysical Research: Solid Earth, v. 104, p. 28957–28981, doi:10.1029/1999JB900248.

Willett, S.D., Fisher, D., Fuller, C., En-Chao, Y., and Chia-Yu, L., 2003, Erosion rates and orogenic-wedge kinematics in Taiwan inferred from fission-track thermochronometry: Geology, v. 31, p. 945–948, doi:10.1130/G19702.1.

Wiltschko, D.V., Hassler, L., Hung, J.-H., and Liao, H.-S., 2010, From accretion to collision: Motion and evolution of the Chaochou Fault, southern Taiwan: CHAOCHOU FAULT, TAIWAN: Tectonics, v. 29, p. n/a-n/a, doi:10.1029/2008TC002398.

Wobus, C.W., Whipple, K.X., Kirby, E., Snyder, N.P., Johnson, J., Spyropolou, K., Crosby, B., and Sheehan, D., 2006, Tectonics from topography: Procedures,

promise, and pitfalls, *in* Tectonics, climate, and landscape evolution, GSA Special Paper 398, p. 55–74.

Yang, Y.J. et al., 2015, Mean Structure and Fluctuations of the Kuroshio East of Taiwan: Oceanography, v. 28, p. 75–83.

Yanites, B.J., Mitchell, N.A., Bregy, J.C., Carlson, G.A., Cataldo, K., Holahan, M., Johnston, G.H., Nelson, A., Valenza, J., and Wanker, M., 2018, Landslides control the spatial and temporal variation of channel width in southern Taiwan: Implications for landscape evolution and cascading hazards in steep, tectonically active landscapes: Variation in channel morphology controlled by landslides in s. Taiwan: Earth Surface Processes and Landforms, v. 43, p. 1782–1797, doi:10.1002/esp.4353.

Yanites, B.J., and Tucker, G.E., 2010, Controls and limits on bedrock channel geometry: Journal of Geophysical Research, v. 115, p. n/a-n/a, doi:10.1029/2009JF001601.

Yanites, B.J., Tucker, G.E., and Anderson, R.S., 2009, Numerical and analytical models of cosmogenic radionuclide dynamics in landslide-dominated drainage basins: Journal of Geophysical Research, v. 114, p. n/a-n/a, doi:10.1029/2008JF001088.

Yanites, B.J., Tucker, G.E., Mueller, K.J., Chen, Y.-G., Wilcox, T., Huang, S.-Y., and Shi, K.-W., 2010, Incision and channel morphology across active structures along the Peikang River, central Taiwan: Implications for the importance of channel width: Geological Society of America Bulletin, v. 122, p. 1192–1208, doi:10.1130/B30035.1.

Yen, I.C., Chen, W.S., Yang, C.C.B., Huang, N.W., and Lin, C.W., 2008, Paleoseismology of the Rueisuei Segment of the Longitudinal Valley Fault, Eastern Taiwan: Bulletin of the Seismological Society of America, v. 98, p. 1737–1749.

Yu, S.-B., Chen, H.-Y., and Kuo, L.-C., 1997, Velocity field of GPS stations in the Taiwan area: Tectonophysics, v. 274, p. 41–59, doi:10.1016/S0040-1951(96)00297-1.

Yu, P.-S., Mii, H.-S., Murayama, M., and Chen, M.-T., 2008, Late Quaternary Planktic Foraminifer Fauna andMonsoon Upwelling Records from the Western South China Sea, Near the Vietnam Margin (IMAGESMD012394): Terrestrial, Atmospheric and Oceanic Sciences, v. 19, p. 347, doi:10.3319/TAO.2008.19.4.347(IMAGES).

Zhang et al., 2019, The Asian Summer Monsoon: Teleconnections and Forcing Mechanisms—A Review from Chinese Speleothem δ18O Records: Quaternary, v. 2, p. 26, doi:10.3390/quat2030026.

CHAPTER 4 SUMMARY

Implications for Landscape Response to tectonics and climate

Many studies have been conducted to understand landscape response to tectonics (Burbank et al., 1996; Snyder, 2000; Kirby and Whipple, 2001; Montgomery and Brandon, 2002; Duvall, 2004). It has been assumed that tectonics can be interpreted from topography, but further investigation has showed that, in many cases, similar landforms can result from different processes (Whipple and Tucker, 1999). Frequently, bedrock-rivers are determined to be detachment-limited systems, allowing for the interpretation of tectonics from topography (Kirby and Whipple, 2001; Cyr et al., 2010). In systems with high sediment transport rates, rivers may adjust due to sediment fluxes which can be a factor of climate (Duvall, 2004; Yanites and Tucker, 2010). This thesis investigated patterns of landscape response to active tectonics in Taiwan across a gradient in topography and uplift. I calculated rates of river incision and timing of terrace deposition to understand the role of tectonics and climate in stream incision and topographic development in southern Taiwan.

Results show that rates of incision reflect the underlying tectonics, as they increase northward with assumed duration of uplift. Incision rates mirror denudation rates suggesting a strong coupling of these systems. Rates of erosion averaged over millennial timescale are within an order of magnitude of uplift rates average over millions of years (Dadson et al., 2003; Chen et al., 2020). The reflection of tectonics in surface processes suggests that a detachment-limited model is appropriate for southern Taiwan on medium timescales (10^4 – 10^6 yrs). However, the presence of terrace deposits on the landscape

represents unsteadiness in patterns of river incision suggesting that a detachment-limited model is not appropriate on all timescales. Dating of terrace deposits showed that climate signals from the orbitally driven EASM system temporarily obscured tectonic drivers of incision on 20 kyr timescales. Over long terms, a detachment-limited model may be appropriate for southern Taiwan, but sediment supply and transport capacity plays a role in drainage development over shorter time periods. It is likely the findings of this study have implications for drainage development in other active orogen. The results suggest that caution should be used when interpreting tectonics from short-term erosion rates.

Recommendations for Future Work

The following are recommendations for future work investigating drainage evolution in southern Taiwan and may be useful for similar studies in other active orogens. The first applies to the application of luminescence dating in Taiwan. The sensitivity of quartz grains is low due to a short sedimentary history. For this reason, in addition to low amounts of quartz sand, it is important to collect ~2x the volume of sediment traditionally collected for luminescence dating. It may prove valuable to collect modern sand samples to understand to test the sensitivity of sediment in the quickly eroding landscape. Additionally, I recommend sampling modern flood deposits to test for partial bleaching as this may have implications for luminescence dating of Holocene fluvial deposits.

In this study, I compare incision rates derived from luminescence ages averaged over the Holocene to late Pleistocene with CRN derived catchment averaged denudation rates averaged over centennial to millennial timescales. The period of time over which

CRN integrates decreases with distance northward as denudation rates increase. In this study, we compare incision rates average over timescales > 10^3 yrs with denudation rates average over centennial timescales in the northern drainages. It would be informative to compare incision rates with paleo-denudation rates derived from CRN sampling of terrace deposits to compare incision rates with denudation rates from periods of terrace deposition. This data may have implications for drainage response to tectonics and inform our understanding of landscape response to climate. Data introduced in this study suggests that terraces are deposited during periods of increased East Asian Monsoon intensity (EASM) because hillslope denudation rates accelerate due to increased precipitation. Paleo-catchment averaged erosion data has the potential to demonstrate further the linkage between climate and landscape processes.

I calculated incision rates from terrace deposits in the southern 100 km of Taiwan as we predicted incision rates would plateau within this area as CRN-derived denudation rates and landslide frequency were shown to (Yanites et al., 2018; Chen et al., 2020). Data introduced here does not show a similar plateau in incision rates. This may because of the large number of samples collected in the Ailiao drainage (n=9) and variety of periods of integration for rates, or because incision rates do continue to increase north of the study area. Future studies could calculate incision rates from drainages farther north to address this question. Additional investigation into the relationship between incision rates and channel steepness and distance from the mountain front could also reveal more information regarding channel response to tectonics. Preliminary work was done to investigate these relationships, but was not discussed in this study.

References

Burbank, D.W., Leland, J., Fielding, E., Anderson, R.S., Brozovic, N., Reid, M.R., and Duncan, C., 1996, Bedrock incision, rock uplift and threshold hillslopes in the northwestern Himalayas: Nature, v. 379, p. 505–511.

Chen, C., Willett, S.D., West, A.J., Dadson, S., Hovius, N., Christl, M., and Shyu, J.B.H., 2020, The impact of storm-triggered landslides on sediment dynamics and catchment-wide denudation rates in the southern Central Range of Taiwan following the extreme rainfall event of Typhoon Morakot: Earth Surface Processes and Landforms, v. 45, p. 548–564, doi:10.1002/esp.4753.

Cyr, A.J., Granger, D.E., Olivetti, V., and Molin, P., 2010, Quantifying rock uplift rates using channel steepness and cosmogenic nuclide–determined erosion rates: Examples from northern and southern Italy: Lithosphere, v. 2, p. 188–198, doi:10.1130/L96.1.

Dadson, S.J. et al., 2003, Links between erosion, runoff variability and seismicity in the Taiwan orogen: Nature, v. 426, p. 648–651, doi:10.1038/nature02150.

Duvall, A., 2004, Tectonic and lithologic controls on bedrock channel profiles and processes in coastal California: Journal of Geophysical Research, v. 109, p. F03002, doi:10.1029/2003JF000086.

Kirby, E., and Whipple, K., 2001, Quantifying differential rock-uplift rates via stream profile analysis: , p. 4.

Montgomery, D.R., and Brandon, M.T., 2002, Topographic controls on erosion rates in tectonically active mountain ranges: Earth and Planetary Science Letters, v. 201, p. 481–489, doi:10.1016/S0012-821X(02)00725-2.

Snyder, N.P., 2000, Landscape response to tectonic forcing: Digital elevation model analysis of stream profiles in the Mendocino triple junction region, northern California: Geological Society of America Bulletin, v. 112, p. 1250–1263.

Whipple, K.X., and Tucker, G.E., 1999, Dynamics of the stream-power river incision model: Implications for height limits of mountain ranges, landscape response timescales, and research needs: Journal of Geophysical Research: Solid Earth, v. 104, p. 17661–17674, doi:10.1029/1999JB900120.

Yanites, B.J., Mitchell, N.A., Bregy, J.C., Carlson, G.A., Cataldo, K., Holahan, M., Johnston, G.H., Nelson, A., Valenza, J., and Wanker, M., 2018, Landslides control the spatial and temporal variation of channel width in southern Taiwan: Implications for landscape evolution and cascading hazards in steep, tectonically active landscapes: Variation in channel morphology controlled by landslides in s. Taiwan: Earth Surface Processes and Landforms, v. 43, p. 1782–1797, doi:10.1002/esp.4353.

Yanites, B.J., and Tucker, G.E., 2010, Controls and limits on bedrock channel geometry: Journal of Geophysical Research, v. 115, p. n/a-n/a, doi:10.1029/2009JF001601.